ACTIVE CONTROL OF PARTICULATE CONTAMINATION FOR A LEO SPACECRAFT ENVIRONMENT

by

JOHN CHARLES CONGER

B.S. Massachusetts Institute of Technology (1991)

submitted to the Department of Aeronautics and Astronautics
in partial fufillment of the requirements for the degree of

Master of Science
in Aeronautics and Astronautics

at the
Massachusetts Institute of Technology
May 1993

Signature of Author_____
Department of Aeronautics and Astronautics
April 23, 1993

Certified by_____
Professor Daniel E. Hastings
Associate Professor of Aeronautics and Astronautics
Thesis Supervisor

Accepted by_____
Professor Harold Y. Wachman
Chairman, Department Graduate Committee

Active Control of Particulate Contamination
for a LEO Spacecraft Environment

by

John Charles Conger

submitted to the Department of Aeronautics and Astronautics
on May 1, 1992 in partial fufillment of the requirements
for the degree of Master of Science in Aeronautics and Astronautics.

Abstract

Spacecraft may actively modify their environment by the release of particulate contamination. Particles may also enter the near-spacecraft environment when spacecraft enter clouds of dust or debris in space. This contamination may seriously hamper the function of systems on board the craft. Two regimes of particulate contamination will be examined. The first is that of particulate contamination in the vicinity of a spacecraft. This may interfere substantially with functions such as electromagnetic observations in the infrared, visible and ultraviolet regions of the spectrum. Second is the tendency of some particles to accumulate on surfaces, such as radiators or solar arrays, and degrade their performance. The background and the problem statement will be discussed in the first chapter.

A computational model is developed to observe the behavior of particulate contamination in the spacecraft environment. This model self-consistently monitors the forces and charge on the particle. Three methods of actively controlling the particles are introduced to the simulation. These methods are cold gas jets, electric field manipulation via high voltage wires, and charge adjustment using an electron beam. In the second chapter, this model will be examined and the behavior of the particles will be discussed.

The effects of the control methods will be examined and evaluated based on their ability to affect the particles and their effects on the spacecraft system. The third chapter will analyze the effectiveness of the control methods when used to reduce optical contamination in the view angle of a sensor. The fourth chapter will analyze the effectiveness of these active control methods when used to reduce contamination accumulation on a surface.

The fifth chapter will state conclusions and suggestions for directions of future work on this subject.

Acknowledgements

At this point I would like to say thanks to a few of the people who made this research possible. In this section, and in the Dedication, I reserve the right to write the way I talk... a passing salute to what this thesis may have been like to read had it not been edited and reedited and... well, you get the picture. There are so many people to thank, and I'm not sure where to start. Perhaps with the people closest to me.

First I'd like to say thanks to my Dad. You've always been a good friend, as well as a father. I've always appreciated having you there. Hey, if it wasn't for you I might have ended up a lawyer like Mom wanted instead of being an engineer. But you always stood by me. Thanks. I'm going to say thanks to Mom, too... but she gets her own section, after this one.

I want to say thanks to everyone who was there for me when my Mom passed away. I really appreciated the support and friendship you all gave me. It would have been a lot harder getting here without you. Especially Steph. (Bet you wondered if I'd mention you in here. Well, I did.) I couldn't have made it through that without you.

I would like to thank Professor Hastings for his help and guidance. He has always pushed me to perform at the best of my ability, without actually seeming like he was pushing. I'm still not sure how he did that. Its been a pleasure working with you, Professor.

I should also acknowledge everyone who helped support my research, and as a correlary, my degree. So here I would like to thank NASA for the Space Grant

Fellowship; Johns Hopkins University Applied Physics Lab; and MIT for the James Clerk Maxwell Teaching Fellowship.

Well, I guess that's about it. The tenses are all wrong and this is far too folksy, but this is only the acknowledgements. Now if you'd please proceed on to the Dedication and then to the dry and proper thesis, complete with correct tenses and no folksy speech, that I've toiled on for the last two years... Enjoy.

Dedication

I would like to dedicate this thesis to my mother, who passed away during my first year here in graduate school. Mom, I cannot help but feel sadness that you didn't live to see me get my degree, or that you didn't even see Chris graduate from high school. But I know that you are always with us anyway, and I hope you're proud of us. I've always done the my best, like you taught me, and it got me to the finest institution in the world. Thanks for everything, Mom. I love you.

Table of Contents

List of Figures

Chapter 1 : Introduction

Spacecraft environmental interactions is a broad field encompassing many factors which must be considered when designing a spacecraft. These interactions with the environment can cause serious problems with spacecraft systems if not anticipated and accounted for. In his survey of spacecraft environmental interactions, A. C. Tribble states that the interactions a spacecraft has with its environment may be characterized by five major categories : vacuum, neutral, plasma, radiation, and micrometeroroid/orbital debris.[1]

Because of the vacuum nature of the orbital environment, there is no natural protection from the ultraviolet radiation of the sun. This radiation increases the solar absorbtance characteristics of the surface materials on the spacecraft. This makes the temperature of the spacecraft much harder to control. An additional problem related to this UV radiation is that it has a tendency to cause molecules to attach to surfaces and remain there, forming a coating that can degrade the performance of solar arrays or thermal control surfaces.[2]

The low density neutral environment will induce a low drag force, and may be responsible for the decay of spacecraft orbit over time. This effect is stronger at lower altitudes where the neutral density is higher. At lower altitudes one may also encounter the effects of physical sputtering. This is an erosion effect resulting from the impact of molecules at high speeds with the spacecraft surface. Usually physical sputtering is not a problem, but may be an issue for certain materials or for long term missions. Another

issue in the neutral environment is that of atomic oxygen. Atomic oxygen is plentiful in the neutral environment and is a very reactive substance. It will react with many spacecraft materials, changing their properties or eroding them.

The plasma environment results in manipulation of charge or the potential around the spacecraft. In low earth orbit, the plasma has a high density but a low energy. The opposite is true in geosynchronous orbit. The electron current dominates in the LEO environment, causing a negative potential to develop on the spacecraft. High voltage solar arrays may interact with the ambient plasma in such a way as to cause an effect called arcing. This results in an intense discharge current which can cause serious damage to the array.

Radiation, such as found in the Van Allen belts, may have adverse effects on the spacecraft. It can damage electronics and solar arrays. Also, the radiation may affect humans and any other living organisms on the spacecraft. Because of these effects, shielding must be used to protect sensitive areas.

Micrometeorites, or orbital debris, pose a serious problem to spacecraft. Any collision with a particulate would take place at a very high speed. The kinetic energy released could result in catastrophic failure of the vehicle.

Spacecraft modify their own environment in numerous different ways. The resulting modifications to the near spacecraft environment may also seriously hamper the function of systems on board. One way in which this may occur is by the release of material to the environment around the spacecraft. Thruster firings release a great deal of material. The shuttle periodically performs water dumps. These are examples of large material releases, but they can be more subtle too. Water molecules from the atmosphere may accumulate on the surface of the craft while it is in the atmosphere, and then will slowly diffuse, or outgas, from the spacecraft surface during its lifetime into the surrounding vaccuum. Spacecraft surfaces may also degrade over time due to

environmental wear or stress due to thermal cycles. This degradation results in small parts of the skin being released into the environment around the spacecraft.

This material may cause a variety of complications on spacecraft systems. Particles in the environment around spacecraft may affect the potential field around the spacecraft if in sufficient numbers. They may interfere with electromagnetic sensors. Particles also cause problems when they accumulate on spacecraft surfaces. They may impede temperature control by changing the absorbtivity of the spacecraft surface. They may accumulate on radiators, causing them to become less effective. Accumulation on solar arrays also lowers the amount of power they may collect.

These particulate-related problems are discussed in this chapter, and the idea of active control to mitigate their effects is introduced.

1.1 Particulate Contamination in the Spacecraft Environment

Particulate contamination in the vicinity of spacecraft may interfere substantially with electromagnetic observations in the ultraviolet, visible and infrared regions of the spectrum. Particulates have been observed around manned spacecraft[3] including a number of Shuttle missions[4]. Most recently contamination problems of this sort have hampered the Magellan[5] and the Mars Observer[6] spacecraft. On both the Magellan and the Mars Observer spacecraft the optical scattering from the particulates was responsible for the periodic loss of the star tracker lock. More generally, calculations show that remote observations will be affected by micron class particles due to solar illumination, earth radiation and particulate self-emission[7]. If the particulates are moving slowly with respect to the spacecraft then they will only pass slowly through the field of view. Hence they will provide a noise background which will be present much of the time. A constant flux of more rapid particles from the spacecraft can produce a noise background as well.

There are several sources of these particulates on orbit. Firstly, particulates which collect on vehicle surfaces on the ground may be carried to orbit and shaken loose during spacecraft operations. Secondly, on a micron scale many surfaces can be quite rough. Many composite materials may have fiber fragments which are micron sized at the surface. Alternatively, under atomic oxygen attack, surfaces may become textured on the micron scale. In orbit, micron size particulates can break off due to forces associated with solar illumination, thermal stresses due to terminator crossing or electrostatic repulsion due to differential charging in the space plasma. Third, particulates are created by firing of rocket motors, especially solid rocket motors, and effluent dumps. It is well known on the Shuttle that water dumps sometimes lead to spectacular clouds of ice crystals. In addition, on vehicles where the placement of thrusters is done without regard to plume impingement problems, surfaces where the plume impinges may be coated with large numbers of particulates or volatile exhaust products.

For larger amounts of dust which a spacecraft may encounter in the vicinity of a comet or around an asteroid, the physical impact of the dust on the spacecraft may be deleterious to the health of the spacecraft. The relative velocity between the dust and the spacecraft may be very high, leading to a large amount of energy which must be dissipated by the particles when they strike the satellite.

The kinetics of dusty plasma clouds is a matter of active research for the understanding of cometary environments as well as for the ring systems of planets such as Jupiter and Saturn. Scientific issues that need to be addressed are the potential formation in the cloud as well as the self-consistent motion of the dust plasma cloud relative to the release source.

Dusty plasmas or plasmas with particulates have been studied in two major space related contexts. The first has been in astrophysics where there has been work on dust in the Jovian ring[8] system and work on the basic physics of dusty plasmas[9,10,11]. The second area has been in the control of reentry wake radar signatures. The introduction of

a wake quenchent made of fine particles can act as a collection source for charged particles. Direct attachment of the electrons to the particles will reduce the electron density and thus reduce the radar cross section of the wake.

The dust cloud potential relative to the ambient plasma is also found to depend on whether the dust cloud is tenuous or not. In a tenuous cloud, the dust cloud potential is very low while the potential on each dust particle is close to that for an isolated particle. In a dense cloud, the dust cloud potential approaches a maximum while the potential on each dust particle decreases to zero with increasing dust density.

The potential in the cloud and the potential in the background plasma are important parameters in determining the dynamics and structure of the dust cloud relative to the spacecraft. The two potentials are obtained from the requirement of charge balance in the grain. It has been shown that these two equations may have multiple solutions[12]. These can arise when several different dominant balances can be established among the currents carried by ions, electrons and particles. The presence of multiple solutions means that the dust-plasma system may be subject to plasma instabilities and the formation of double layers in the interior of the system.

The motion of the dust cloud relative to the spacecraft depends very sensitively on the self consistent potential in the cloud. This is exactly the same as what was found for the plasma cloud examined in previous work[13]. This raises the possibility that the motion of the dust cloud may be controlled from the spacecraft by the controlled application of electric fields and charges from the spacecraft. Even for a loose set or particulates the motion of the particulates will depend sensitively on the local electric forces[5]. This suggests the ability to actively control of the environment from the spacecraft. This would allow alleviation of undesirable consequences rather than only responding passively to the deleterious situation.

1.2 Particulate Contamination of Spacecraft Surfaces

In the design of any space power system which operates subject to the second law of thermodynamics, one of the major concerns is the disposal of heat. Since the only mechanism for heat removal in space is by radiative cooling, all space power systems must have surfaces which emit waste heat and reflect solar radiation. These thermal control surfaces then determine the operational temperature of the system. The spacecraft electronics, power, propulsion and payload are designed to work most effectively within a band centered around the design operational temperature. Contamination of the thermal control surfaces typically causes an increase in the solar absorptance and therefore degrades the ability to emit waste heat. This causes an increase in the operational temperature of the spacecraft which in extreme circumstances may cause immediate system failure but usually shortens the lifetime of the spacecraft systems below the design life. For example, lack of control over the system temperature can lead to enhanced boil-off of cryogens and therefore a reduction in the life of cryogenically cooled spacecraft sensors. In addition, a rise in the system temperature will modify the IR signature of the spacecraft making it easier to detect. For solar arrays the accumulation of contaminants on the solar cell covers can cause a loss of power due to direct obscuration of the solar cells as well as due to the decrease in conversion efficiency associated with the rise in the cell temperature. This is now the accepted explanation for the loss of power on the 6 GPS Block I satellites. These satellites had a beginning of life power of 560 W and a design power after eight years of 460 W with the loss of power being due to radiation degradation. Instead, after eight years the average power is 380W. This power loss is well modeled by phenomenological models of contaminant deposition in addition to radiation loss.[14]

The deposition of contaminants on sensitive thermal control surfaces can be controlled to a significant degree by careful design of the system with potential effluent sources placed far from thermal control surfaces. This, however, constrains the design of

the spacecraft and may be impractical in some instances. In addition, the contaminant flux to a surface can never be reduced to zero because of self scattering and contaminant attraction to sensitive surfaces by local electric fields. Contaminant self scattering and atmospheric backscattering around a spacecraft will provide a flux of contaminant molecules with no direct line of sight to other spacecraft surfaces.

These constraints suggest that an active and autonomous system which could reduce contaminant deposition or remove contaminant deposits would enable significant gains in spacecraft performance. In addition, it may be possible to use new materials currently forbidden for contamination reasons on spacecraft. This would expand the design options available for a spacecraft designer.

1.3 Control of Particulate Contamination

In the current generation of spacecraft, the deleterious spacecraft environmental interactions are handled either by design (that is, modifying the design to eliminate them) or by changing the operation of the spacecraft or by redundancy so that failure of critical parts will not be catastrophic. Methods for passive control of contamination from particulates have been developed. These methods do not require specific action at the time of contaminant presence. For example, a structure may be placed about the sensor to impede the close approach of particles, or the data processing software can remove or ignore some spurious signals. This has been the manner in which both the Magellan and Mars Observer spacecraft have dealt with their particulate contamination problems, which caused temporary loss of the star tracker lock when software attempted to identify particles as stars. In the case of the Mars Observer, the amount of allowable uncorrelated targets in the software was increased, and this allowed the star tracker to ignore extraneous particles. These methods, however, will not necessarily result in complete removal of contaminating signals.

In the next generation of spacecraft it will be possible to actively control some of the interactions. This is because of growth in the capability to sense and compute locally the environment with very fast microprocessors. One benefit of active control is that it will be possible to accommodate a changing environment (both spatially and temporally). However, the major benefit of active control of any design limiting problem is that it opens up whole new regions of design space for a spacecraft designer to explore. This is being tried with active control of performance limiting instabilities in gas turbine engines, with active control of large space structures and active control of fluid flow over aircraft wings. What makes all of these possible is the ability to very rapidly sense the onset of the design limiting problem and compute a response to it before it becomes catastrophic. Hence it allows a designer to operate in previously forbidden space.

This work involves examination of active methods to control particulate and molecular fragment contamination. There are three methods which are examined in this research. The first is through use of cold gas jets. Gas jets are fired to move particles away from a critical region near the spacecraft, such as the view angle of a sensor or the surface of a radiator. A second technique for affecting the particles is to modify the electric field that surrounds the spacecraft such that the particles are repelled from the critical region. The third method for active control of the particulate contamination is to use electron beams to charge up the particles. The high negative charge induced will allow the particles to be swept away by the electric field.

Each of these cases will be examined in terms of their benefits weighted against their potential system effects on the spacecraft. The modification of the field can use a relatively large amount of power, and it does not reach very far from the spacecraft. The use of an electron beam will also draw power and have little direct physical effect, though it can affect the plasma atmosphere about the spacecraft. In addition, at reasonable power levels this control method is not effective far from the spacecraft. The cold gas jets have an effect farther away from the spacecraft, but they also cause the most physical

disruption to the spacecraft. Thrusters must be strategically located on the spacecraft to compensate for any potential orbit alteration. The control jets and the compensation thrusters will result in an increase in the mass of the spacecraft.

Active control methods are analyzed and compared by including them in a particle trajectory simulation. This simulation and the active control methods will be described in more detail in Chapter 2. In addition, the behavior of micron scale particles in the spacecraft environment is discussed.

These methods will then be inserted into the simulation of two different contamination problems. In Chapter 3, simulation results are discussed regarding the effectiveness of the methods in reduction of the particulate contamination in front of a sensor on a spacecraft in LEO. In Chapter 4, simulation results are discussed regarding the effectiveness of control methods in deterring particles from landing on a solar array surface. Chapter 5 will detail conclusions from these results, and suggest directions for future work.

Chapter 2: Simulation Model

The task of analyzing particulate behavior around a spacecraft, and how the control methods affect it is accomplished using computer simulation. Both two and three dimensional simulation models are introduced in this chapter. Particles are tracked from the point they are released from the spacecraft to the point which they leave the computational domain. The force and charge on the particle are calculated self consistently.

In this chapter the domain within which the particles will move is discussed, as well as the particles that are modeled. The capability of the simulation is reviewed. In addition, the behavior of the particles is examined in detail.

2.1 Description of Domain

In two dimensions, the spacecraft is modeled as a rectangle. The leading edge of the spacecraft makes an angle of 90 degrees with the radial vector from the Earth and the sun angle is taken as a variable. The orbit is taken to be equatorial, and the altitude is variable. For definiteness, the spacecraft is taken to be two meters in length by one meter in height. (See Figure 2-1) In three dimensions, the spacecraft is modeled as a cylinder such that a crossectional cut through the equatorial plane will yield the two dimensional model. The particles are tracked in a domain five body lengths on either side of the spacecraft, and in front of the spacecraft the particles are tracked for up to a kilometer. This is because the strength of the neutral wind will tend to blow particles in this region

back toward the spacecraft. The particles that are modeled in this domain are taken to be uniform spheres with a crossectional area of πr^2.

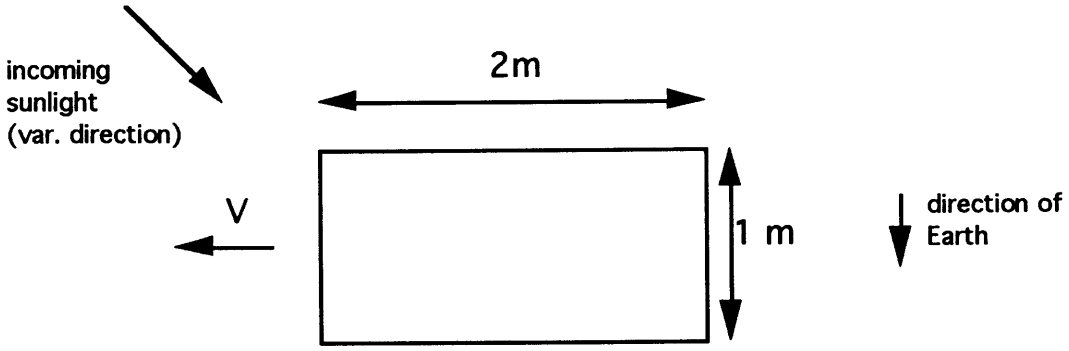

Figure 2-1 : 2D Spacecraft schematic

Once the orbit of the spacecraft is specified, the ambient neutral environment is calculated using the US Standard Atmosphere model. The plasma environment is determined using the International Reference Ionosphere model in the three dimensional case. In the two dimensional simulation, the ambient electron density is taken as $10^{11}/m^3$ and the electron temperature is taken to be .1 eV. The potential on the spacecraft is assumed to be fixed or controlled at some given value. It is assumed that there will be a grounding surface away from areas of interest which will allow the net current to be zero. The potential in the vicinity of the spacecraft is calculated from a hybrid-PIC code which uses fluid electrons and kinetic ions.[15] The solution is two dimensional and is extended to the three dimensional case by use of rotational symmetry. This model is discussed in more detail later in this chapter in the section regarding the electric field modification.

2.2 Computational Approach

The computational approach involves the simple forward integration in time of the equations of motion and the charge balance equation for the particles. All integration is done using *dlsode* integration software. The equations of motion are

$$\frac{dx}{dt} = v_x \qquad \frac{dv_x}{dt} = a_x \tag{2-1}$$

$$\frac{dy}{dt} = v_y \qquad \frac{dv_y}{dt} = a_y \tag{2-2}$$

$$\frac{dz}{dt} = v_z \qquad \frac{dv_z}{dt} = a_z \tag{2-3}$$

Equations 2-1 and 2-2 are used in the two dimensional code, and equations 2-3 are included in the three dimensional code. In addition, there is the charge equation for each particle which is updated each time step:

$$\frac{dq}{dt} = I_i + I_e \tag{2-4}$$

where the currents are the ambient ion and electron currents. For simplicity, the secondary electron and photoelectric currents are neglected in this simulation.

The forces used to obtain the accelerations for these formulae are elaborated upon in the next three sections. Then the methods used to obtain the ambient currents are explained.

2.3 Ambient forces

When a particle is released into the environment it is acted upon by a number of ambient forces. The ambient forces included in this simulation are solar pressure, neutral wind drag, Lorentz force due to the Earth's magnetic field. These forces are independent of the spacecraft and its configuration, but depend on its location in the atmosphere.

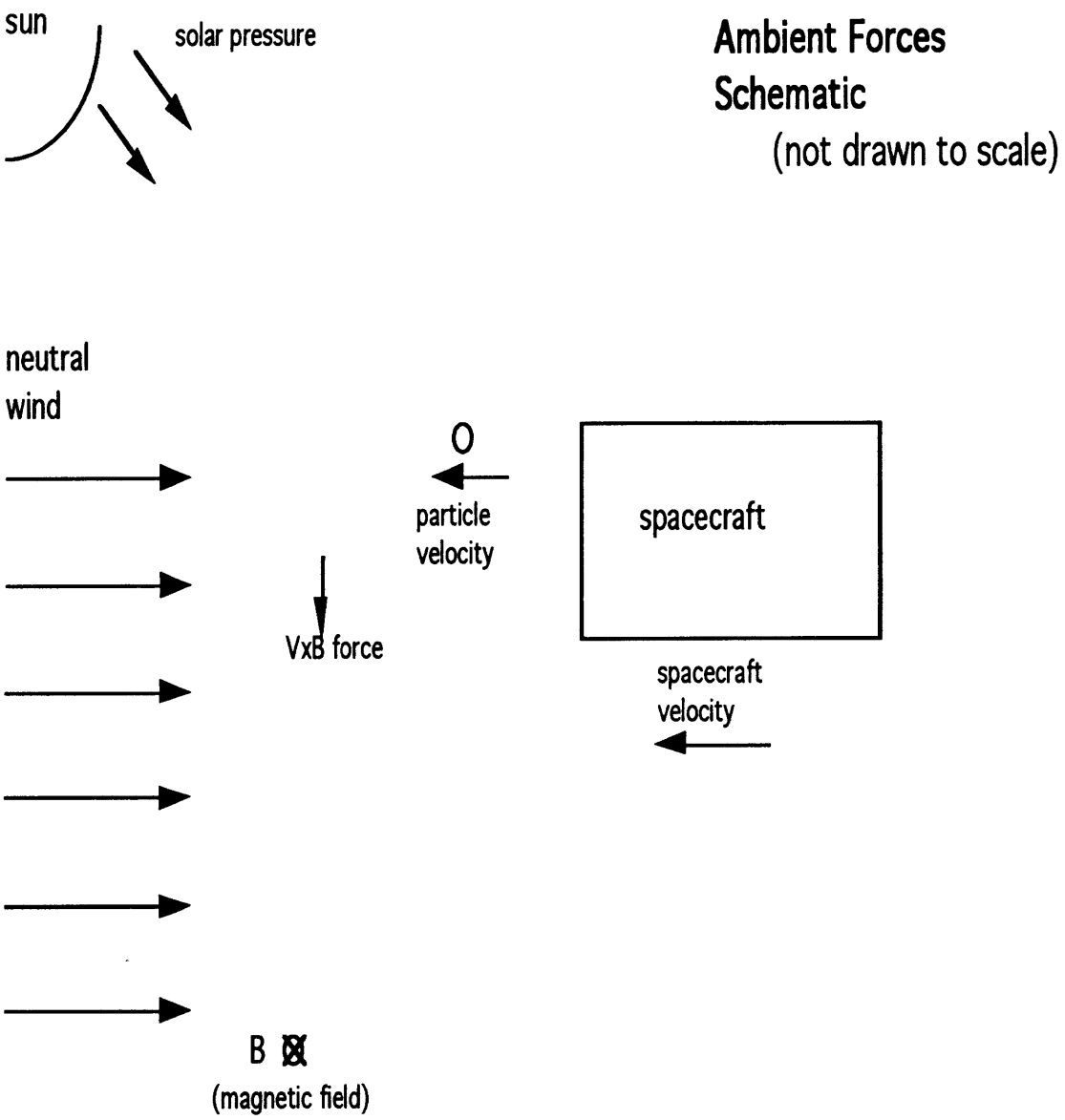

Figure 2-2 : Ambient Forces Acting on a Particle

2.3.1 Solar Pressure

The intensity of sunlight at the earth's orbit is defined by the solar radiation constant, Γ_S = 1370 W/m^2. The momentum flux asociated with the photons is Γ_S/c, where c is the speed of light. The formula for the actual force on the particle is

$$\vec{F}_s = \frac{\Gamma_s}{c} A_p K \hat{s} \tag{2-5}$$

where A_p is the crossectional area of the particle, and K is an accommodation coefficient. If there is total absorption then K = 1, and if there is total reflection, then K = 2. We shall take K as one, corresponding to particles which absorb the photons striking them, yielding the formula:

$$\vec{F}_s = \frac{\Gamma_s}{c} A_p \hat{s} \tag{2-6}$$

The unit vector $\hat{s}$ represents the direction of the force, pointing from the sun to the particle.

2.3.2 Neutral Wind

The neutral wind is the gas dynamic drag force that acts on the particle released from the spacecraft due to the rapid velocity with which the spacecraft is moving through the ambient atmosphere. This force depends primarily on the altitude, which determines the density of the ambient neutral gas. The formula for the neutral drag force is

$$\vec{F}_w = \tfrac{1}{2} \rho V^2 c_d A_p (-\hat{V}) \tag{2-7}$$

The neutral density is ρ, which goes through significant changes as the altitude is varied. V is the relative velocity between the particle and the neutral gas. This is equivalent to v_S - v_p, where v_S is the velocity of the spacecraft and v_p is the velocity of the particle in the

spacecraft frame. Since, in general, $v_S >> v_p$, this value will usually be equivalent to the velocity of the spacecraft. The coefficient of drag for a sphere is $2 + (\tau - \sigma)$, where τ and σ are the tangential and normal momentum accommodation coefficients respectively. These coefficients are assumed equal, and thus c_D is set to 2 for the particles. A_p is the crossectional area of the particles. The term $(-\hat{V})$ represents the unit vector in the negative V direction. Thus, this force is directed in the opposite direction to the particle velocity.

The density drops a large amount at high altitudes (Figure 2-3), such that this force goes from being dominant at 150 km to practically nonexistent at 1000 km (Figure 2-4). The plot in Figure 2-4 uses a spherical particle which is five microns in radius, and it is clear as the altitude changes, that the neutral drag force is driven down by the decrease in the neutral density.

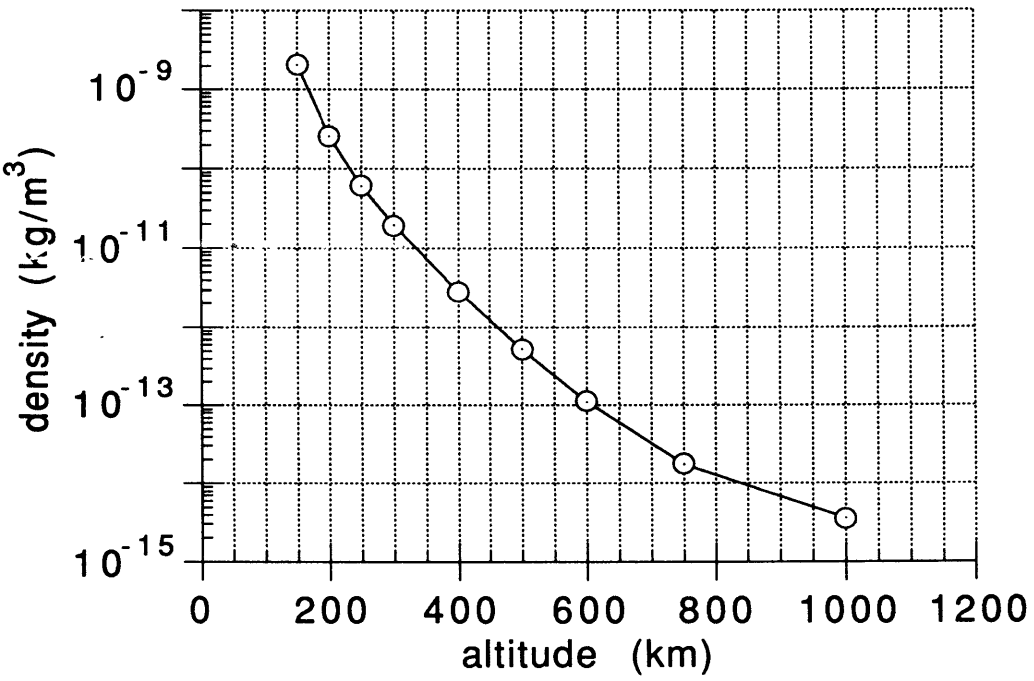

Figure 2-3 : Ambient Density vs. Altitude

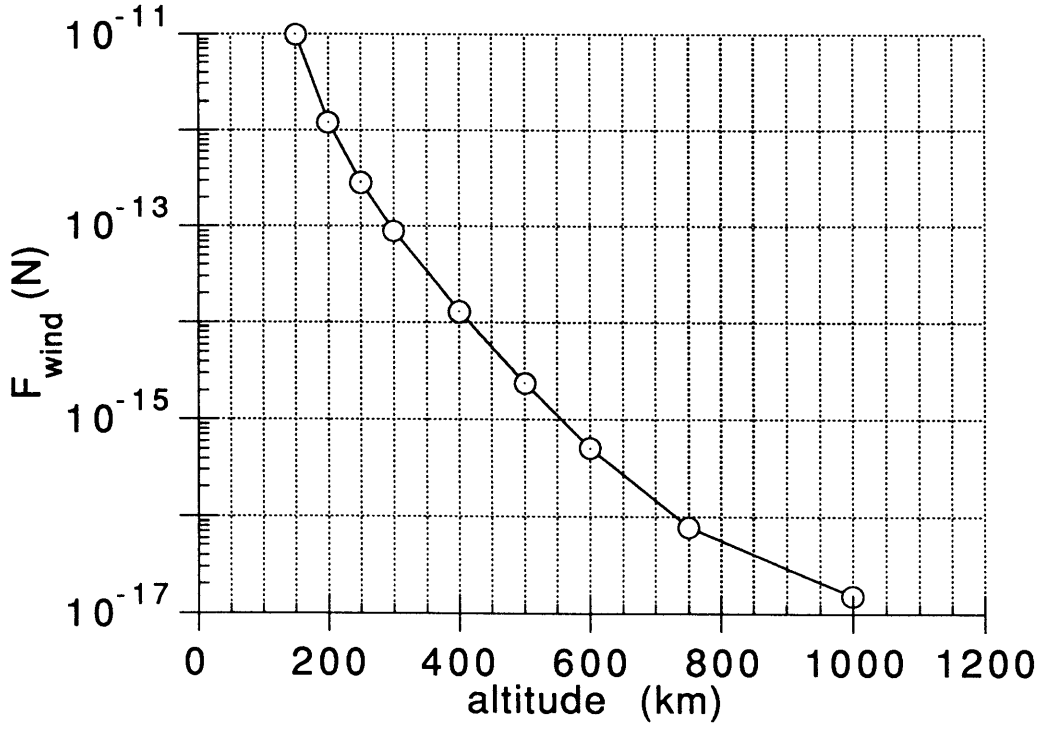

Figure 2-4 : Neutral Wind Drag vs. Altitude

The density is modified in the wake region. A model of the wake behind a rapidly moving object of circular cross section was obtained from the reference by Al'pert, Gurevich and Pitaevskii.[16] The wake model is derived in this reference by integrating the neutral distribution function and using perturbation theory to obtain $\delta n(x,y,z)$, the perturbation from n_o, the ambient neutral density. They transform to polar coordinates (ρ,ϕ,z coordinates) and make the assumption that the body is rapidly moving. The model is a far field model ($z^2 >> r^2$), thus for the spacecraft modeled in this work, it will not be valid for the first few meters behind the spacecraft. However, our area of interest is not within this region. This wake model is included for the sake of completeness.

$$-\delta n(x,y,z) = 2n_o \exp\left[-\frac{MV_o^2}{2\kappa T}\left(\frac{\rho}{z}\right)^2\right]^{-\frac{R_o}{z}\sqrt{\frac{MV_o^2}{2\kappa T}}}_{0} \int \tau e^{-\tau^2} I_o\left(-\frac{\rho}{z}\sqrt{\frac{2MV_o^2}{\kappa T}}\tau\right)d\tau \qquad (2\text{-}8)$$

In this formula, n is the neutral density, M is the molecular mass of the neutral particles, V_O is the velocity of the spacecraft, R_O is the radius of the circular cross section, T is the temperature of the neutrals, and I_0 is the Bessel function of zero order having an imaginary argument. From this they get a chart of values for the ratio of the local neutral density $n(\rho,z)$ to the undisturbed neutral density, n_O.

	$\frac{z}{R_o}\sqrt{\frac{2\kappa T}{MV_o^2}}$										
ρ / R_o	0	-0.2	-0.4	-0.6	-0.8	-1.0	-1.2	-1.5	-2.0	-4.0	-8.0
0.0	0	0	0	0.06	0.21	0.37	0.50	0.64	0.78	0.94	0.98
0.2	0	0	0.01	0.09	0.24	0.38	0.51	0.65	0.78	0.94	0.98
0.4	0	0	0.06	0.14	0.28	0.42	0.53	0.67	0.78	0.94	0.98
0.6	0	0.04	0.11	0.23	0.36	0.48	0.57	0.69	0.79	0.94	0.98
0.8	0	0.09	0.27	0.39	0.48	0.56	0.63	0.71	0.80	0.94	0.98
1.0	0.50	0.51	0.54	0.58	0.62	0.65	0.68	0.75	0.82	0.94	0.98
1.2	1.00	0.92	0.78	0.76	0.75	0.74	0.75	0.78	0.84	0.94	0.98
1,5	1.00	1.00	0.96	0.88	0.87	0.86	0.84	0.84	0.86	0.94	0.98
2.0	1.00	1.00	1.00	0.97	0.95	0.95	0.93	0.91	0.90	0.94	0.98
4.0	1.00	1.00	1.00	1.00	1.00	1.00	0.99	0.99	0.99	0.97	0.98
8.0	1.00	1.00	1.00	1.00	1.00	1.00	1.00	1.00	1.00	0.99	0.99

Figure 2.5 : Ratio of $n(\rho,z)$ to n_O

2.3.3 Lorentz Force

The sum of the electromagnetic forces acting on the particle is known as the Lorentz force. The Lorentz force is represented by the following formula:

$$\vec{F}_L = q(\vec{E} + \vec{v} \times \vec{B}) \qquad (2\text{-}9)$$

The charge is q, E represents any electric fields present, v is the velocity of the particle in the Earth frame, and B is the Earth's magnetic field. We ignore the ionosphere electric field, which leaves only the second term in the equation. As the spacecraft travels through the Earth's magnetic field, there are two components of this velocity vector. The

first is the velocity of the spacecraft. This is a constant, and the vector product of the spacecraft velocity and the magnetic field results in a constant force. Therefore, it is referred to as the motional electric field. In the spacecraft's frame, it acts as an electric field on the particle pointing in the $\vec{v}_s \times \vec{B}$ direction. The second component of the velocity vector is the velocity in the frame of the spacecraft. This is usually a much smaller force, acting in the $\vec{v}_p \times \vec{B}$ direction.

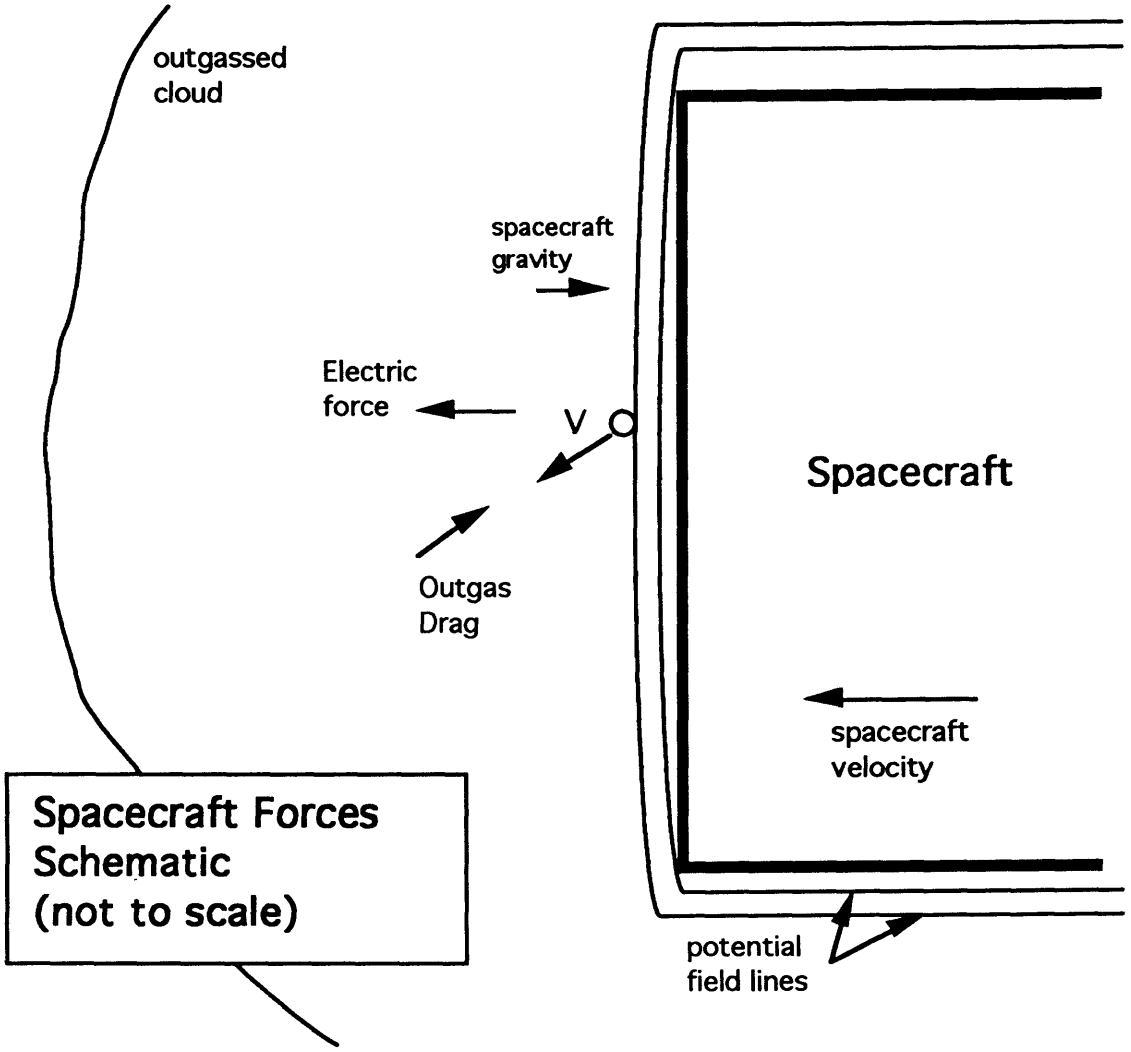

Figure 2-6 : Spacecraft Forces Acting on a Particle

2.4 Spacecraft Forces

2.4.1 Spacecraft Electric Field

The electric field of the spacecraft applies the force $F_e = qE$, where q is the charge of the particle, and E is the strength of the electric field generated by the spacecraft at a given point in space. The force will act in the direction of the electric field. The model used for the electric field is a modified version of a code written by Wang[15]. It is a hybrid PIC code that uses fluid electrons and kinetic ions.

The governing equations for the code are:

$$\nabla^2\phi = -\frac{e}{\varepsilon_o}(n_i - n_e) \tag{2-10}$$

$$n_e = n_o \exp\left(\frac{e\phi}{KT_e}\right) \tag{2-11}$$

where n_i is obtained from the positions of the ion particles. The ion motion is determined by:

$$\frac{d\vec{x}_i}{dt} = \vec{v}_i \;;\quad \frac{d\vec{v}_i}{dt} = -\frac{q_i}{m_i}\nabla\phi \tag{2-12}$$

Wang's code was specifically designed to model flat plates. To arrive at the fields desired for this particulate tracking code, the boundary conditions were changed. In the figure below is shown a potential contour plot of the two dimensional spacecraft generated when the flat plate boundary was changed to a rectangle. The spacecraft in this case was held at a potential of -1 V. Contours are at -.2 V, -.4 V, -.6 V, -.8 V, -1 V. Each unit of length on the plot represents .04 meters; 25 units are equivalent to one meter. The potential drops off extremely quickly near the leading edge of the spacecraft.

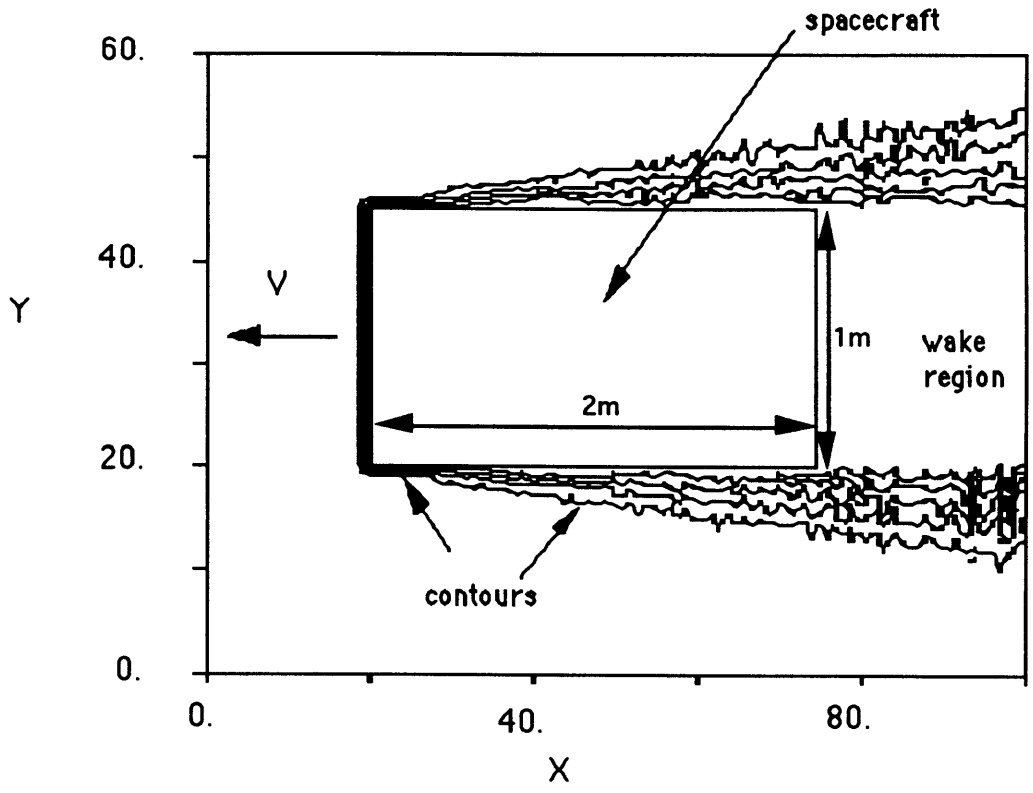

Figure 2-7 : Potential Contours around a Rectangle Moving at High Velocity

2.4.2 Outgassing Drag

A spacecraft will have a cloud of gas, such as water, around it at any point in time due to release of molecules from the spacecraft surface. This is called outgassing. In this simulation, the effects of the drag due to this cloud around the vehicle were included. In this model, the same drag formula(2) as in the neutral wind case is used. A point source model was used to determine the outgas density. Using the continuity equation

$$\frac{1}{r^2}\frac{\partial}{\partial r}(r^2 \rho u) = 0 \qquad (2\text{-}13)$$

one can obtain the result,

$$\rho u = \frac{C}{r^2}, \qquad (2\text{-}14)$$

where C is a constant. Assuming that the gas is expanding at the thermal velocity, one can write the density in the form

$$\rho = \frac{C_1}{r^2}, \tag{2-15}$$

where C_1 is simply the constant C/u. Taking the outgas rate to be a constant Γ_o and $r=r_o$ at the spacecraft surface, one can obtain the equation

$$\rho = \frac{\Gamma_o}{v_{th}}\left(\frac{r_o}{r}\right)^2 \tag{2-16}$$

where v_{th} is the thermal speed of water molecules. Because of the point source, this model is valid only in the far field. It is extrapolated into the near field of the spacecraft to get a reasonable approximation of the cloud density near the spacecraft.

Finally, using the drag equation 2-17, we get the resultant drag force. Notice that this is basically the same equation as 2-7, albeit with a different velocity vector.

$$\vec{F}_{drag} = \tfrac{1}{2}\rho v_p^2 c_D A_p(-\hat{v}_p) \tag{2-17}$$

In this case, the velocity used is v_p, the particle velocity in the spacecraft frame. The outgassed water molecules, released from the spacecraft, are assumed to be moving with the spacecraft, as is the particle, and only the relative velocity is important. In addition, the direction is different. This force acts in the direction opposite to the unit velocity vector of the particle in the spacecraft frame, and this direction is represented in the formula by $-\hat{v}_p$.

2.4.3 Gravitational Force

This simulation takes into account the gravity force between the particle and the spacecraft. Since it is a near field model, the force on the particle and the ship due to the Earth's gravity are taken to be equal and thus it is neglected.

The force between the particle and the spacecraft is

$$\vec{F}_g = \frac{Gm_p m_s}{r^2}\hat{g} \tag{2-18}$$

where G is the gravitational constant, $6.67 * 10^{-11}$ m^3/kg-s, m_p and m_S are the masses of the particle and the spacecraft respectively, and r is the distance between the particle and the center of mass of the spacecraft. The unit vector $\hat{g}$ represents the direction from the particle to the center of mass of the spacecraft, which in this case is its geometrical center.

2.5 Control Forces

2.5.1 Gas Jet Plume Model

The analytical model used to determine the density of the gas from these jets is a far field model obtained from a survey article by Dettleff[17].

$$\frac{\rho}{\rho_E} = \frac{\kappa_4}{2}\left(\frac{r_E}{r}\right)^2 (\cos\theta)^{\kappa_4} \tag{2-19}$$

where κ_4 is the hypersonic parameter:

$$\kappa_4 = \gamma(\gamma-1)M_E^2 \tag{2-20}$$

In these equations, ρ/ρ_E is the ratio of density to exit density of the thruster, r/r_E is the ratio of the distance from the source point of the thruster model to the exit radius of the thruster. M_E is the mach number at the exit of the thruster, and γ is the ratio of specific heats. The value θ represents the angle from the plume centerline. The model is a far field source model, and therefore is not accurate for values of r close to zero, so the approximation is made in the simulation that when the density value is larger than the exit density, it is simply set to equal the exit density. The gas in this plume is assumed to have reached the maximum velocity for a pure isentropic expansion:

$$u_{lim} = \sqrt{\frac{2\gamma}{\gamma - 1} RT_o} \tag{2-21}$$

These jets are assumed to use diatomic nitrogen as fuel. The exit radii are set to two centimeters. The area ratio, and corresponding exit mach number, decide how quickly the density will fall off with angle away from the centerline. The two cases that were run were at M_E=5.914 (which corresponds to an area ratio of 50) and M_E=2. Below are plotted the decrease of the term, $(\cos\theta)^{\kappa 4}$, in the density equation with angle from the centerline for a range of exit mach numbers (Figure 2-8). The density fall off is more accurately displayed by the plot of $\kappa_4 (\cos\theta)^{\kappa 4}$ shown in Figures 2-9 and 2-10. It is clear from the first of these two that the thrusters with higher exit mach numbers have a higher density region near θ=0, but these thrusters also drop off far more quickly. The lower mach numbers produce less thrust near the centerline, but keep their effectiveness over a greater span of area.

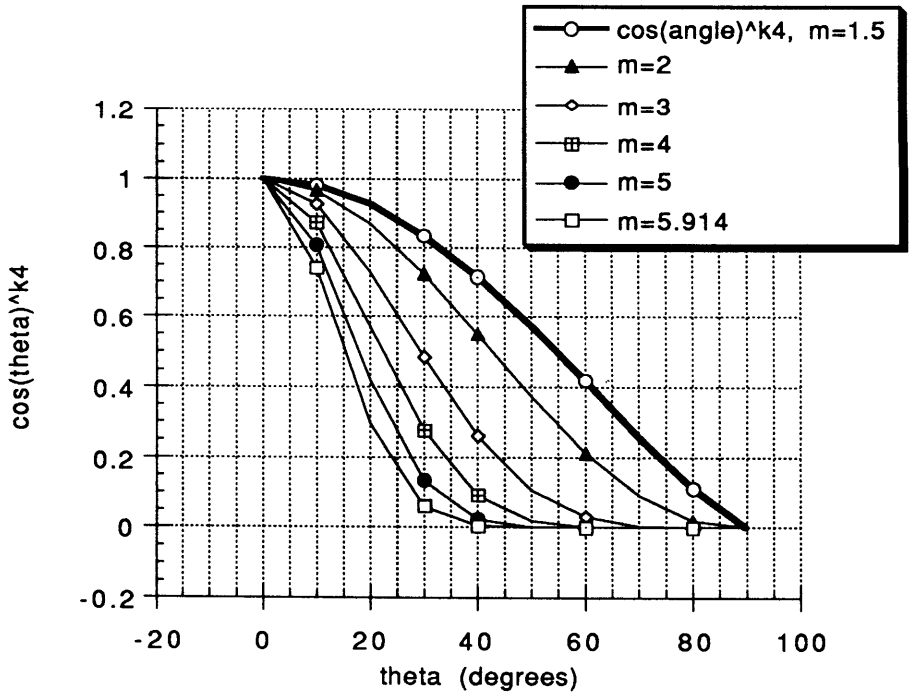

Figure 2-8 : Rate of Density Fall Off with Angle from Centerline for 1.5>M_E>6

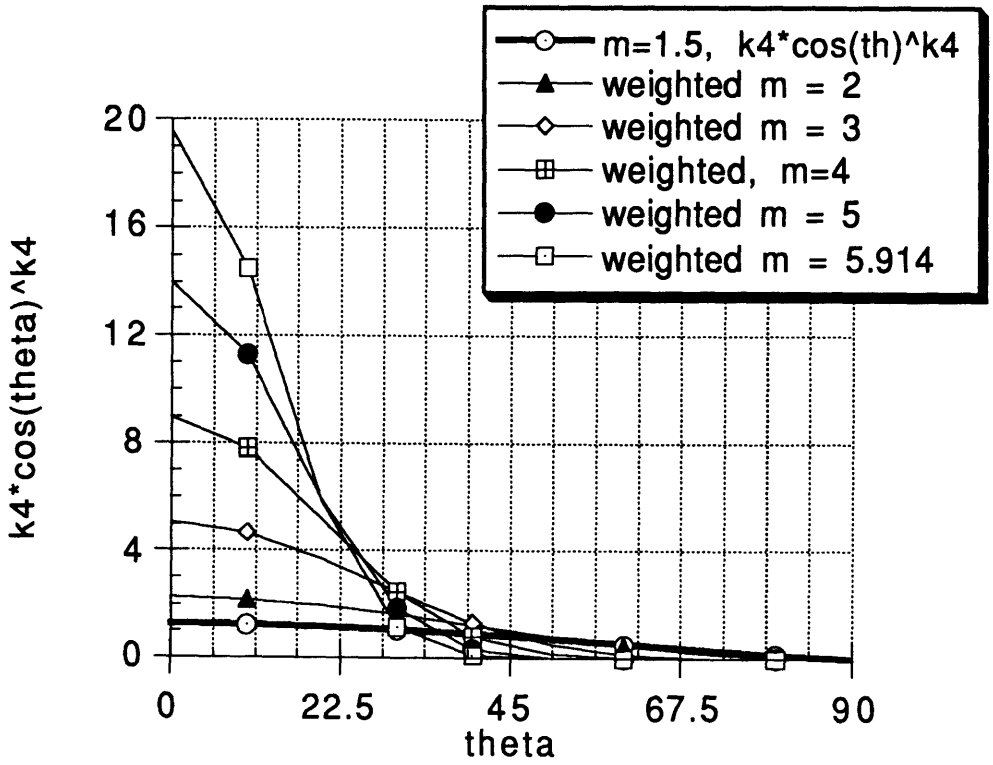

Figure 2-9 : Weighted Density Fall Off, $1.5>M_E>6$

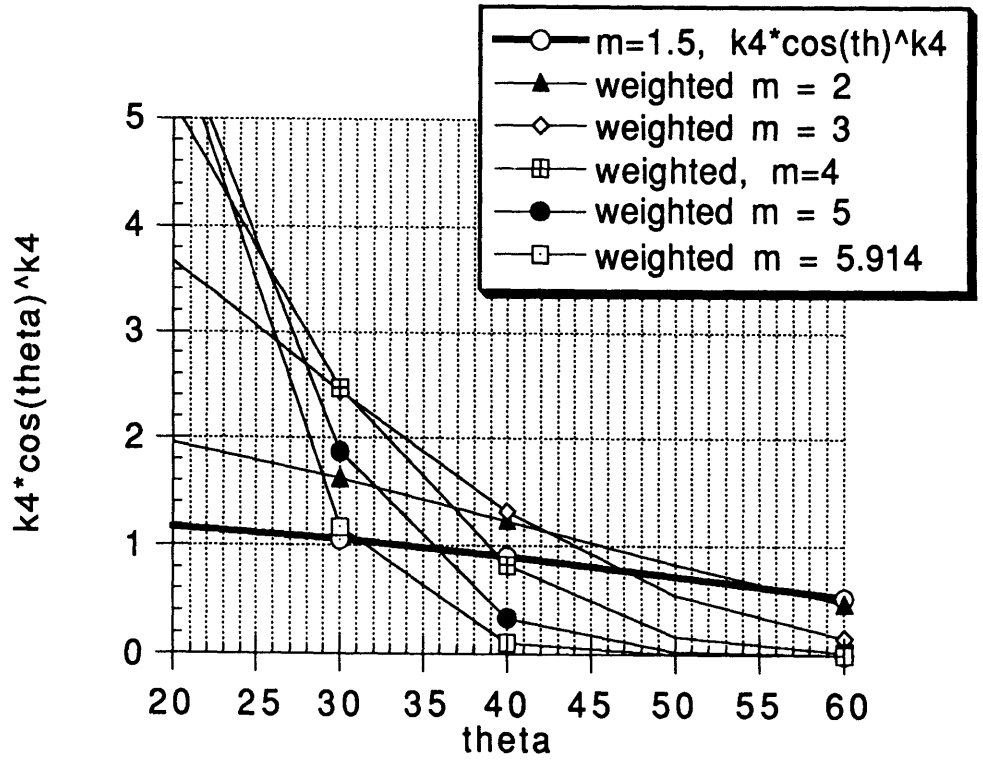

Figure 2-10 : Close-up of Weighted Density Fall Off, $1.5>M_E>6$

2.5.2 Modified Electric Field Model

For some of the cases that are examined, the electric field is modified using high negative voltages. The aim of this modification is to repel the particles from certain regions of the spacecraft using the force generated by the electric field acting on the negatively charged particle. The specific electric fields that are used for the cases examined are described in their respective sections.

2.5.3 Electron Beam Charge Modification

The aim of this modification is to increase the effect of both the motional electric field and of the spacecraft generated electric field. There is a limiting factor, however, in the amount of charge that one can deposit on an individual particle. This is a function of the dielectric strength of the particle. As an initial test for this method, the charge of the particles in the simulations were simply set to the maximum charge that they could hold without breaking up (based on the dielectric strength of the particle), in an attempt to examine whether this was an effective path to take.

First the maximum charge must be derived. We start with the Poisson equation for potential around a sphere

$$\frac{1}{r^2}\frac{\partial}{\partial r}\left(r^2\frac{\partial \phi}{\partial r}\right)=0 \qquad (2\text{-}22)$$

Solving this, we get

$$\frac{\partial \phi}{\partial r}=\frac{c_1}{r^2}, \qquad (2\text{-}23)$$

and then,

$$\phi = -\frac{c_1}{r} + c_2. \tag{2-24}$$

Next we solve this for conditions inside the sphere and outside the sphere. For ϕ to be regular, c_1 must be zero inside the sphere. This yields the result $\frac{d\phi}{dr} = 0$ inside the sphere. In addition, at an infinite distance from this charged object, the field must have died away to zero. Therefore, c_2 must be zero outside the sphere. Thus at the surface of the sphere, we get the relation between these two constants,

$$c_2 = -\frac{c_1}{r_p}, \tag{2-25}$$

where r_p is the radius of the spherical particle.

Now, the charge density is defined by the equation

$$\sigma = \frac{q}{4\pi r_p^2} \tag{2-26}$$

since the charge is distributed over the surface of the sphere. In addition, one can define the charge density as

$$\sigma = \varepsilon \underline{E} = -\varepsilon \frac{d\phi}{dr} = -\varepsilon \frac{c_1}{r_p^2} \tag{2-27}$$

Now we solve for the constant c_1 and get

$$c_1 = \frac{-q}{4\pi\varepsilon}. \tag{2-28}$$

Therefore,

$$E = \frac{q}{4\pi\varepsilon r_p^{\,2}} \tag{2-29}$$

So maximum charge that the particle can hold is governed by the equation:

$$q_{max} = 4\pi\varepsilon\varepsilon_o r_p^{\,2} E_{str} \tag{2-30}$$

where ε is now the *relative* dielectric constant of the material, ε_o is the permittivity constant of free space (8.85×10^{-12} F/m), r_p is the radius of the particle and E_{str} is its dielectric strength in V/m.

2.6 Charge Equations

The charge on the particles in this simulation is calculated self-consistently using the electric field that was generated. The field is not recalculated at each time step, since for a small number of particles, the effect on the overall field is negligible. The charge calculation is made using the electron and ion ambient currents. The formulae for these currents are given below for the case in which the particle potential is higher than the ambient and vice versa, respectively.

$\phi_p > \phi_{amb}$:

$$I_e = -A_p e n_{e\infty} \frac{\bar{c}_e}{4}\left(1 + \frac{e(\phi_p - \phi_{amb})}{\kappa T_e}\right) \tag{2-31}$$

$$I_i = A_p e n_{i\infty} V_o \left(1 - \frac{e(\phi_p - \phi_{amb})}{\tfrac{1}{2} m_i V_o^{\,2}}\right) \tag{2-32}$$

$\phi_p < \phi_{amb}$

$$I_e = -A_p e n_{e\infty} \frac{\bar{c}_e}{4} e^{-e(\phi_p - \phi_{amb})/\kappa T_e} \tag{2-33}$$

$$I_i = \frac{A_p}{2} e n_{i\infty} V_o \tag{2-34}$$

In these formulae, A_p is the surface area of the spherical particle, e is the unit charge, $n_{e\infty}$ and $n_{i\infty}$ are the ambient electron and ion densities, which are taken to be equal. C_e is the electron velocity, T_e is the electron temperature, and V_o is the velocity of the spacecraft.

These currents enable the calculation of dq/dt over each time step. The value of f_p is obtained for the comparison from the equation

$$q_p = C\phi_p \tag{2-35}$$

where C is the capacitance of the particle and is obtained using

$$C = \frac{\varepsilon A_p}{r_p}. \tag{2-36}$$

Recalling that the assumption was made that these particles were spherical, $A_p = 4\pi r_p^2$, and the capacitance becomes

$$C = 4\pi\varepsilon r_p. \tag{2-37}$$

2.7 Discussion on Particle Behavior

It is common to have quartz insulating cloth covering the surface of a spacecraft. However, when the system is under stress, parts of the quartz can break off and enter the environment around the spacecraft. On the Magellan spacecraft, it was discovered that when the spacecraft would roll, thus revealing a different area to the sun, quartz fragments would be released.[5] This is likely due to a thermal cycle causing stress on the quartz and causing some to break free. Such an event might occur with other stresses as

well, such as a sudden vibration to the spacecraft from a thruster firing. In any case, these quartz particles interfered with the star trackers, acting as false signals. The simulated particles are taken to be spheres whose radii range from one to ten microns, with a maximum initial velocity taken to be five meters per second.

When no active control methods are being used, there are two main regions of particle behavior. The first is at the lower altitudes, where the behavior is dominated by the gasdynamic drag force imparted by the neutral wind. In this first region, the particles are blown back and swept behind the spacecraft. The second is the region of higher altitudes where the drag force dips below other forces such as the solar pressure and the motional electric field. (Figure 2-11) In the figure below, the forces acting on the particle are plotted against altitude. A sample particle of 5 micron radius was used, and simple characteristic locations near the spacecraft were taken when the force was location dependent. The charge was taken to be the steady state charge, equivalent to approximately -0.26 volts. This plot portrays the neutral drag as a clearly dominant force up to 400 km. At that point, the electric field generated by the spacecraft skin generates a higher force, but only at the wall. This field falls off quickly, however. The solar pressure is comparable to the neutral wind at approximately 600 km.

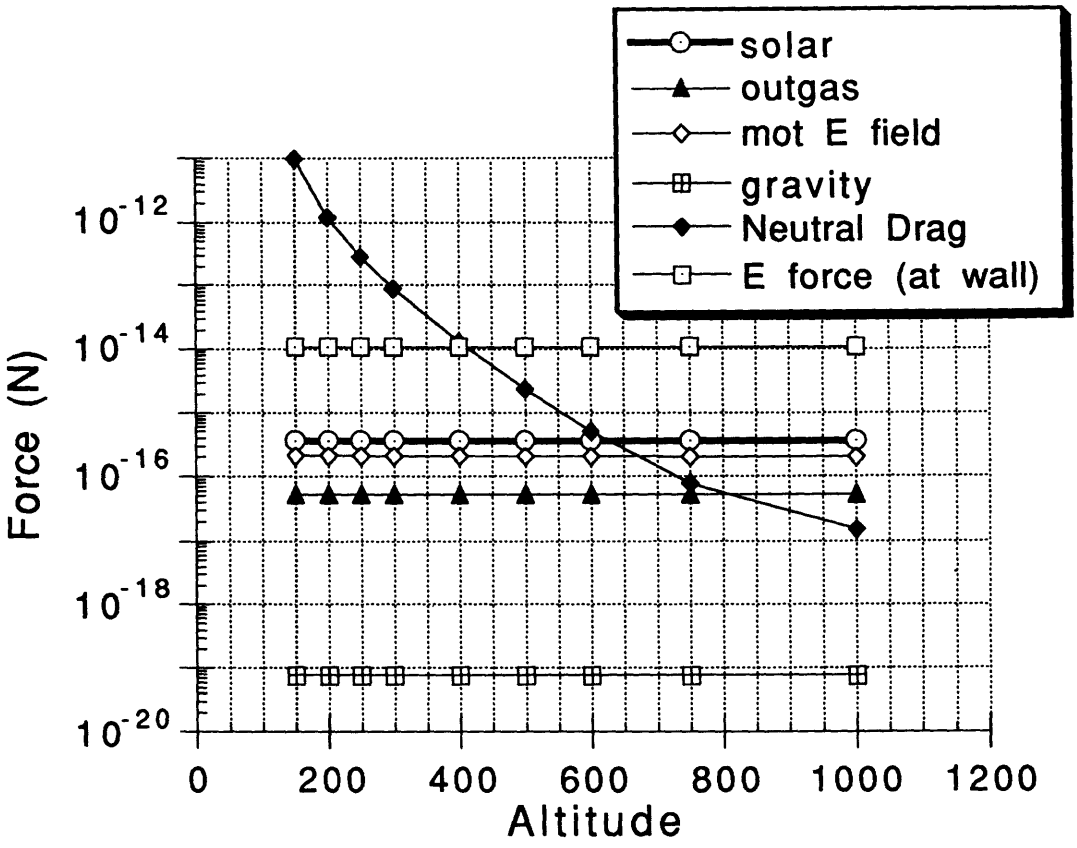

Figure 2-11 : Force (N) vs. Altitude(km) on a 5 micron particle

At this point, when the neutral wind has decreased to the point of being comparable to the solar pressure, the particle trajectories are ballistic, following their initial velocity vectors. In reality, it is at even lower altitudes than this point that the transition is seen, closer to 350 km of altitude. (see Figure 2-12) These trajectories are for 5 micron particles with an initial velocity into the neutral wind of -1 m/s.

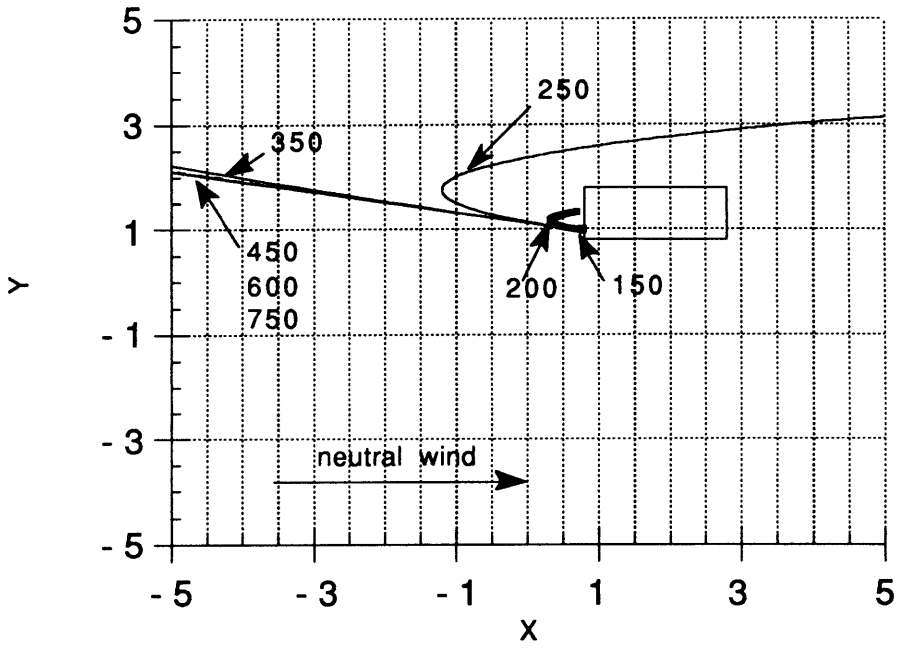

Figure 2-12 : Particle Trajectories for Variable Altitude

To demonstrate further the difference in particle behavior between these two regions, figures are shown for each region which display particle locations in front of the spacecraft leading edge. The only particles plotted in these plots are the ones that are released from the leading edge of the spacecraft, as these dominate the region in front of the leading edge. The lower altitude region behavior is characterized by a case at altitude of 200 km, and the higher altitude region is characterized by a particle behavior at 600 km. The particle sizes are randomly chosen with an even probability distribution between one and ten microns radius. The initial velocity is taken to be specular with maximum velocity randomly chosen with an even probability distribution for each particle varying between zero and five meters per second. The starting location on the front of the spacecraft is also randomly chosen. Small particles (between 1 and 4 microns radius) are denoted by an x; the medium sized particles (4-7 microns radius) are denoted by a circle; the large particles (7-10 microns radius) are denoted by a square. The cloud

of particulates are seen at one , three and ten seconds after initially released. The domain to be examined in these plots will extend a small distance on either side of the spacecraft in the y-direction, but in the direction of velocity it will extend from the leading edge of the spacecraft to the farthest particles from it.

Figures 2-13 a,b,c show the behavior in region 1. A cloud of particles can be seen in front of the spacecraft after one second. Notice that the particles that have made it the farthest distance from the spacecraft are the heavier ones. By the time three seconds have gone by, the particles have spread out considerably. Note, once again, that it is the heavier particles that have resisted the neutral wind enough to make it farther away from the spacecraft. The smaller particles have either been blown back behind the leading edge, or are close to it. In Figure 2-13c, one can see that almost all of the particles have been swept away by the wind. Only a few large particles remain.

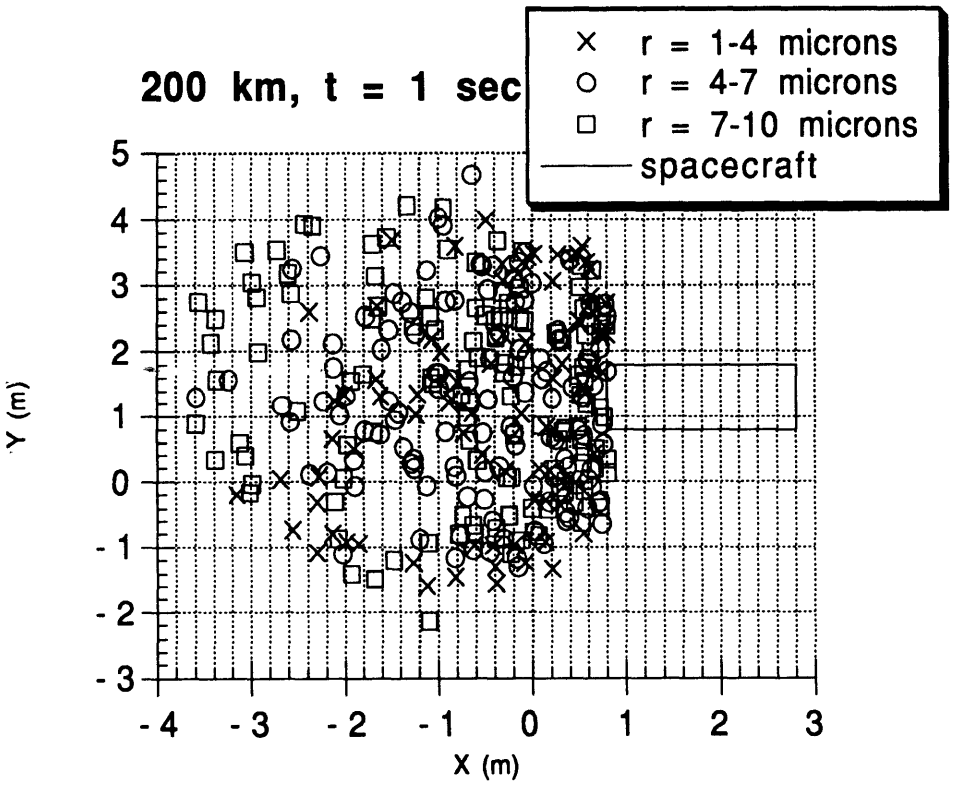

Figure 2-13a : Scatter plot Display of Particle Locations (200 km, t=1 second)

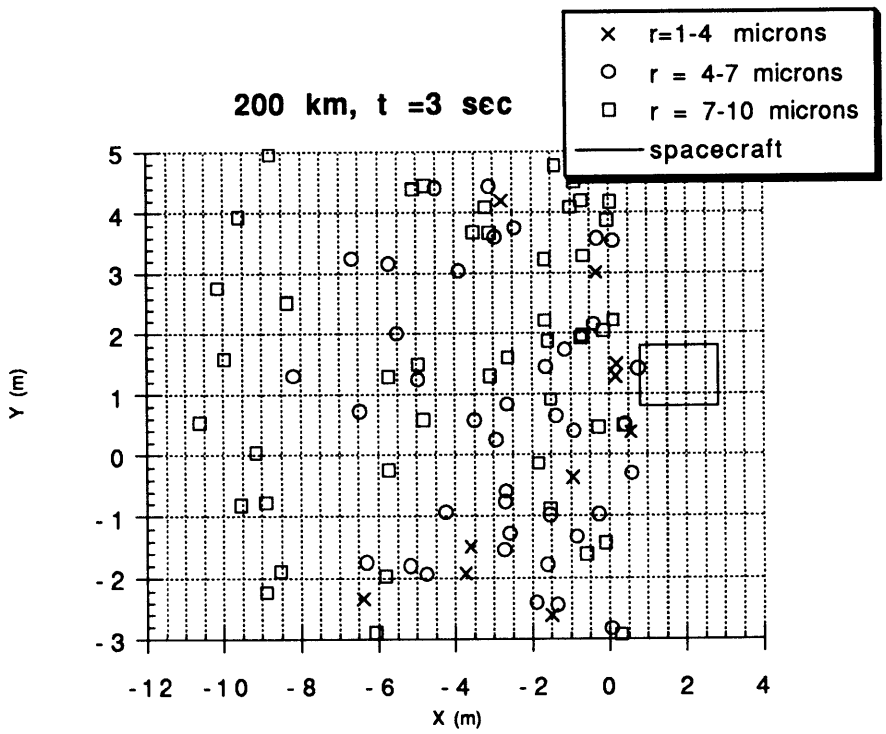

Figure 2-13b : Scatter plot Display of Particle Locations (200 km, t=3 seconds)

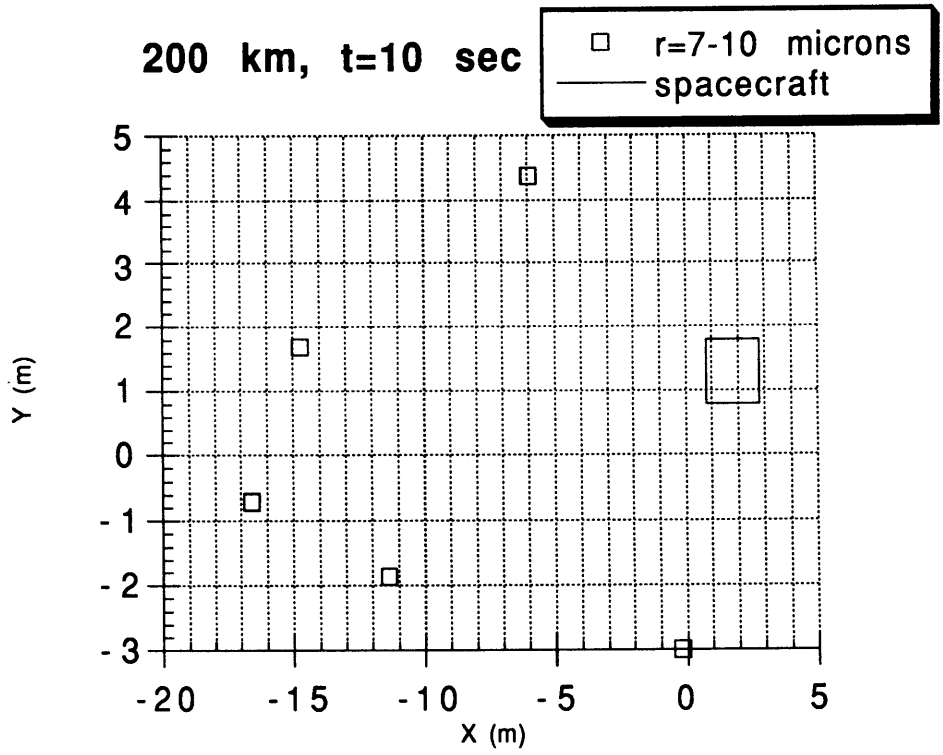

Figure 2-13c : Scatter plot Display of Particle Locations (200 km, t=10 seconds)

Figures 2-14 a,b,c show typical behavior in the upper altitude regions. In the first of these three plots, the cloud of particles in front of the sensor looks very similar, although slightly more extended to the right, to the one for 200 km. By t = 3 seconds, the particle clouds have taken on slightly different characteristics. Note that in the 600 km plot, the leading edge of this expanding particle cloud has gotten further than in the 200 km plot. In addition, light particles are among those that have traveled the farthest into the neutral wind. Another interesting feature is the fact that there are more particles evident in figure 2-14b. This further demonstrates the fact that the particles aren't being blown back in the higher altitude case. Plot 2-14c shows the most remarkable contrast with Figure 2-13. At 200 km, nearly all of the particles have been blown away by the neutral wind by t = 10 seconds. At 600 km, there is still a considerable cloud. By this time, however, some of the particles have begun to slow. The lighter particles are not present in the farthest regions of this expanding cloud. There is a clearly visible region (approximately $40<x<50$) in which there are only heavy particles. There is also another region (approx. $30<x<40$) in which there are primarily medium sized particles. The region behind this seems to have representation from all sizes of particles. This implies the lighter particles are being slowed, as these regions aren't clearly noticeable in the earlier plots.

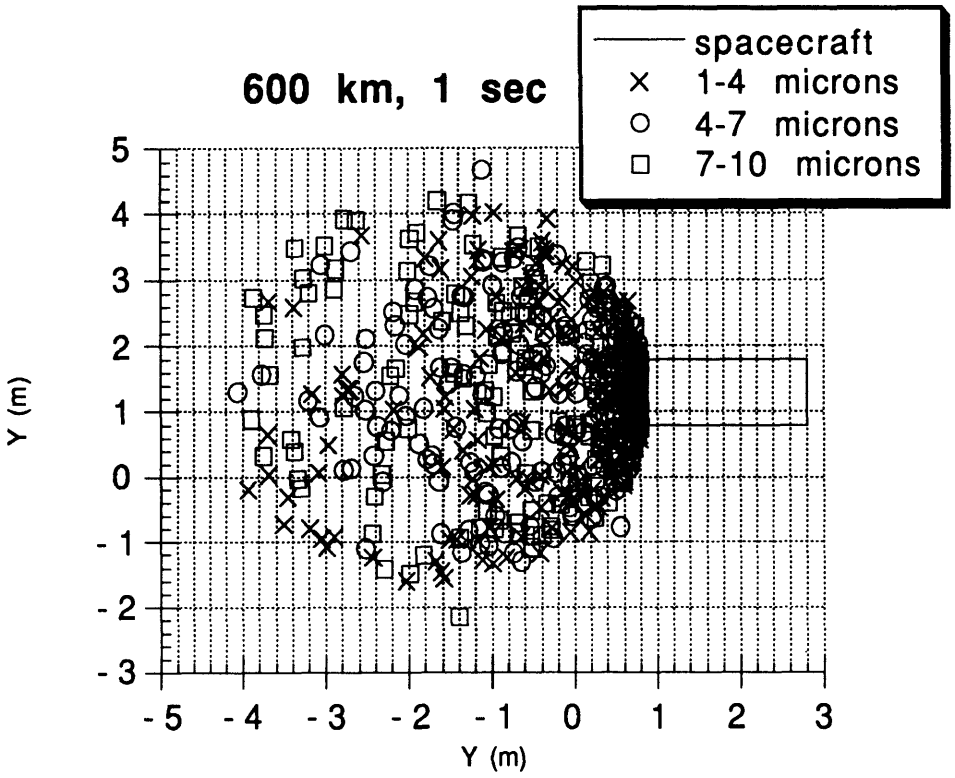

Figure 2-14a : Scatter plot Display of Particle Locations (600 km, t = 1sec)

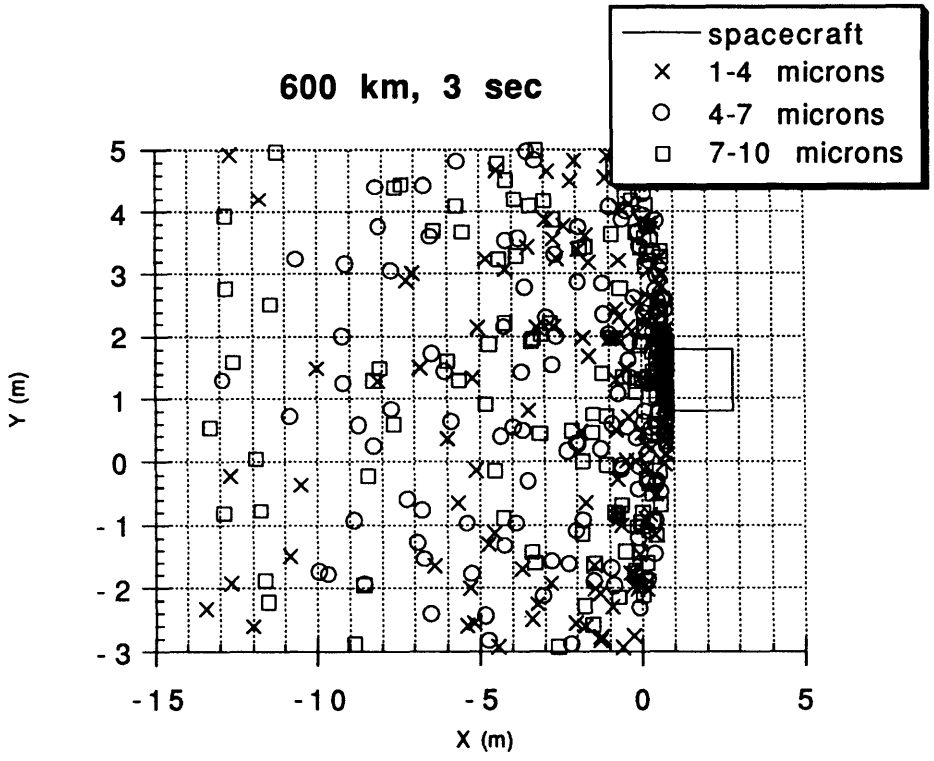

Figure 2-14b : Scatter plot Display of Particle Locations (600 km, t = 3sec)

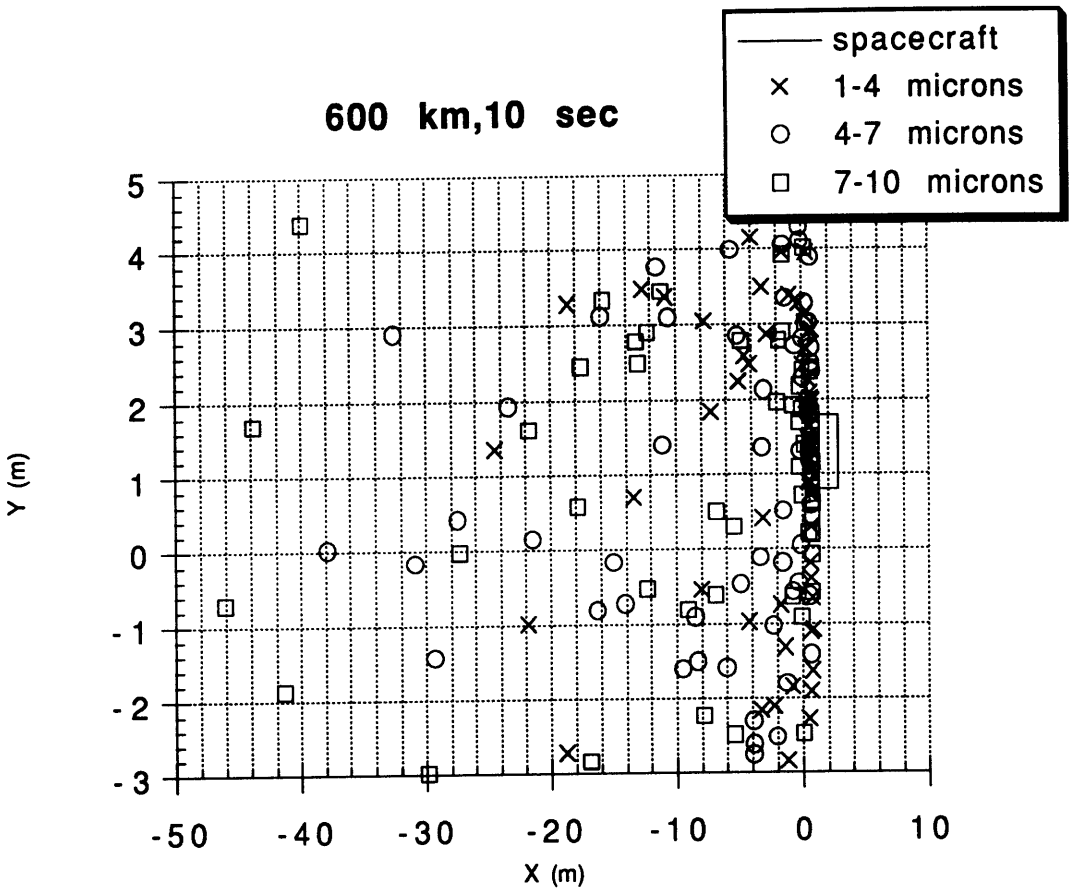

Figure 2-14c : Scatter plot Display of Particle Locations (600 km, t = 10sec)

It is clear that these particles are significantly less influenced by the lower forces at higher altitudes. The particle momentum cannot be overcome by forces on this order of magnitude. The effects of the initial momentum as the initial velocity is varied between one and five m/s on a five micron particle are displayed in Figure 2-15.

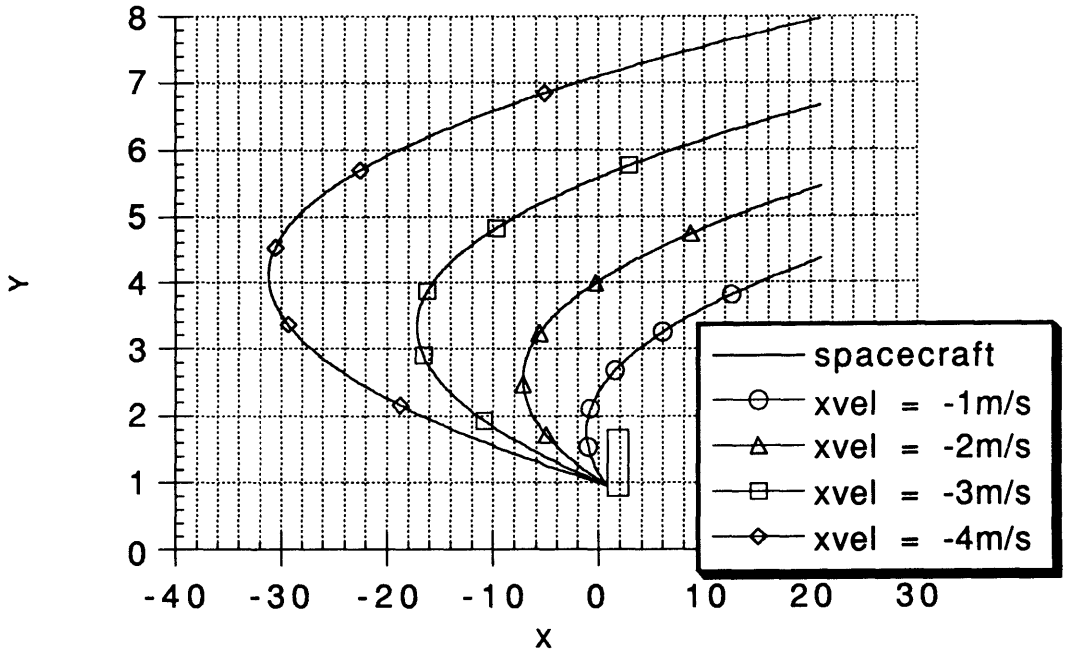

Figure 2-15: Variable Initial X-Velocity at 250 km

The altitude here is set to 250 km, in the lower altitude region, so that the reduction in the effect of the neutral drag is clear as the initial velocity, and thus the initial momentum, increases. There is also a change in the trajectory plots if the initial mass is varied. (Figure 2-16) This case involves not only the variation in initial momentum, but also has an effect on the drag force that bleeds off the particle momentum, as it is directly proportional to the crossectional area of the particle.

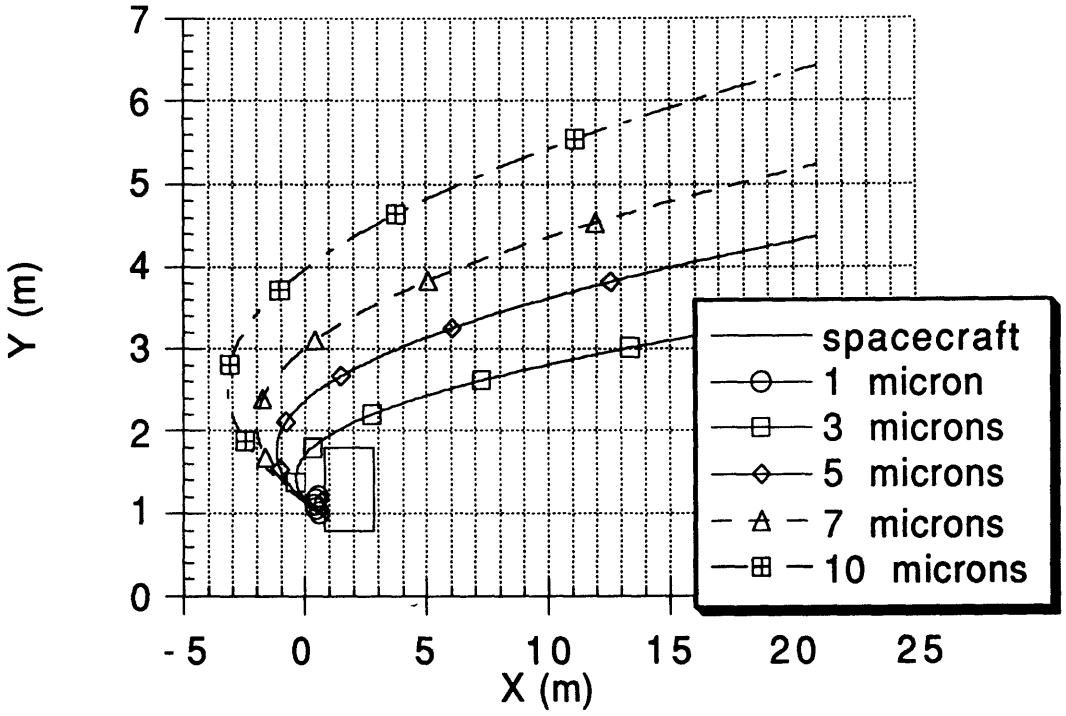

Figure 2-16 : Trajectories with Variable Sized Particles at 250 km

One would normally expect charged particles to travel in circular patterns in the upper atmosphere, but once again the high mass of the particles does not allow it. Where the gyroradius in LEO of an electron at would be 2cm, and that of a simple hydrogen ion with unit charge would be 1 m, the gyroradius of even the 1 micron particle at its steady state charge would be 1.59×10^{10} m. This is exceedingly high, and thus in the near field region which is examined in this research, the circular motion is simply not evident.

In this section the behavior of spherical quartz particles of radii ranging from one to ten microns has been examined. The particles act far less dominated by electromagnetic effects than by neutral wind effects, and this gives some insight into which control methods will work better.

Chapter 3: Particulate Contamination in the Spacecraft Environment

The primary type of contaminating effects that is investigated is that of particulates in the environment of a spacecraft. These particulates may impair the function of spacecraft systems while in the environment around the spacecraft, and not simply by accumulating on a surface. This surface contamination case is examined in Chapter 4. In the case that will be examined here, light is scattered into electromagnetic sensors, adding a background of noise to the desired readings. First, the conditions under which the simulation occurs are described, including a discussion of what modifications are made to the spacecraft in attempts to reduce contamination. Next, there is a discussion of how the scattered intensity of sunlight from each of these particulates is determined. Finally simulation results are presented and discussed.

3.1 Description of Sensor Case

In this analysis, a sensor is located in the center of the leading edge of the spacecraft. For definiteness, the sensor is taken to be circular and .1m in diameter. This is so that it is much smaller than the body length of the leading edge of the spacecraft. Its view field is taken to be a cylinder extending out along the velocity vector from the sensor. A baffle is placed about the sensor for two reasons. First there is the practical purpose of preventing extraneous scattered light from entering the sensor from areas not in the view field, off to the side. Secondly, the baffles will prevent large amounts of

scattering from particles getting too close to the sensor. Control mechanisms are located around the sensor. In the two dimensional case, the gas jet control is implemented by placing a jet on either side of the thruster, blowing particles out and away before they can get to the view field of the sensor. (Figure 3-1a) In the case of the electric field modification, high voltage wires are placed on either side of the sensor, to repel the negatively charged particles. (Figure 3-1b)

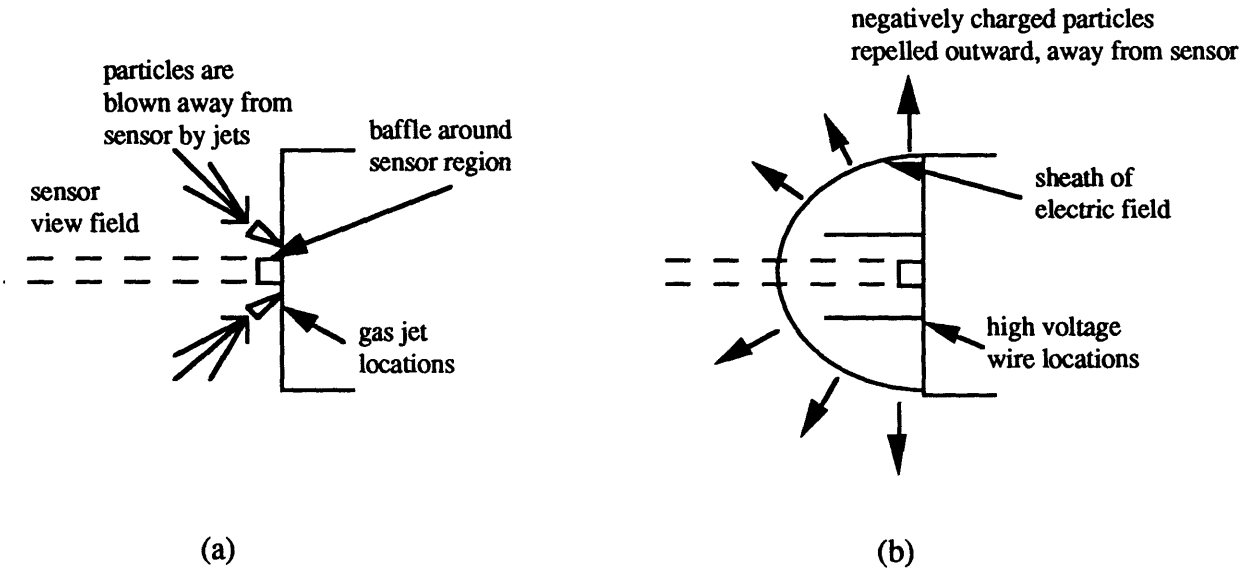

Figure 3-1 : Sensor and Control Mechanism Locations

The potential field that results from the high voltage wires (b) can be seen in Figure 3-2.. Figure 3-2a shows the field around the entire spacecraft, including the wake and the wire region. The second figure, 3-2b, is a close-up of the high voltage wire region. The potential decrease radiates from the wires. The resultant electric field is perpendicular to these lines. The contours are not chosen to demonstrate the magnitude of the gradient, only its shape. This implies an electric field which pushes negatively charged particles radially outward, away from the view field. This was the reason for using the extended wires. The influence of this imposed electric field extends roughly a body length from the spacecraft. The distance at which one charged particle may affect

another in LEO (the Debye length) is approximately one centimeter. The voltage has to be extremely high for the influence of the field to extend this distance from the craft. In the normal case, the potential decayed extremely quickly away from the spacecraft. These wires, set to -1000 V, enable a significant extention of that influence.

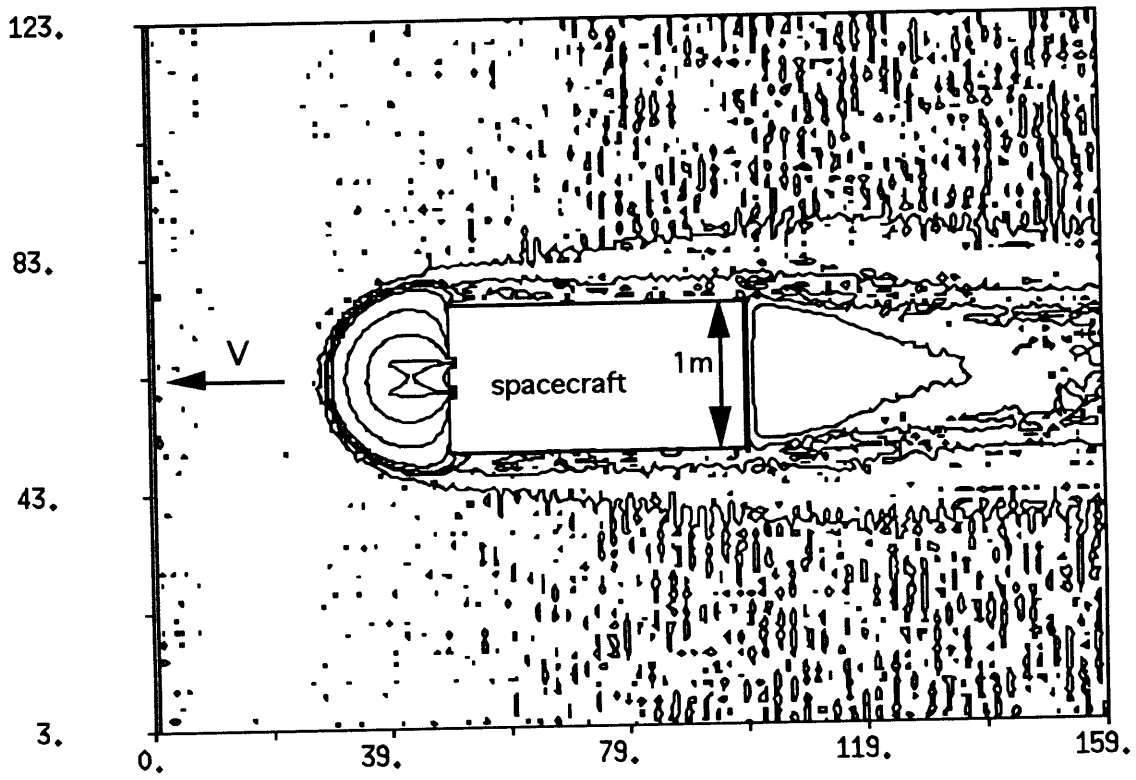

Figure 3-2a : Electric Field with High Voltage Wires

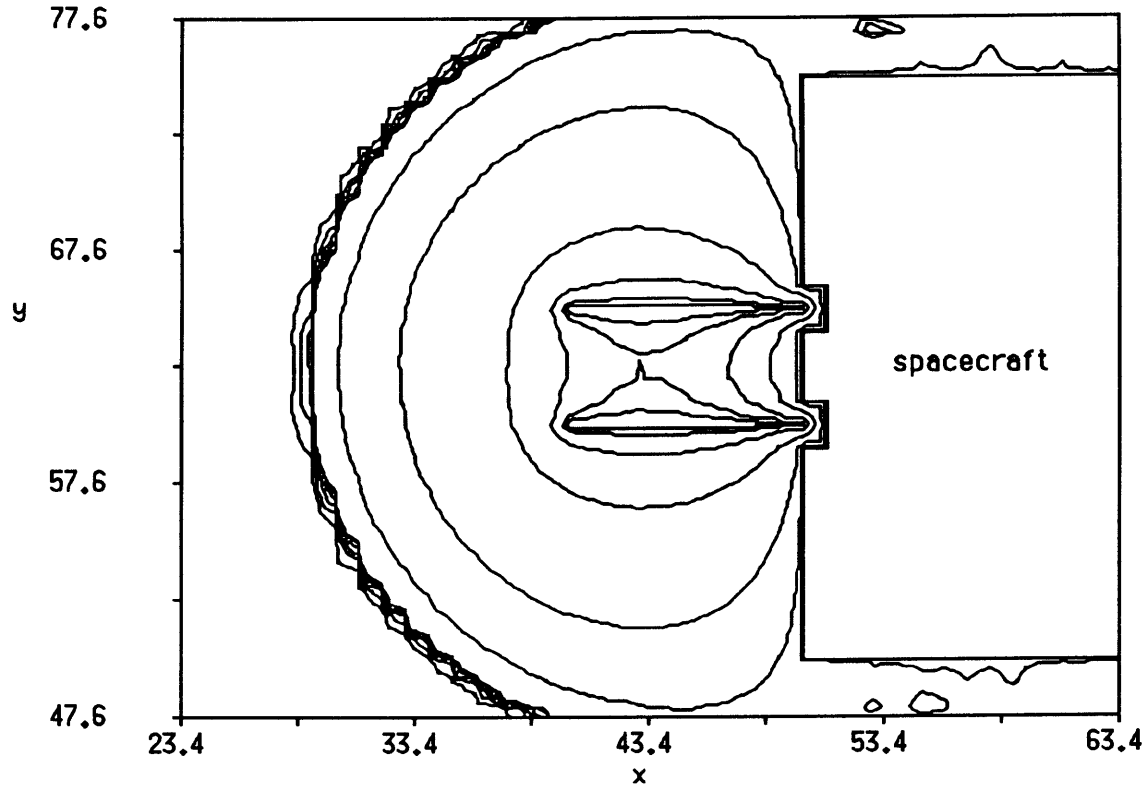

Figure 3-2b : Close-up of High Voltage Wire Region

In the extension to three dimensions, the number of gas jets in increased from two to six, placed symmetrically around the sensor. In the case with the high voltage wires, the electric field is taken to be axisymmetric, representing a cage of high voltage wires circling the sensor, in three dimensions.

A burst of particles from the spacecraft is simulated. That is, several thousand particles are simultaneously released from the surface of the spacecraft. This simulates the effects of a shock to the spacecraft system such as a sudden vibration from a rocket firing or thermal cycle. For the sake of simplicity, particles are taken to be released from all points on the spacecraft (save the sensor location and the area directly around it where control mechanisms may be found) with equal probability. As noted in the previous chapter, the particles simulated are be quartz spheres. Particulates are taken to be evenly distributed one to ten microns in size. The particles exit specularly, with the maximum

velocity varying between zero and five meters per second in an even probability distribution. The number of particles released in the two dimensional simulation is 10000, and 25000 are released in the three dimensional case. These numbers are chosen so that statistically significant numbers of particles would cross the field of view.

3.2 Scattered Intensity

The noise, or scattered intensity of sunlight, resulting from the particles is the parameter by which the various scenarios will be compared. The total contaminating scattered intensity at any point in time is the sum of the scattered intensity from each of the particles in the view field.

The intensity for the individual particles is determined by using Mie scattering theory. The simplifying assumption that the particle radius is large compared to $\lambda/(2\pi)$, i.e. $r_p >> \lambda/2\pi$, where λ is the wavelength of the incident radiation. Since the smallest particles that are considered are one micron in radius, the results for the intensity of the scattered radiation will be valid for visible light and for the short wavelength infrared region. The following derivation for this intensity was obtained from van de Hulst.[15]

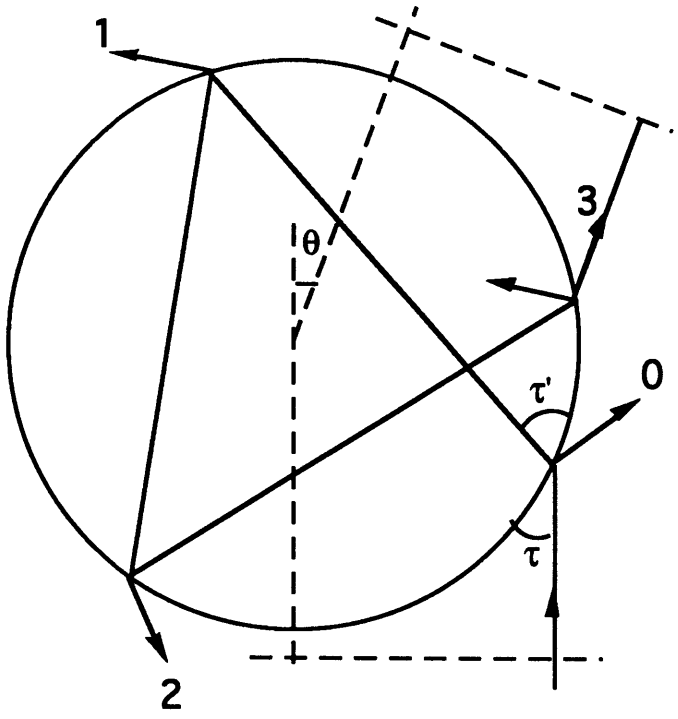

Figure 3.3 : Path of a Light Pencil Scattering Inside a Sphere

In figure 3.3, the path of a ray entering a spherical particle is traced. It bounces around inside the particle, at each point refracting and reflecting partially. The angle between the incident light and the sensor can be seen relative to the angle θ, and τ represents the angle between a single ray of light and the surface it strikes. Next, a finite pencil of light is examined, characterized by $d\phi$ and $d\tau$. The sphere is taken to have the real refractive index m. Therefore the value for τ', using Snell's law, comes out to:

$$\cos\tau' = \frac{1}{m}\cos\tau \qquad (3\text{-}1)$$

The Fresnel reflection coeffictions are:

$$r_1 = \frac{\sin\tau - m\sin\tau'}{\sin\tau + m\sin\tau'} \quad \text{and} \quad r_2 = \frac{m\sin\tau - \sin\tau'}{m\sin\tau + \sin\tau'} \qquad (3\text{-}2)$$

and from them we can get the energies for each subsequent reflected ray formed as a result of the original pencil. (Multiple rays are numbered in the above figure.)

$$\varepsilon_i = r_i \qquad \text{for } p = 0 \qquad (3\text{-}3)$$

$$\varepsilon_i = (1 - r_i^2)(-r_i)^{p-1} \qquad \text{for } p=1,2,3 \qquad (3\text{-}4)$$

Note that p denotes the subsequent reflections of the pencil of light inside the sphere. As p increases, it decreases in energy.

The pencil of light emerging in one of these directions is characterized by a small range $d\theta$ around the scattering angle θ. We may derive from figure 3-3, that the total deviation from the original direction is

$$\theta' = 2\tau - 2p\tau \qquad (3\text{-}5)$$

which defines the scattering angle in the interval $(0,\pi)$ by

$$\theta' = k \cdot 2\pi + q\theta \qquad (3\text{-}6)$$

where k is an integer and q = +1 or -1. Differentiation with use of Snell's law gives

$$\frac{d\theta'}{d\tau} = 2 - 2p\frac{\tan\tau}{\tan\tau'} \qquad (3\text{-}7)$$

which defines

$$d\theta = \left|\frac{d\theta}{d\tau}\right| d\tau \qquad (3\text{-}8)$$

The emergent pencil spreads into a solid angle $\sin\theta d\theta d\phi$, i.e., over an area r^2 times this solid angle at a large distance r from the sphere. Dividing the emergent flux by this area we obtain the intensity

$$I_i(p,\tau) = \frac{\varepsilon_i^2 I_o a^2 \cos\tau \sin\tau d\tau d\phi}{r^2 \sin\theta d\theta d\phi} = \frac{a^2}{r^2} I_o \varepsilon_i^2 D \qquad (3\text{-}9)$$

where i is 1 or 2, depending on the polarity, and

$$D = \frac{\sin\tau\cos\tau}{\sin\theta|d\theta'/d\tau|} \qquad (3\text{-}10)$$

Then this intensity is summed over τ, i and p to get the total intensity scattered into the sensor. The final result, therefore, is an expression which is simply

$$I = f(\theta)\frac{a^2}{r^2} I_O, \qquad (3\text{-}11)$$

and thus the nondimensional intensity I/I_O is proportional to $\frac{a^2}{r^2}$. The scattered intensity is larger for larger particles and for ones that are closer to the sensor.

3.3 Simulation Results

The purpose of this simulation is to determine the comparative effectiveness of the different active control methods that are being reviewed. These methods are 1) using gasdynamic forces to blow the particles away from the view field of the sensor; 2) modifying the spacecraft electric field; and 3) using electron beams to increase charge on the particles, and thus to increase the impact of the electromagnetic forces about the spacecraft (primarily the motional electric field which is the largest ambient

electromagnetic force contribution), to sweep them from the domain. These methods are first examined for the two dimensional case, and then for the three dimensional case. Finally, potential system effects are examined.

3.3.1 The 2D Case

For an initial review of this problem, a two dimensional model is used. As mentioned in chapter 2, a two meter by one meter rectangle is used to model the spacecraft in two dimensions. These simulations are performed using characteristic LEO values for electron density and temperature ($n_e=10^{11}/m^3$; $T_e=.1$ eV).

3.3.1.1 No Active Control (2D Case): First examined is the case of particle release using no active control. The intensity profiles with time (Figures 3-4:abcdefgh) display the scattered light contamination in the scenario for 150, 200, 250, 300, 350, 450, 600 and 750 km of altitude. These plots display log plots of the normalized intensity with respect to time. The intensity is normalized by the incident light, i.e. sunlight. The "zero" line at 10^{-16} represents the edge of the domain. It is the intensity that would be caused by one 10 micron particle at a distance of 1km. This is established as a reference value.

The plots display an increase in the amount of time that the contamination can appear in the viewfield. At higher altitudes, particles are not swept out of the domain by the neutral wind as easily, and thus particles stay in the domain for much longer. As a result, contamination appears in the viewfield much longer after the release time. At 150 km, the particles are all swept back so strongly that particles only cross the view field within the first two seconds. This time can be seen to gradually increase as the cases get higher altitudes.

There are a number of common characteristics in these plots. First, there is always a peak near t=0, when the particle release occurs. This represents the bulk of the particles moving at the fastest speeds. The peak is slightly higher in the lower altitudes,

as particles are blown back by the neutral wind such that they are closer to the sensor and the resultant scattering they cause is increased. After the peak, there is a decrease with time, as particles which cross the viewfield are crossing farther from the sensor, thus the later time of crossing.

In the plots representative of region 1 (lower altitudes), there are several points at which the intensity rises to a sharp peak and then is quickly reduced. This is occuring due to particles approaching the sensor while in the view field. Each of these peaks is likely due to a single particle. These particles have been turned around by neutral drag and are heading toward the spacecraft.

A feature that is common to the region 2 plots is that of small isolated peaks of intensity later in the time domain. These particles which arrive later tend to cross at farther distances from the sensor, as shown by the shorter intensity peaks. At these farther distances, the particles are less densely populated, and thus they cross the viewfield less frequently.

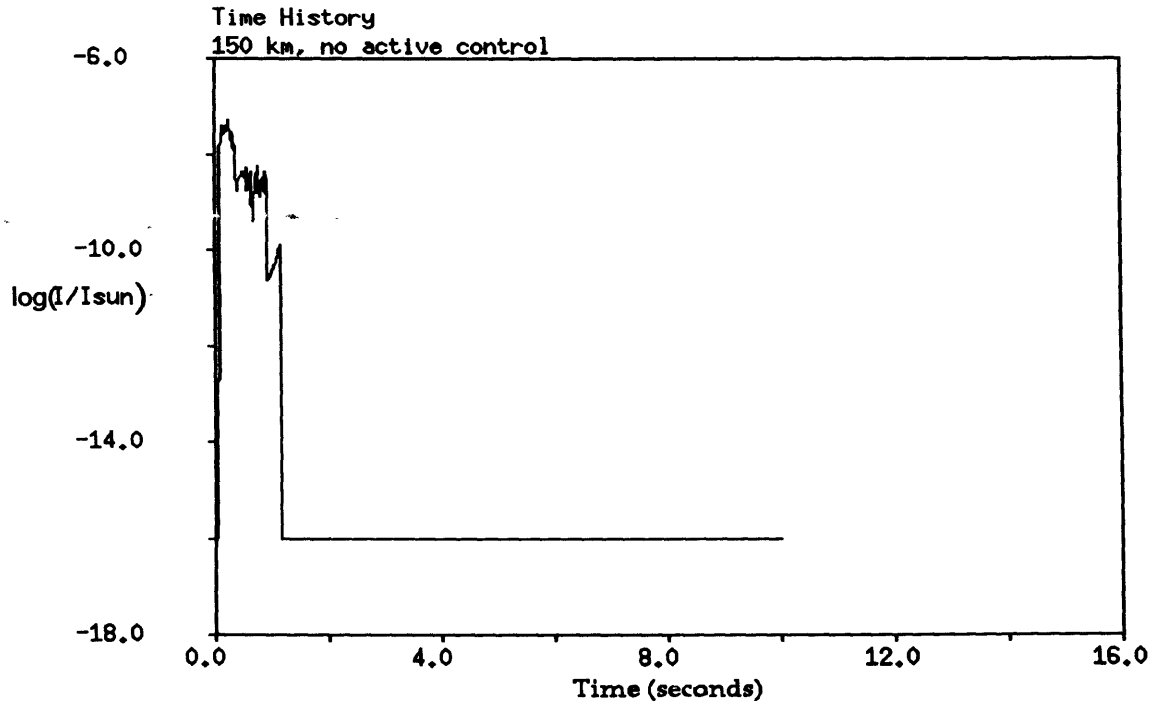

Figure 3-4a : Time History of Intensity at 150 km; No Active Control

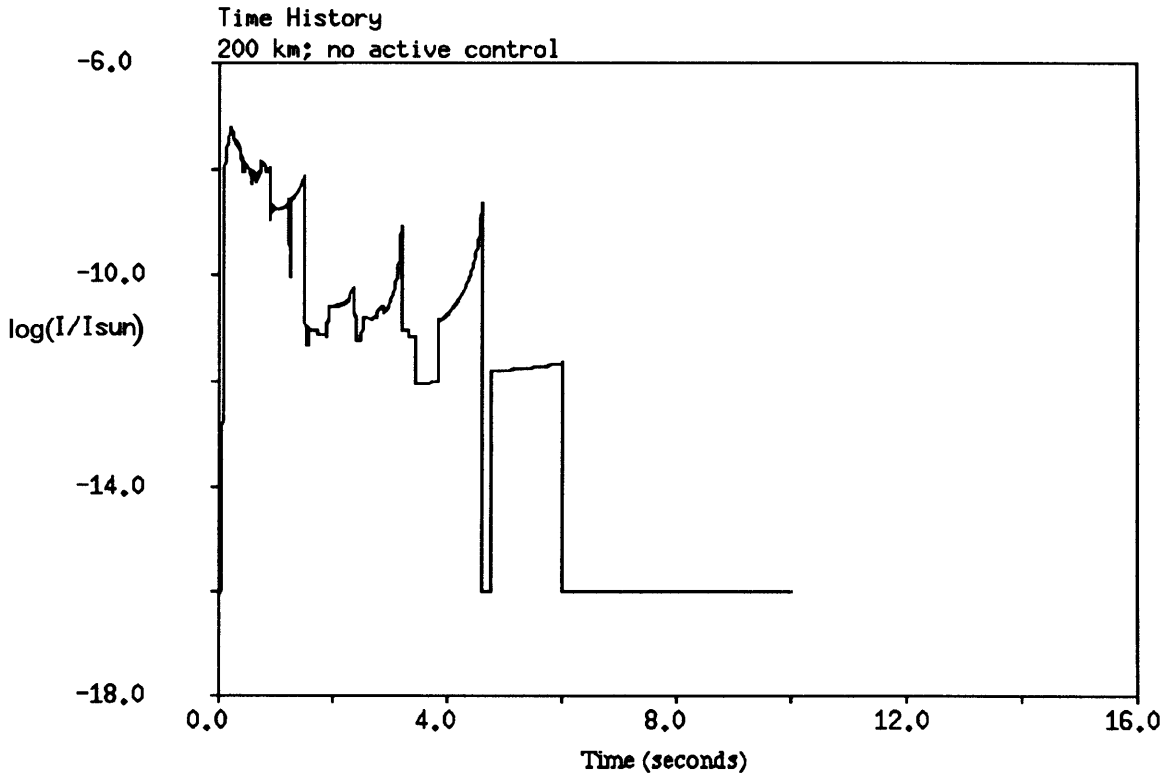

Figure 3-4b : Time History of Intensity at 200 km; No Active Control

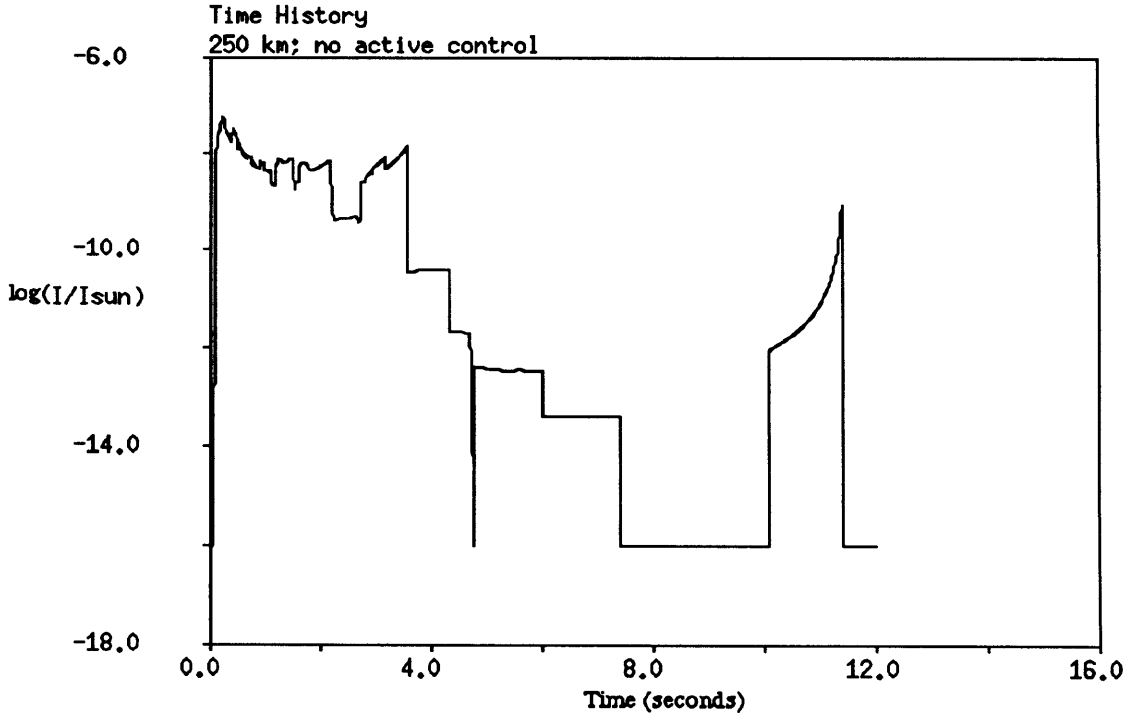

Figure 3-4c: Time History of Intensity at 250 km; No Active Control

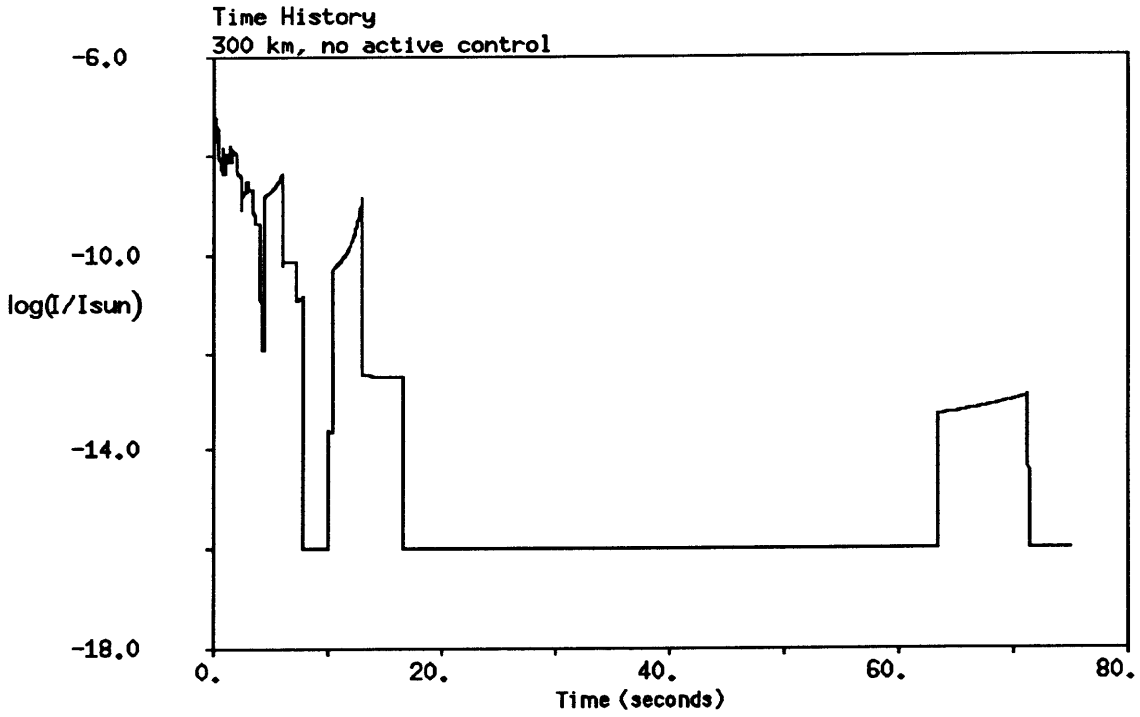

Figure 3-4d : Time History of Intensity at 300 km; No Active Control

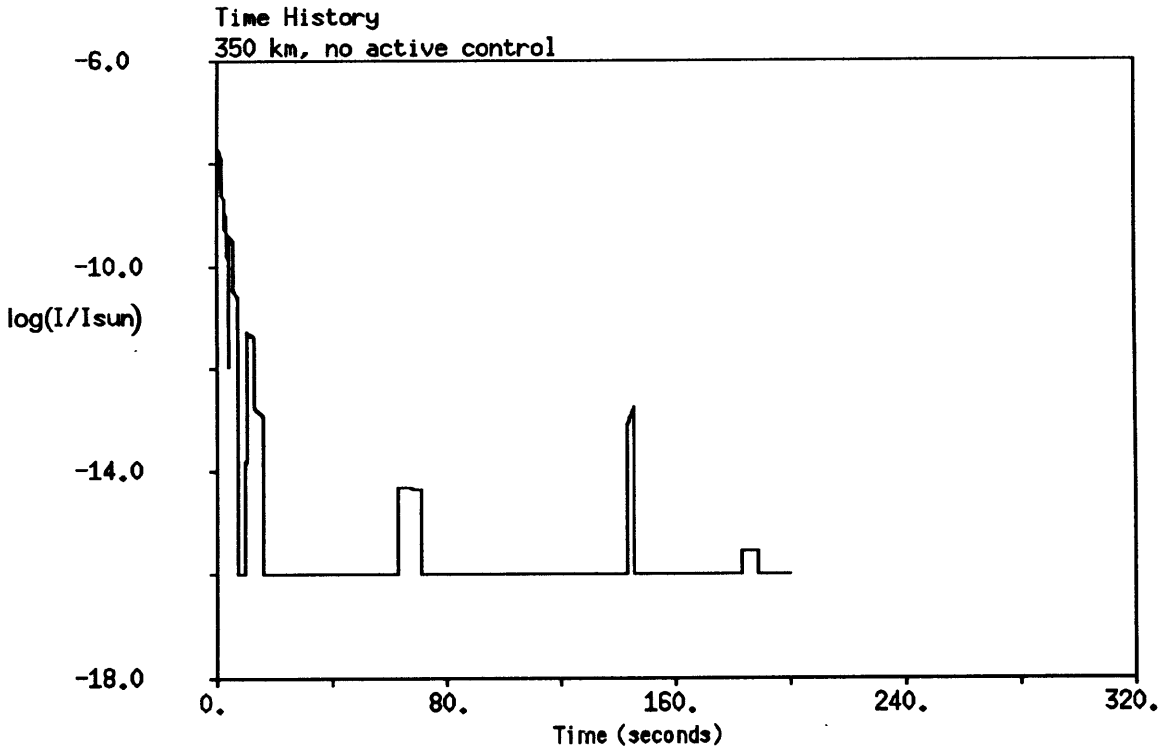

Figure 3-4e : Time History of Intensity at 350 km; No Active Control

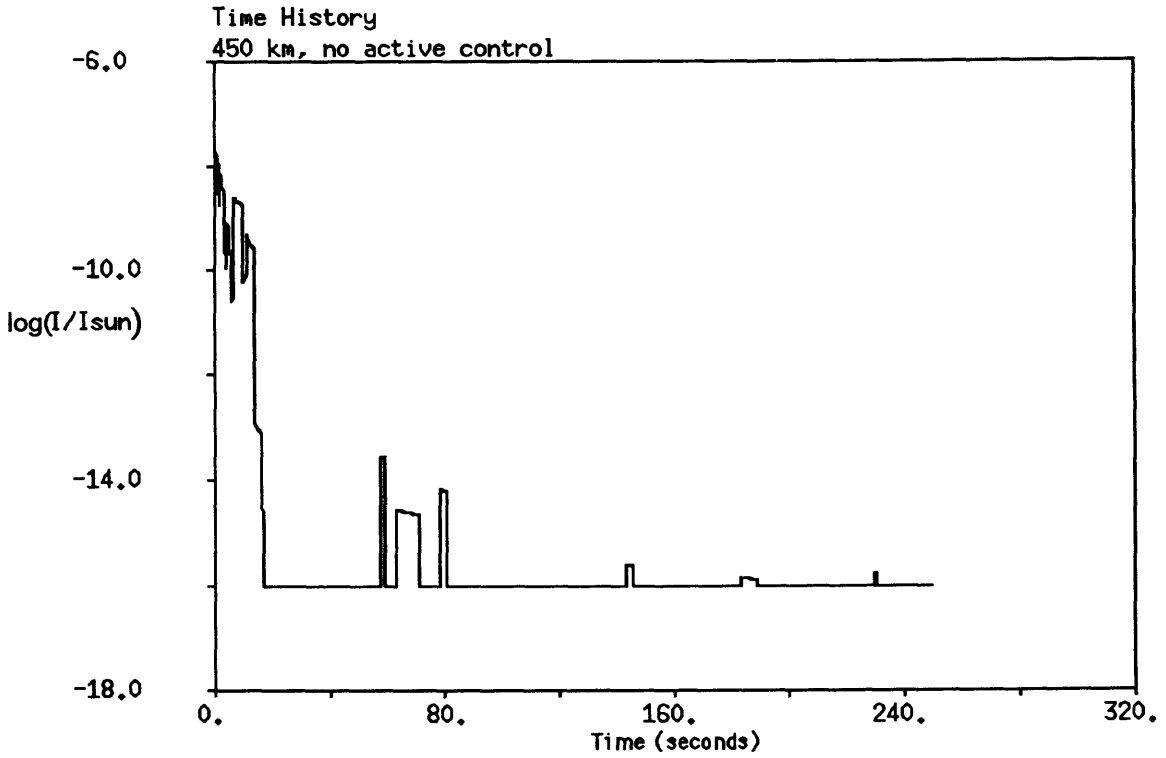

Figure 3-4f : Time History of Intensity at 450 km; No Active Control

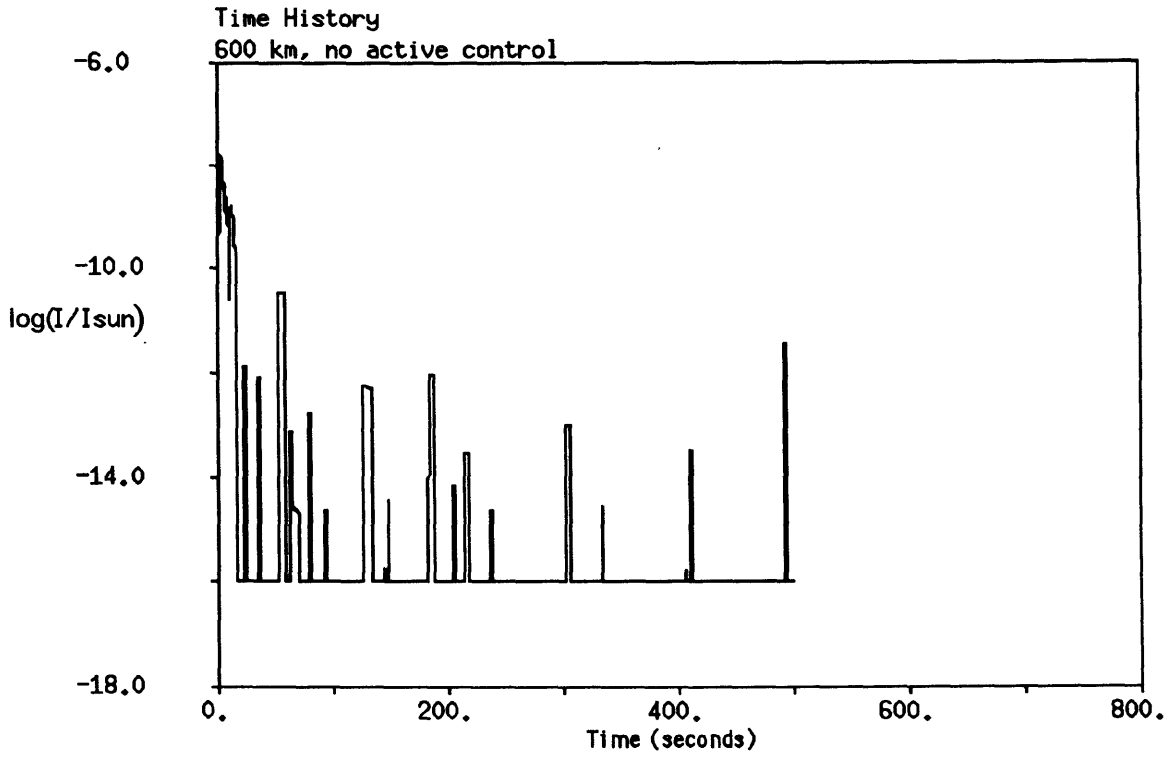

Figure 3-4g : Time History of Intensity at 600 km; No Active Control

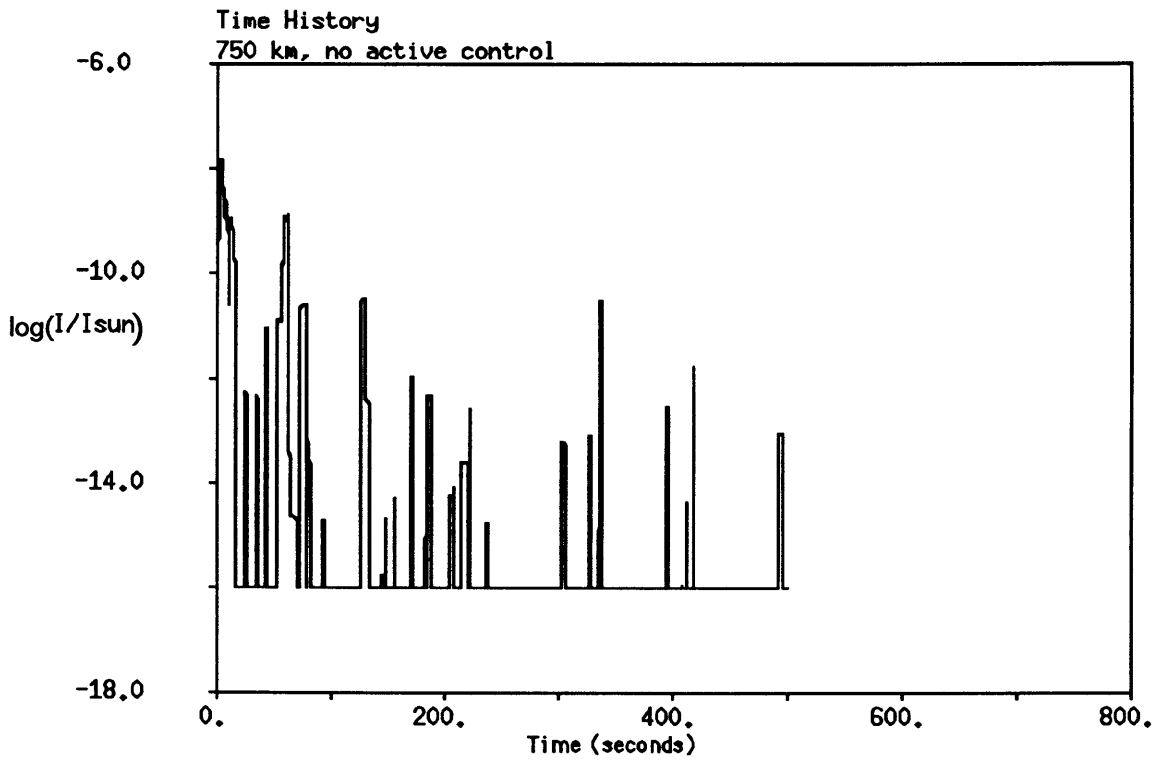

Figure 3-4h : Time History of Intensity at 750 km; No Active Control

The total intensity at each time was averaged over the first ten seconds for each plot. This is a region containing the peak, and thus the chief disturbance. This time average for the cases where no active control was used in the 2D case is shown in Figure 3-5. The time average is lower for the lower altitudes. This is because of the short duration of contamination at 150 km. Over the range of time from $0 < t < 10$ there is a long period without the presence of contamination. This has the effect of decreasing the time average intensity over this period. The neutral wind, in the low altitude regions, is acting as another contamination control method, reducing the average scattered intensity. Because it is less effective at higher levels, the intensity levels off. The error bars display the standard deviation of each average.

The values displayed here have no absolute meaning, because the number of particles released is completely artificial. The contaminant intensity increases with

increased numbers of particles. What is important is the relative values between this and the values that will be produced by the use of active control methods.

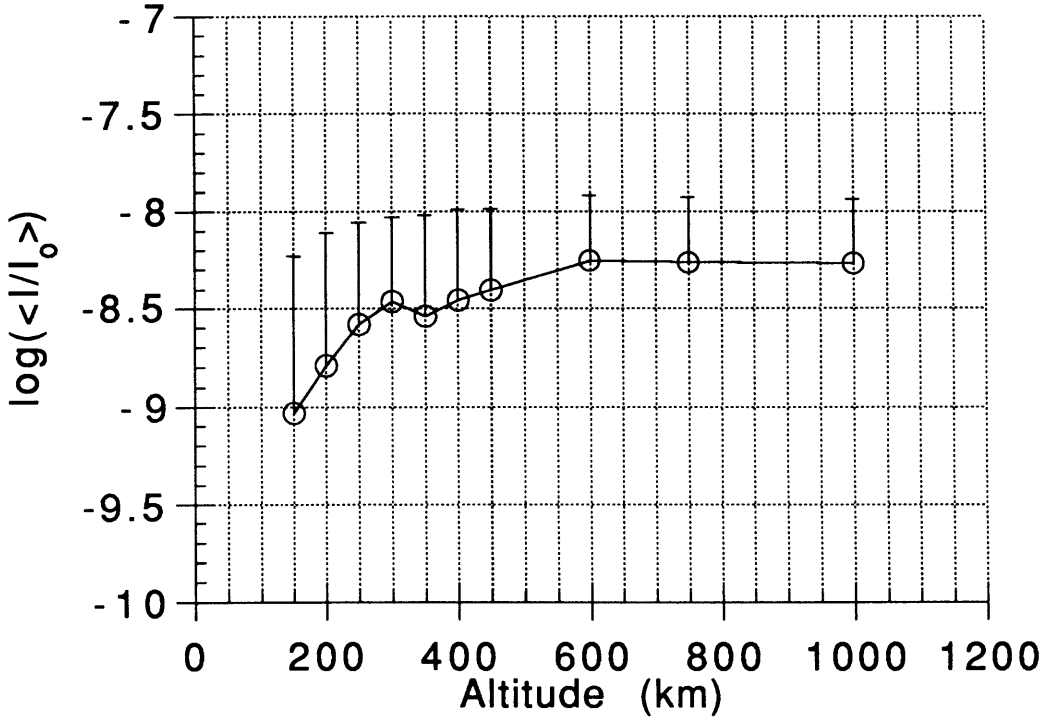

Figure 3-5: 2D Intensity Plot, No Active Control

3.3.1.2 Gas Jet Control (2D Case): Next, different control methods are added to this simulation to see what sort of effects they may have. The first that is examined is the gas dynamic control force imparted by the cold gas jets. The thrusters are located on either side of the sensor such that they could blow particles away from the view field. Due to considerations regarding fuel usage which are discussed later, the thrusters are limited to 10mN of force and to a single second firing duration starting immediately after the particle release event. To determine an optimal firing angle, the jets are fired at 30, 60

and 90 degrees with respect to the sensor view vector and the effects at each angle are compared.

First, a set of intensity time histories for altitudes of 200 km (Figure 3-6 abc) and 600 km (Figure 3-7abcd) are examined. In figure 3-6, the plots from region 1, the amount of contamination is visibly diminished between the 30 degree and 60 degree runs. The peak is lower and the final time that contamination appears is sooner. In the 90 degree simulation, another phenomenon can be seen. At approximately t=4 seconds, a particle can be seen entering the view field and approaching the sensor. This particular orientation of the thruster has changed the trajectory of the particle such that it produces a sharp intensity peak. In addition, the initial peak in this scenario is more spread out than in the 60 degree case.

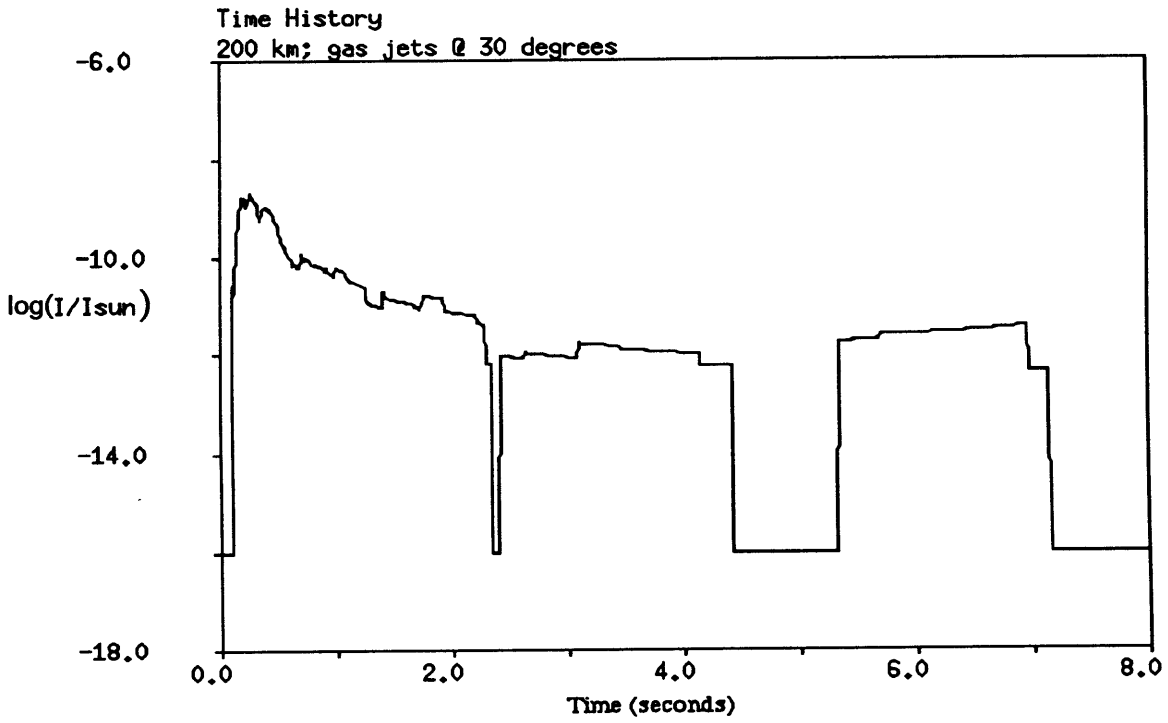

Figure 3-6a : Time History of Intensity at 200 km; Gas Jets at 30 degrees

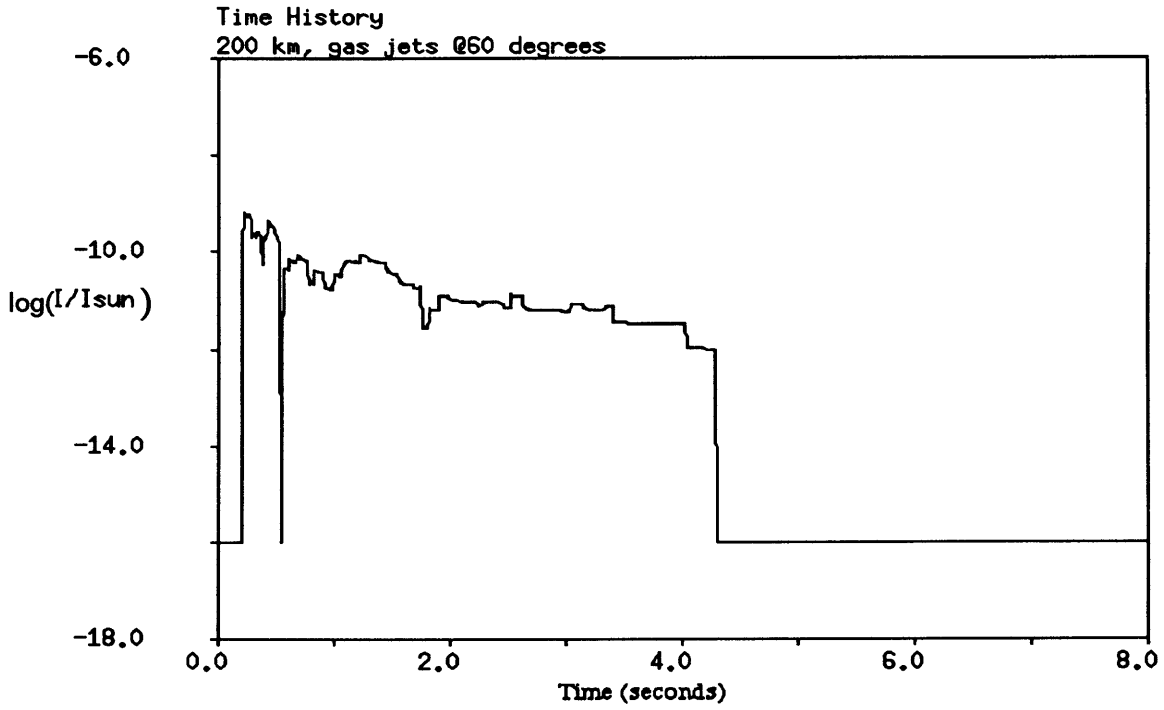

Figure 3-6b : Time History of Intensity at 200 km; Gas Jets at 60 degrees

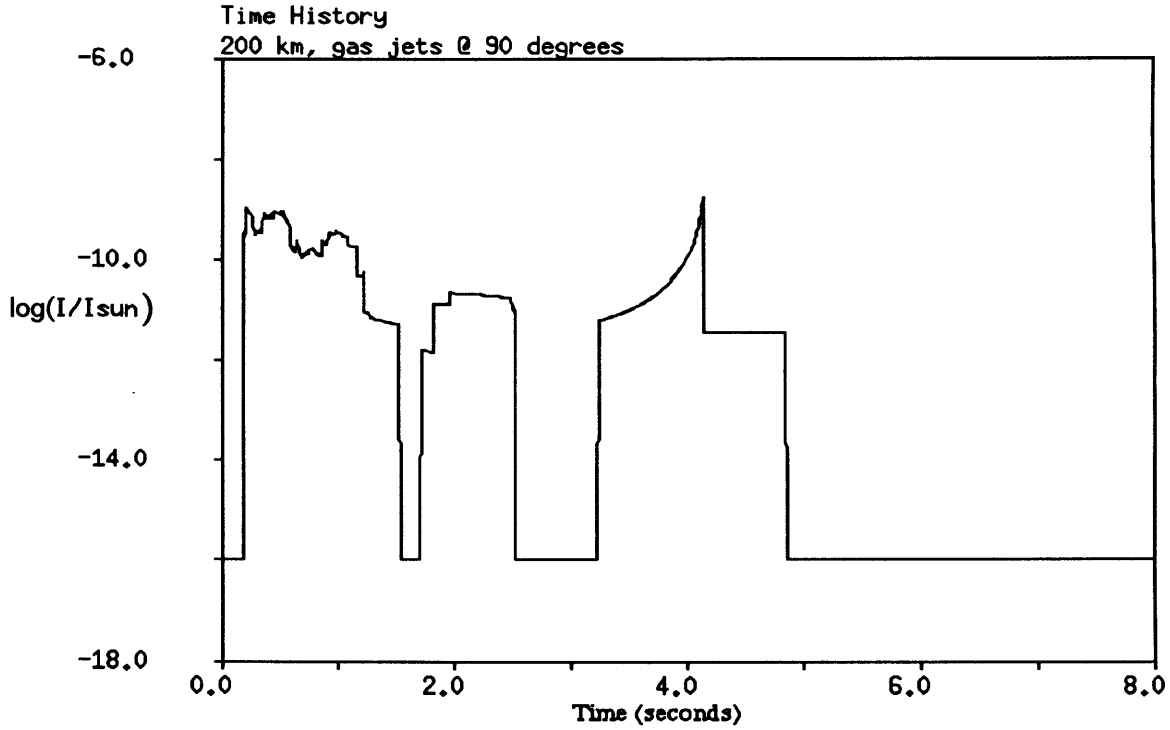

Figure 3-6c : Time History of Intensity at 200 km; Gas Jets at 90 degrees

Figure 3-7 shows the effects of varying the thruster angle in region 2. The specific plots are of intensity time histories at 600 km. The behavior seen in figure 3-7a is reminiscent of the behavior seen in the case modeling the absence of active control. They both possess similar "isolated short duration peak" structures. However, there are far fewer in the case where the thrusters are used, and they stop appearing sooner. In the 60 and 90 degree inclination runs, these effects are mitigated still more. In the 90 degree case, as is seen in Figure 3-7c, there is still one late particle appearance. It must have had enough forward momentum to make it through the thruster plume while being blown on such a course that it crossed much later and much farther away (as is implied by the small size of the peak.) A closer up view of the main body of contamination for this case is displayed in Figure 3-7d.

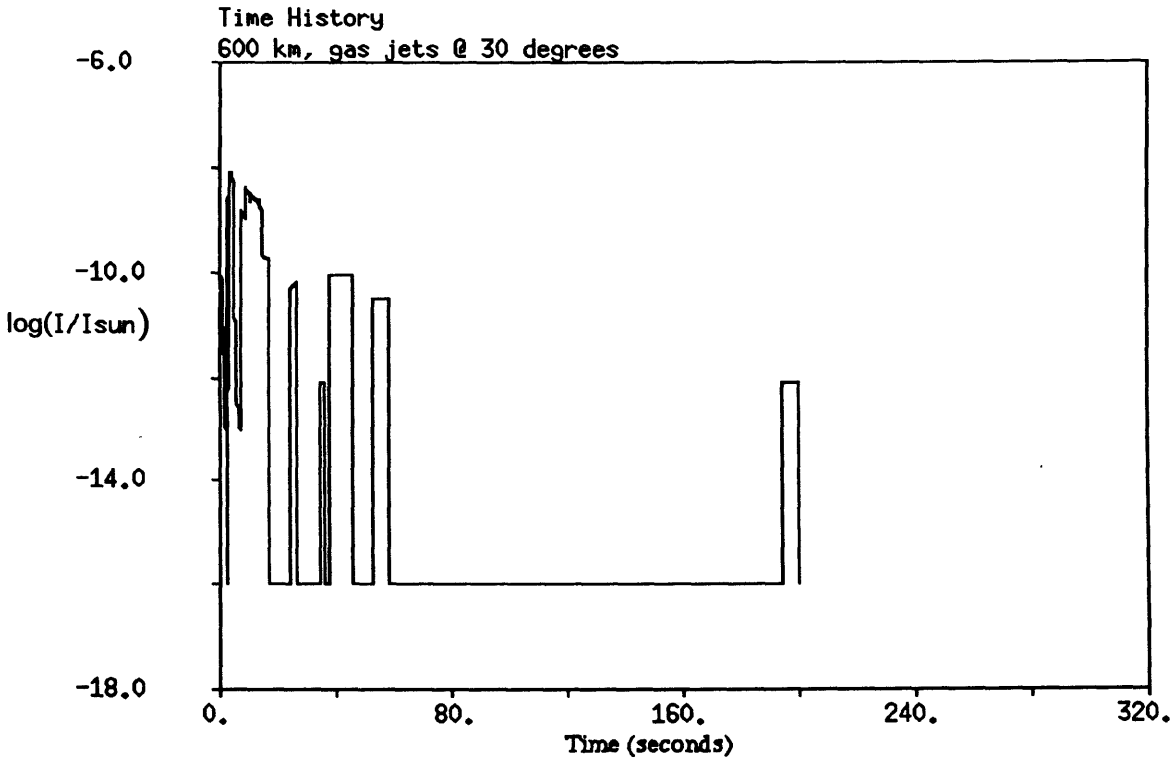

Figure 3-7a : Time History of Intensity at 600 km; Gas Jets at 30 degrees

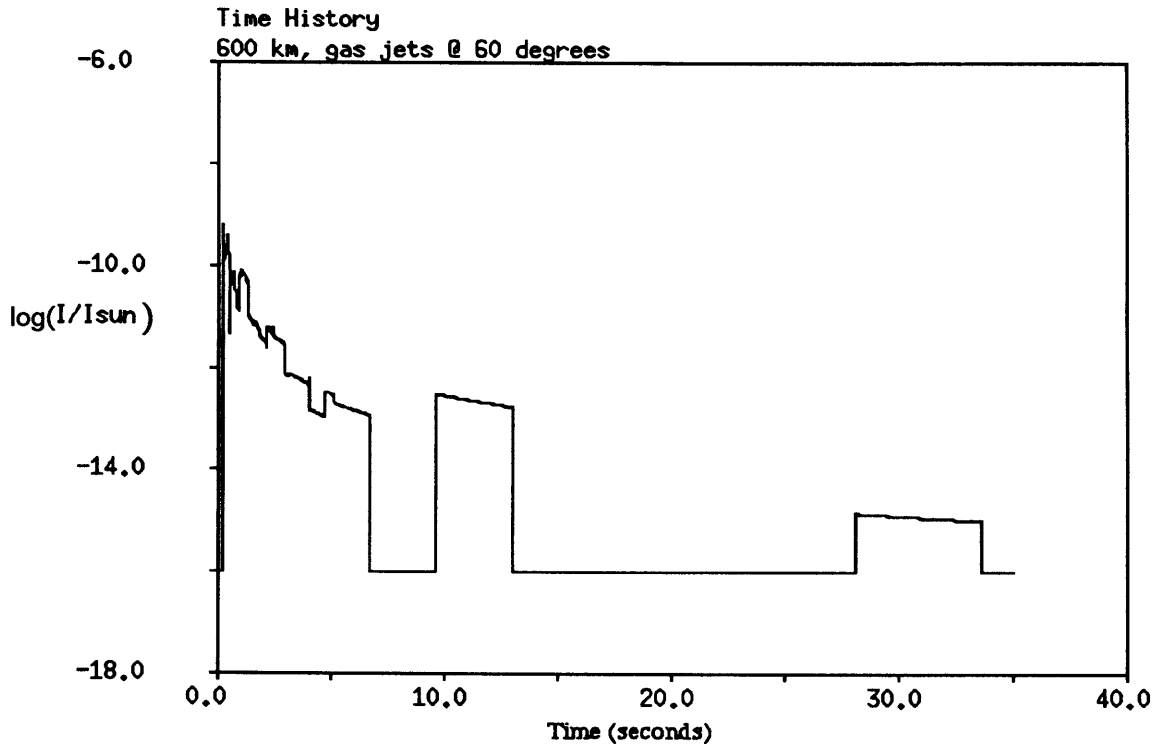

Figure 3-7b : Time History of Intensity at 600 km; Gas Jets at 60 degrees

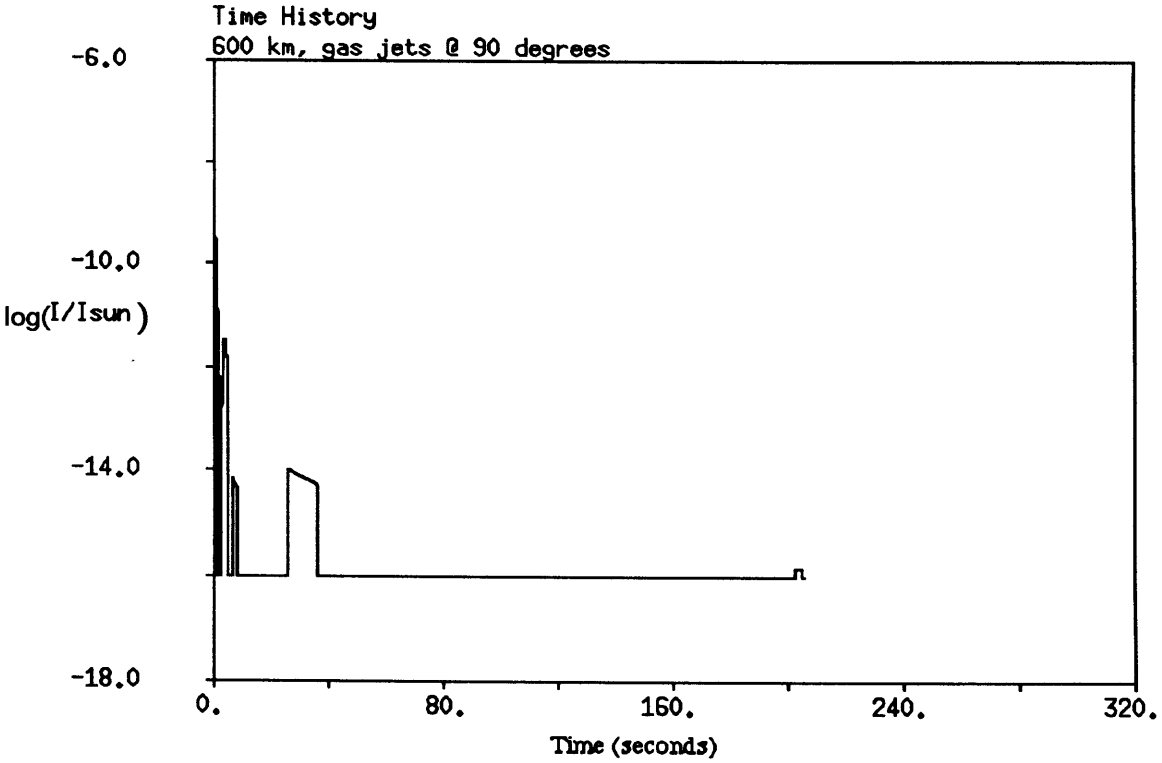

Figure 3-7c : Time History of Intensity at 600 km; Gas Jets at 90 degrees

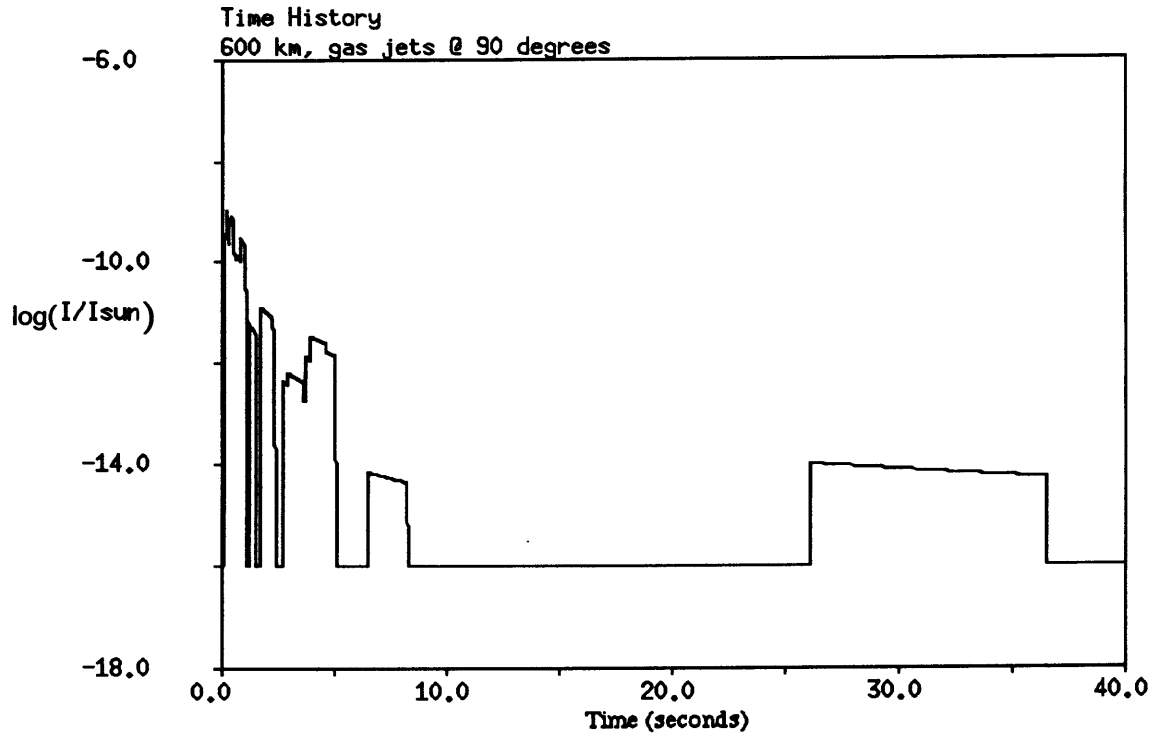

Figure 3-7d : Close up : Time History of Intensity at 600 km; Gas Jets at 90 degrees

The intensity data is averaged over the first ten seconds as with the case of no active control (Figure 3-8). Once again, the bars represent standard deviation of the time averaged data. There are two fairly interesting points about these results to note. First is the tendency of the 60 and 90 degree cases to decrease with altitude rather than increase as was seen in Figure 3-5. One way in which gas jets reduce the scattered intensity due to the particles is to push particles away from the craft, thus increasing their distance from the center. The strong neutral wind at low altitudes acts against this and the gas jet effectiveness due to this component at low altitudes is reduced.

Secondly, there is the effect of the 30 degree inclination plot rising up after approximately 300 km and becoming fairly high. This is due to the fact that some particles do not reach the region of primary influence of the jet, since the angle points farther away from the leading edge of the spacecraft, before the one second firing time is

up, and thus are not turned away by t = 1s. These are either slower low momentum particles which haven't yet reached the significant part of the plume or they are higher momentum particles which have not yet been turned around by the plume but have now become lower momentum particles due to the plume's effects. At lower altitudes, the neutral wind would sweep them away once the thruster switched off. However, at higher altitudes, the wind is too weak, and the amount of contamination proceeds to increase. This increase occurs while the wind gets weaker. The value at high altitudes is still lower than the in the case with no active control, thus representing the decrease that these thrusters produce alone. This line implies an optimum balance between the positive effects of the neutral wind in reduction of particulates, and the negative effects of the neutral wind in reducing the effectiveness of the thrusters by exercising a strong force opposite to them.

Overall, these cases show a significant improvement over the cases using no active control whose values as seen in Figure 3-5 are orders of magnitude worse than the best cases here.

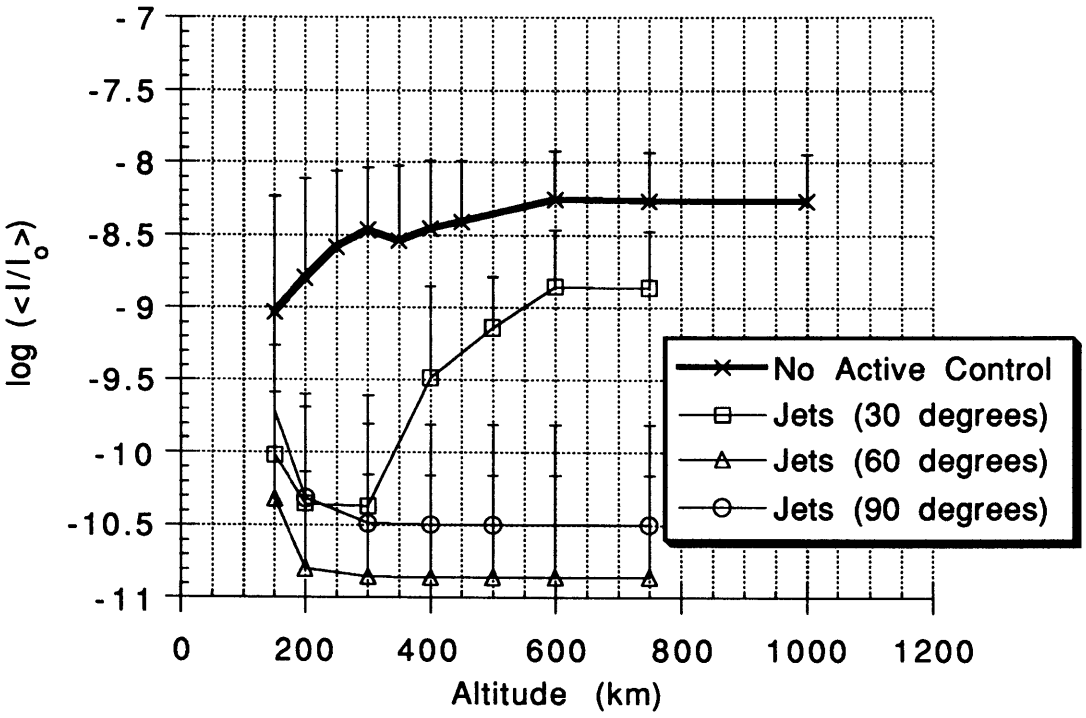

Figure 3-8 : Intensity Plot (2D) for Gas Jets at Varied Inclinations with Respect to Viewangle

3.3.1.3 Electric Field Modification (2D Case): The next control method examined is that of modifying the electric field to attempt to repel the particles from the domain. The field is set up as described in section 3.1 and it is assumed to be on through the duration of the simulation.

A few time history plots are shown next in Figures 3-9a, b and c. These plots correspond to 200, 300 and 600 km of altitude. These can be compared to the plots of the corresponding altitudes with no active control. It can be seen that using this electric field does not seem to have a significant effect. The 200 km plots with no active control (Figure 3-4b) and with the high voltage wires (Figure 3-9a) are remarkably similar. The most significant difference is the spike (just to the left of t = 4.0) in Figure 3-4b that

cannot be found in Figure 3-9a. There are more differences between the two 300 km plots (3-4d and 3-9b). The differences between the two 600 km plots are more visible. There are fewer late-arriving isolated peaks in Figure 3-9c than in Figure 3-4g. In addition, the initial peak is smaller in the electric field case for this altitude, implying a greater effect at higher altitudes.

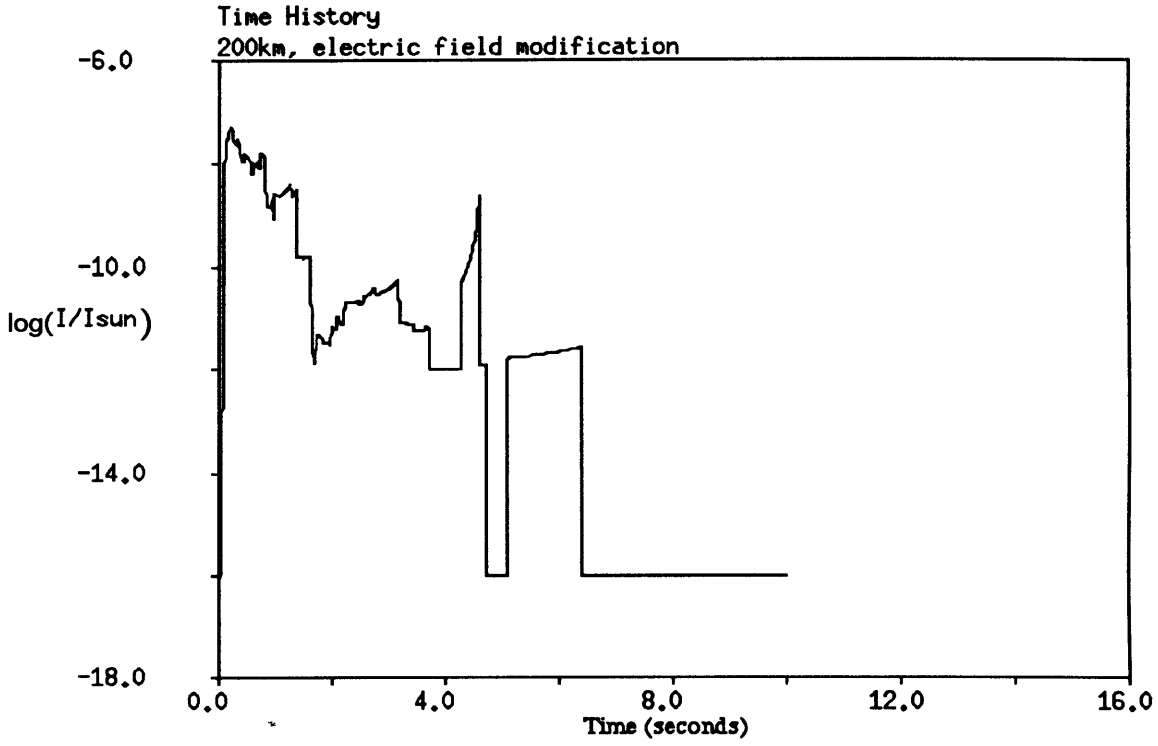

Figure 3-9a : Time History of Intensity at 200 km; Modified Electric Field

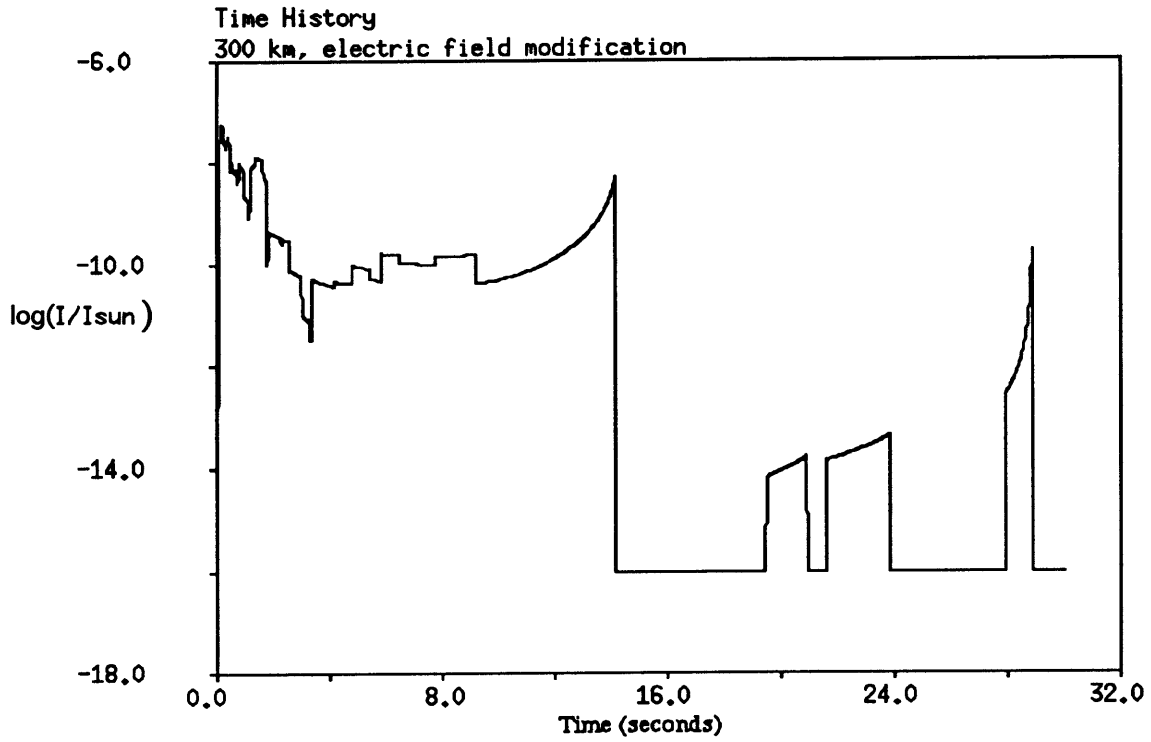

Figure 3-9b : Time History of Intensity at 300 km; Modified Electric Field

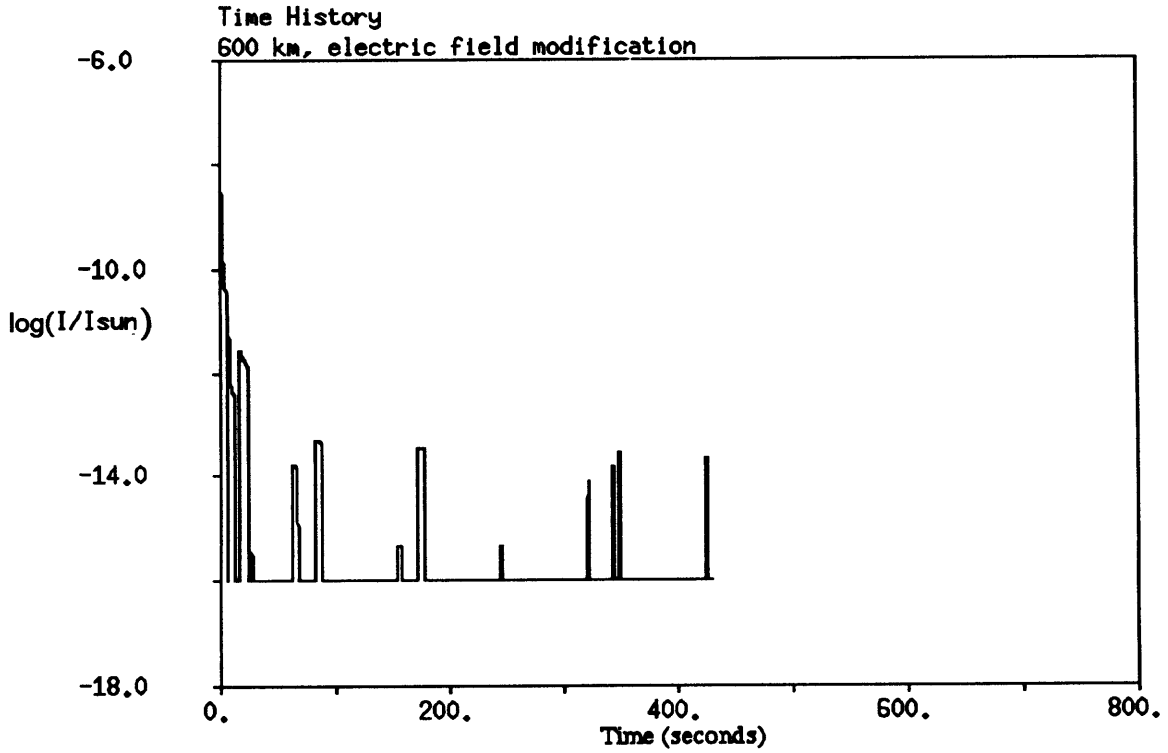

Figure 3-9c : Time History of Intensity at 600 km; Modified Electric Field

Time averaging the intensity for each of the runs done with the electric field, Figure 3-10 is generated. The lower altitude results are very similar, but the differences become more pronounced between the higher altitude averages. This is due to the neutral wind. At low altitudes, the neutral wind is strong enough to sweep away all of the particles that would have been affected by the electric field. As the altitude increases, the wind becomes weaker, but the electric field does not. The electric field modification method results in a lower average intensity in the absense of the neutral wind, than with no control method at all. Even though this is true, the higher altitude averages are still within a standard deviation of each other, and therefore these results do not display a significant improvement.

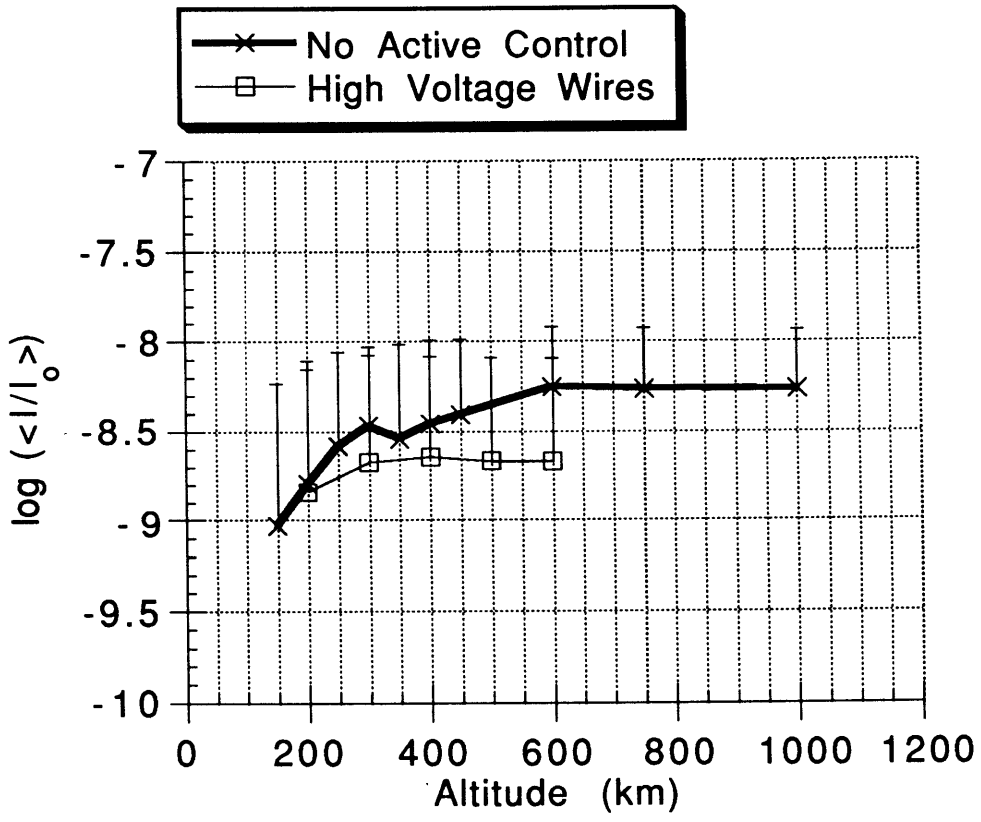

Figure 3-10 : Intensity Plot (2D) with Electric Field Modification Case

3.3.1.4 Electron Beam Charge Modification (2D Case) : The addition of charge to the particles had negligible effects on the motion of the particles. There is a limit based on their dielectric strength placed on the amount of charge that these particles can hold (Section 2.5.3) . This limit is not high enough to significantly affect their motion. In Figure 3-11 below the time averaged intensity of these runs is compared with the runs using no active control method.

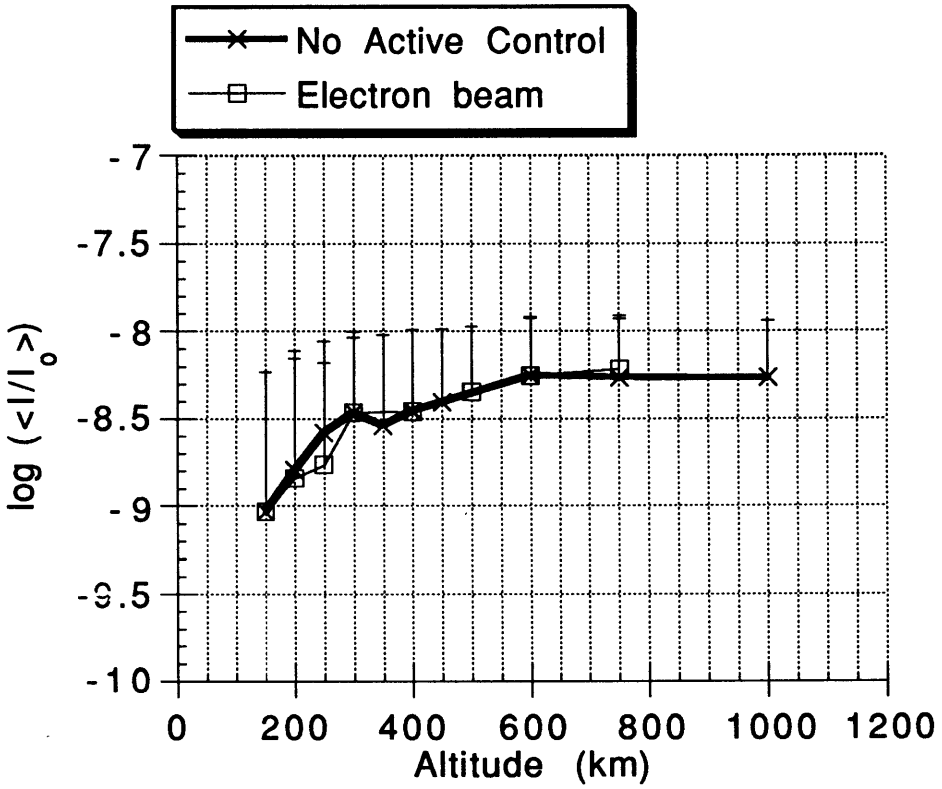

Figure 3-11 : Intensity Plot (2D) with Electron Beam Charge Modification

The two lines that are shown here display nearly the same behavior, implying that even when each particle is set to its maximum charge, the change is insignificant.

3.3.1.5 Summary of 2D Case Results Figure 3-12 compares the averaged intensities of all of the methods. It is clear from the plot which method is the most effective at

reducing the scattered light into the sensor. The gas jets, specifically the gas jets angled at 60 degrees from the view field, result in an extremely large improvement over the case with no active control, whereas the electric field modification yields marginal gains at high altitudes, and the electron beam charge modification shows no gains whatsoever.

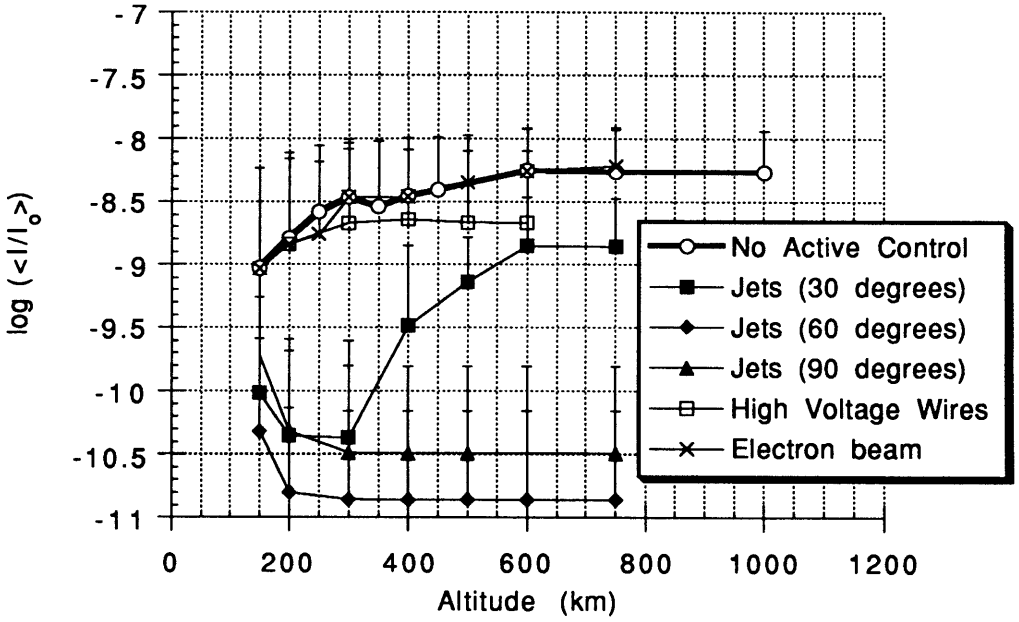

Figure 3-12 : Intensity Plot (2D) Comparing All Control Methods

3.3.2 The 3D Case

In three dimensions, the rectangular model of the previous set of simulations is rotated to form a cylinder. The geometry of the spacecraft allows the electrical field to be determined by taking the two dimensional electric field and assuming it was axisymmetric about the centerline of the cylinder. Rather than using characteristic values for electron density and temperature, as in the two dimensional case, this set of simulations uses the International Reference Ionosphere model to get values for each altitude.

The number of particles which are used in these cases is 25000. This resulted in fewer particles crossing the view field during each simulation than in the two dimensional cases, which uses a 10000 particle release across the spacecraft. Primarily this is because there is a much higher chance in the 2D case that any particle released will cross the view field. Releasing more particles increases the number of particles crossing the viewfield, and thus results in more computational data to analyze, however, the computational cost was too great.

Due to the fact that fewer particles cross the sensor viewfield in these cases, there is a change in appearance in the intensity time history plots. In Figure 3-13a, the peaks in the initial region are less continuous than in Figure 3-4b, the analagous plot for the two dimensional case. In addition, the reduction in particles crossing the sensor viewfield result in a smaller contribution to the scattered intensity, which causes a smaller peak. This results in lower values for the average intensity in the three dimensional simulations than the two dimensional simulations, for the cases without active control (Figure 3-14). A characteristic time history plot for the higher altitude region is displayed in Figure 3-13b. Due to the fact that there are fewer particles crossing the sensor viewfield, the final particle appears much sooner than in the analogous two dimensional case (Figure 3-4h).

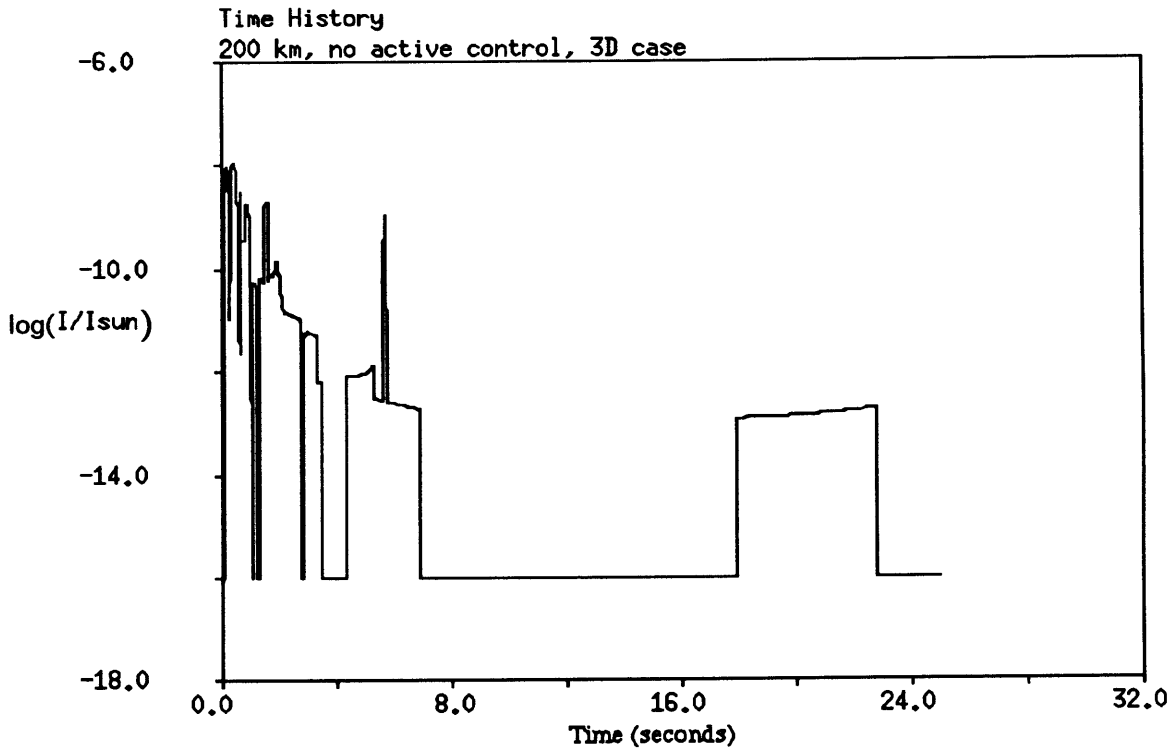

Figure 3-13a: Intensity Time History (3D) at 200 km, No Active Control

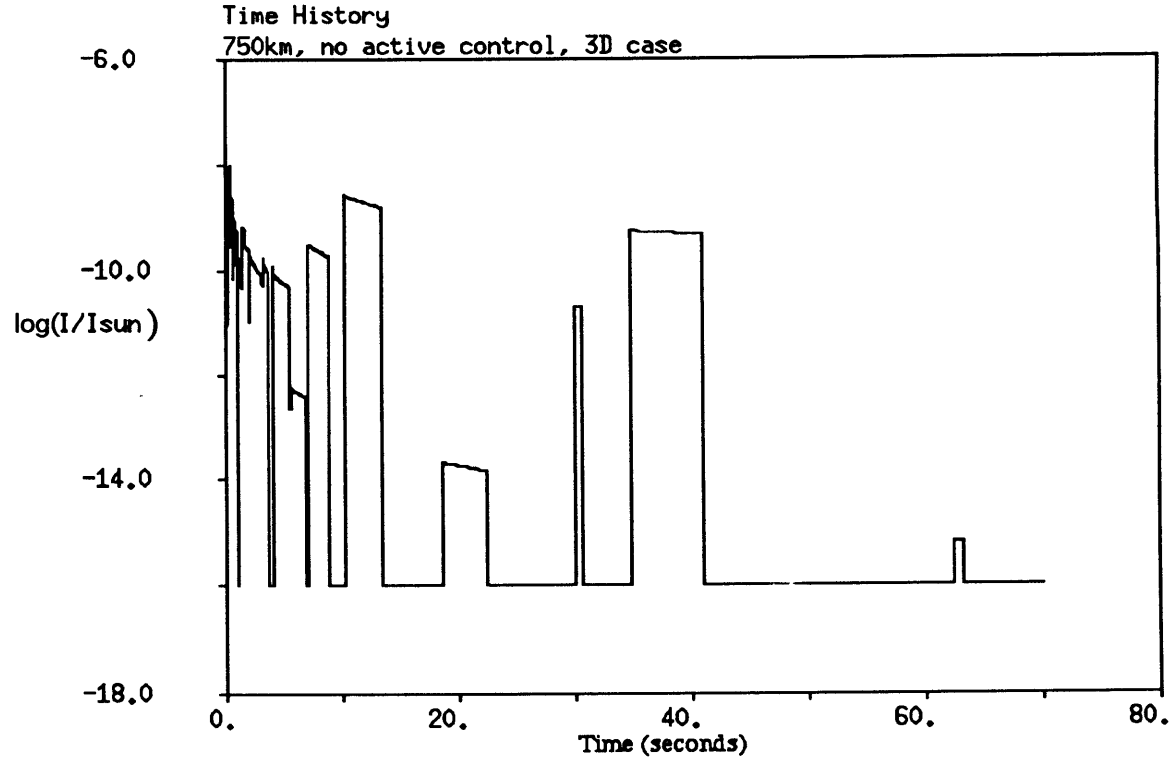

Figure 3-13b: Intensity Time History (3D) at 750 km, No Active Control

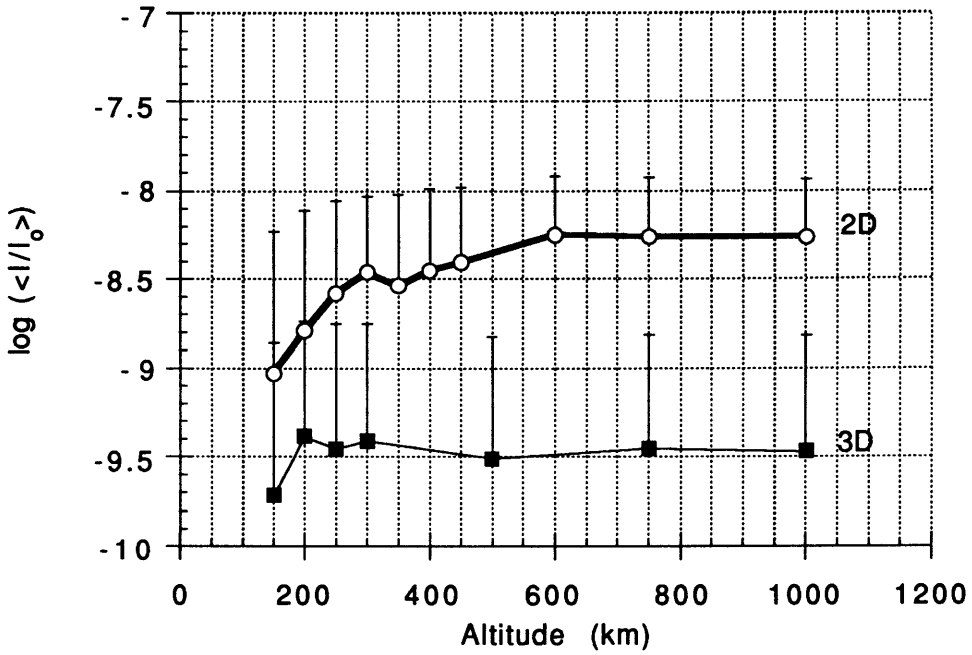

Figure 3-14 : Intensity Plots for No Active Control Scenarios

Next, the effects of the active control methods in three dimensions are discussed. The first method analyzed is gas dynamic control using cold gas jets. The first runs that are done use thrusters of area ratio 50, and therefore exit Mach numbers of 5.9. Six of these thrusters are placed symmetrically about the sensor, with 60 degree inclinations with respect to the view angle. These runs show considerably less effect than was shown in the corresponding two dimensional runs. (Figure 3-15) This occurs because the particles are no longer compelled to travel through the centerline of the thruster to get to the sensor view field. In addition, thrusters with this exit mach number experience rapid plume density fall-off away from the centerline. (see section 2.5.1) In order to affect more area with the gas jet plume, the exit Mach number is reduced to 2. This is more effective than the other jets (see Figure 3-15), however they are still less effective than the two dimensional scenario. The behavior in this line again implies an optimum neutral

wind velocity to balance the aid that the wind gives in reducing the contamination and the negative effects in reduction of the effectiveness of the thrusters.

The electric field modification used in the two dimensional case is extended to three dimensions as an axisymmetric version of the former. The physical model for this is a cage of high voltage wires surrounding the sensor. This method, as in the two dimensional runs, has some effect in the higher altitude region but not at the lower one. Again, the contamination controlling effects of the wires are small compared to the strong neutral wind at lower altitudes, but at higher altitudes the effects are visible. The effect that it had was much smaller than in the two dimensional case, as well. Figure 3-15 shows that the case with the modified electric field is better than the case without active control, but the two are very close, well within the standard deviation lines.

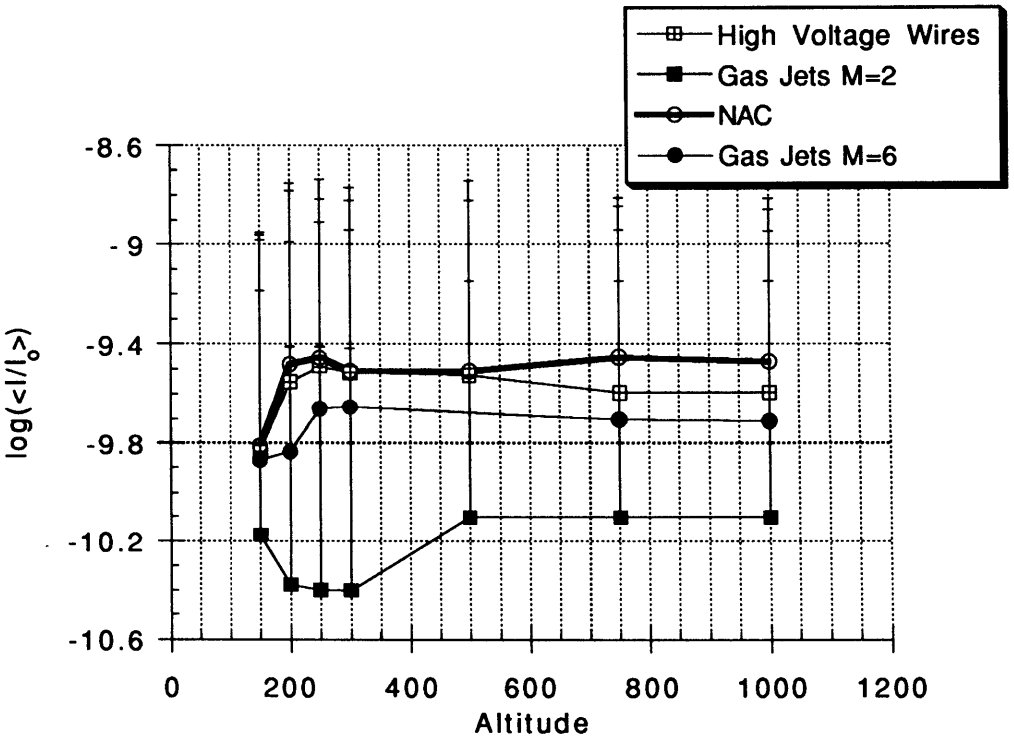

Figure 3-15 : Intensity Plot (3D) Comparing Effectiveness of Control Methods

The electron beam modification in this case shows no appreciable difference with the case without control, just as in the two dimensional case.

Additionally, despite the fact that the gas jet scenarios do not affect the intensity as much as they did in the 2D case, they do cause significant reduction of the amount of particles that were permitted to cross the viewfield. These numbers are not valuable in an absolute sense but in a relative one. The gas jets with exit Mach number equal to 5.9 reduced the number of particles crossing the sensor view field by half. The second gas jet case, using an exit Mach number of 2, showed an even greater reduction in the amount of particles crossing the sensor during the simulation. (Figure 3-16) Therefore, though these methods do not reduce the scattered light intensity in the three dimensional case, they do accomplish a significant reduction in particle numbers crossing the viewfield.

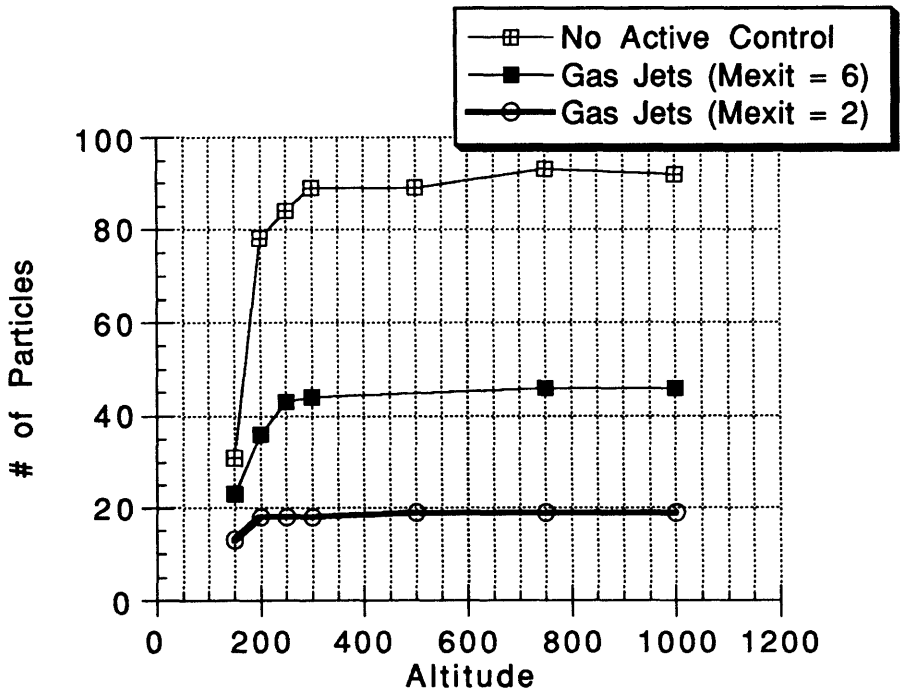

Figure 3-16 : Particles Crossing Viewfield in 3D Simulations

3.3.3 System Effects

The other measure of effectiveness for the control methods in these simulations is that of the effects and demands each one may place on the spacecraft. The goal is to find the most effective control method while minimizing system effects. This section will discuss the mass and power penalties of the three active control methods examined in this

section, in addition to qualitatively addressing the potential problems that might be incurred by using each of these methods.

The gas jets primarily incur mass penalties. These will be due to fuel and containment systems. The fuel consumption is simply a function of the mass flow rate of the thruster and the amount of time that the jet will spray gas. The cold gas thruster used was taken to be 10 mN. This number was obtained to minimize the mass flow necessary while still obtaining significant effect. The low thrust does the added benefit of relieving the system of the need for heavy pressure tanks which would be needed to hold gas at the high pressures necessary to generate high thrust from cold gas thrusters. The thruster was previously chosen to be a cold gas thruster of I_{sp} = 70 sec. Using the thrust and the I_{sp}, the mass flow rate was determined to be .000015 kg/s. The duration of the jet firing, chosen to balance fuel conservation and effectiveness, had been chosen to be one second each firing. This results in a mass cost of .000015 kg per thruster per firing. In addition, these thrusters cause a net force which slows the spacecraft. Therefore, compensation thrusters must be placed at the rear of the spacecraft to maintain the orbit. The thrusters which are angled at 60 degrees with respect to the velocity vector, the retarding force per thruster is half of the force of that thruster. For simplicity, we assume that the compensation thrusters are of the same type as the contamination control thrusters. This results in the following mass cost for one firing:

$$m = 3/2 * (6 * .000015 \text{ kg/s}) * (1 \text{ s}) = .000135 \text{ kg}$$

If the event which caused the particle releases was that of thermal shock, then it would occur twice per orbit: when entering and leaving eclipse. The number of orbits in a given year varies for each altitude. The difference is small, however, compared to the number of orbits. The number of orbits that spacecraft at 200 and 600 km will complete in a year are 5942 and 5438 respectively. It is thus possible to arrive at values for the mass cost in fuel per year. The cost per year is 1.60 kg for the lower orbit, and 1.47 kg for the higher one.

The power cost of the electric field modification was determined using the voltage of the extended wires, and multiplying it by the ion current to them. The ion current is determined by the field generating code. This will result in the power necessary to maintain the wires at the constant voltage. The current was determined to be 3 mA by the field code. This, combined with the fact that the wires are set to -1 kV, results in a power requirement of 3 watts per wire. Using the requirement that the wires be within a Childe-Langmuir length of each other in order for this cage to be effectively modeled by the axisymmetric assumption used in the 3D scenario, then sixteen wires are required using this set-up. This results in a total power requirement of 48 watts. For the electron gun, the power requirements are much less. In order to get at least an electron gyro radius on the order of a body length (1 meter) a voltage of 220 volts is required. This assumes that the gun will be fired soon after the event, before the particles are far from the craft. In order for the beam to scan the necessary area on in an effective amount of time, it will only be on a given particle for .1 ms. This taken with the maximum charge allowable for a ten micron particle (done to get an upper limit for power cost) results in a current on the order of nanoamps, which combined with the 220 volts, gives a power requirement on the order of microwatts. This is negligible. Considering the fact that the effectiveness was negligible as well, this is not surprising.

Chapter 4 : Particulate Contamination on Spacecraft Surfaces

A second problem that is examined is that of reducing particulate contamination on a surface. Solar arrays and radiators have their effectiveness reduced when particles build up on their surface. In this chapter, the case of particles coming to rest on the surface of a solar array is examined. These particles block incident sunlight, reducing the power generated by the array. Due to the negligible effects noted in the previous chapter of the electromagnetic control methods, only the gas jets are examined here. In the first section of this chapter, the simulation conditions are described. Then, results are presented and discussed.

4.1 Description of Surface Case

In this case, the effectiveness of gas jet control in reduction of particle deposition on a solar array surface is examined. This case is only examined in two dimensions, because there is no rotational symmetry, and the electric field cannot be extrapolated accurately into three dimensions. As before, the spacecraft is taken to be one meter by two meters. The array is taken to be of a length on the same order of the spacecraft: two meters. The array is located even with the trailing edge of the craft, .2 meters away from the top edge of the spacecraft. (Figure 4-1) The direction of the sun is oriented such that the maximum amount possible reaches the solar array. Particles are emitted only from

the lateral surface next to the array. The location of the contamination control jet is shown in Figure 4-1.

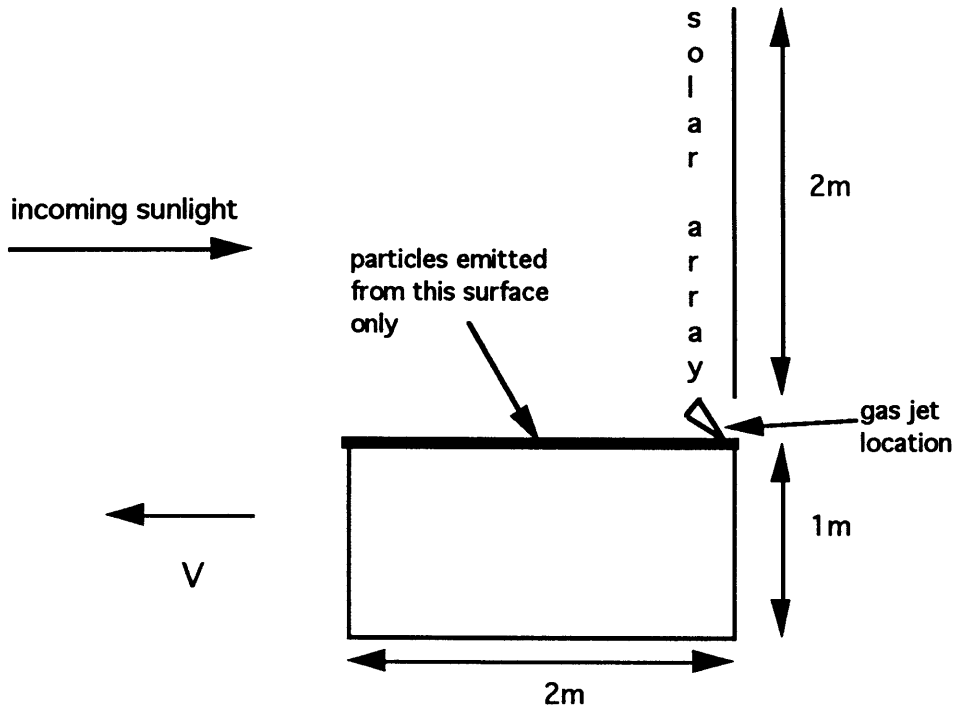

Figure 4-1 : Surface Case Set-Up

The potential on the spacecraft is set at -1 V, as it was in the sensor case. The solar array potential varies linearly from -1 V at the end nearest the spacecraft, to -28 V at the far end of the array. The resultant potential around the spacecraft and the array is displayed in Figure 4-2. The windward surfaces have very short sheath regions, as there is no high voltage region, like in the sensor case, to extend the potential sheath into the incoming flow.

The gas jet that is used in this simulation is the same type that is used in the sensor case, for consistency. The thrust is taken to be 10 mN, and it fires for one second after particle release. The fuel requirements due to using thrusters this size are examined

earier, in the analysis of the sensor case, and is taken to be acceptable. Therefore, using a thruster of this size is taken to be acceptable here, as well.

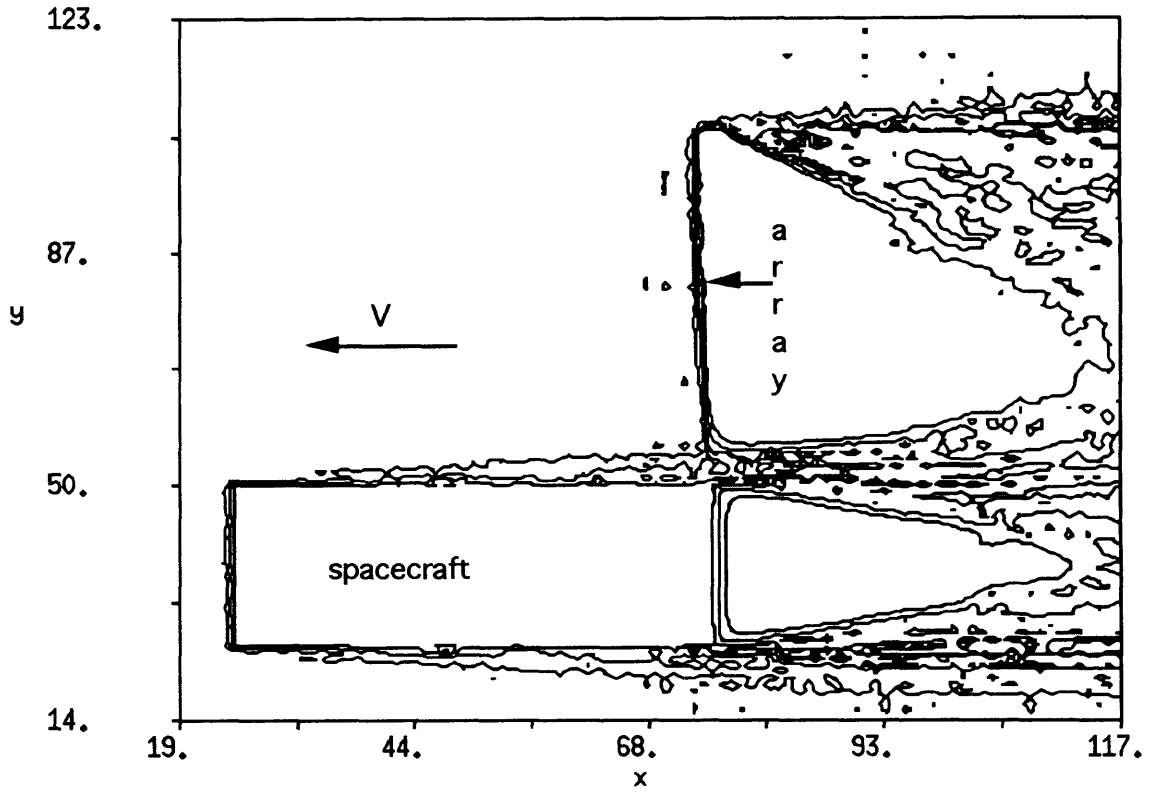

Figure 4-2 : Potential Contours about Spacecraft and Solar Array

In this case, fewer particles need to be released in order to get a statistically significant number of impacts on the solar array surface. This is due to the fact that the particles are only released from one surface. In addition, the array is fairly large and many of the particles will tend to impact it after release. This is especially true in the lower altitude case, where particles will be blown back into it. In this simulation 500 particles are released at time t=0. This is a sufficient number to generate a statistically significant number of particles impacting the surface. Particles will be quartz spheres released with the same velocity and size probability distributions as defined in the sensor case.

4.2 Simulation Results

This simulation is designed to ascertain an initial estimate of the effectiveness of the gas jet control method in mitigating particle accumulation on a spacecraft surface, in this case a solar array. The general analysis of micron sized particle behavior in the second chapter and the control method analysis in the third chapter each imply that the electromagnetic control methods are ineffective. Therefore, only the gas jet effectiveness is examined here.

The neutral wind applies a force to the particles at lower altitudes, and sweeps them back onto the surface. Thus, the number of particles (Figure 4-3) and the area they obscure (Figure 4-4) decreases as the altitude increases.

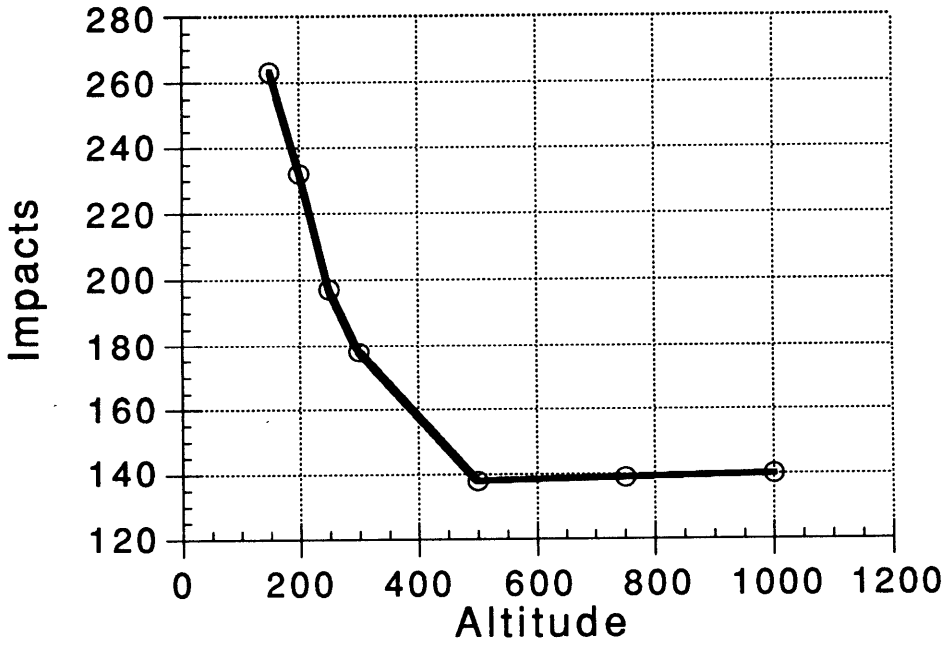

Figure 4-3: Number of Particles impacting Solar Array (out of 500 released)

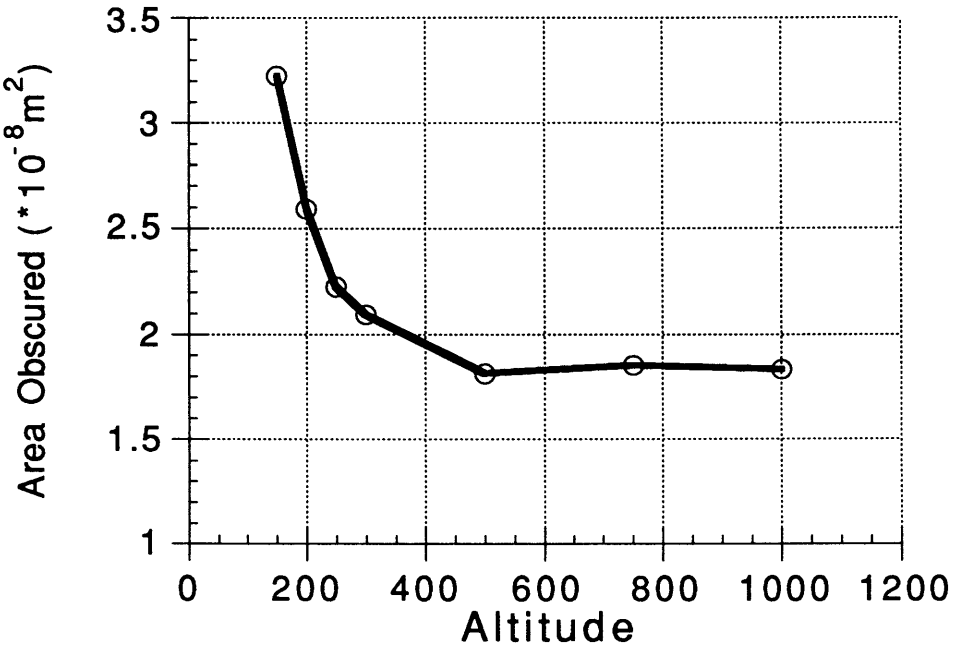

Figure 4-4: Area obscured by particles (for initial 500 particle release)

In addition, at the very low altitudes, many particles are blown back between the array and the spacecraft, into the gap between them. The significance of this can be seen in the next plots, where the effects of cold gas jets in this scenario are examined. Notice that at 150 km, the effect of the gas jet is actually to make the contamination worse. It pushes the particles which would have been blown into the region in between such that some of them impact the solar array. As the altitude increases, the effectiveness of the cold gas jet against the neutral wind improves, and in addition, there are fewer particles that would have been blown into that "safe" intermediate region since the wind is weaker.

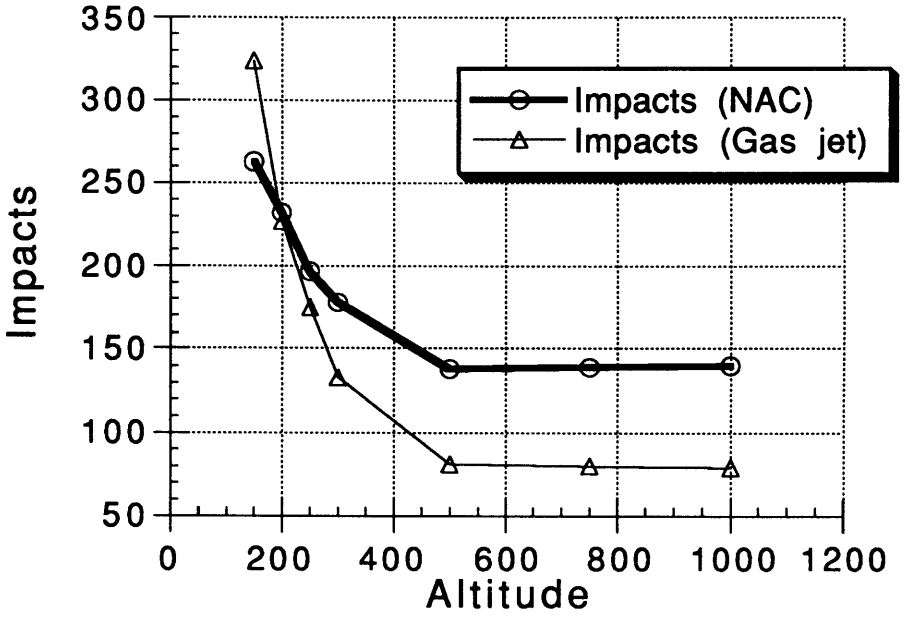

Figure 4-5: Number of Impacts (out of 500 released) :

Gas Jet Control versus No Active Control

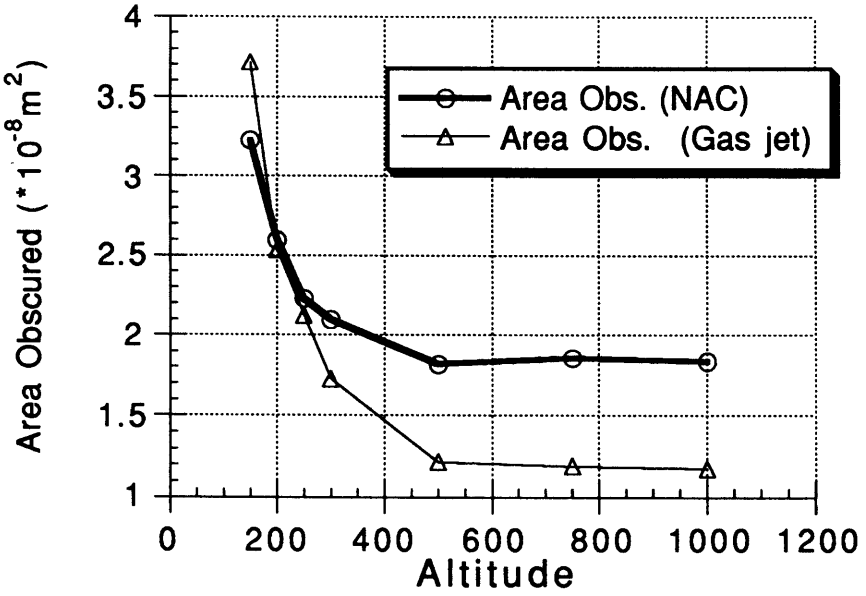

Figure 4-6: Area obscured in each case

At the highest altitudes, specified as region 2 in Chapter 3, the effectiveness of the jet reaches a steady state, reducing the amount of particles that impact the surface by 42% and the area obscured by these particles by 35%. The particles that actually do reach the surface are those with more initial momentum (and thus larger size) so the reduction in area obscured is smaller than the reduction in number of impacts.

Chapter 5: Conclusions

Some problems associated with particulate contamination around spacecraft were addressed in this research. Particles may be jarred from the surface of spacecraft due to sudden vibration from a solid rocket motor firing. In addition, they could be broken loose by stresses resulting from thermal cycles. In this research, active control methods were examined to mitigate the effects of this particulate contamination. The active control methods that were examined were gasdynamically blowing particles from sensitive areas; modifying the electric field to electromagnetically repel the particles, which possessed negative charge; and increasing the charge on the particle to increase the probability that they would be swept away by the motional electric field.

Simulations were developed and presented which would model the paths of released particulates in this environment. The simulation tracks the particles while self-consistently calculating the force and charge on the particle as it moves through the domain. The control methods that were analyzed were inserted into the simulation, and the reduction of contamination that resulted with the use of each was noted.

The second chapter details the simulation that was used, and elaborates on the theory that was used to develop it. In addition, this chapter contains a detailed analysis of the behavior of released particles in the ambient environment. The particles in the simulations were taken to be quartz spheres with radii between one and ten microns. The particles were taken to be released from the spacecraft with velocities ranging from zero to five meters per second. The particles were found to be primarily influenced by the

force due to the neutral wind. The electromagnetic forces in the spacecraft environment had a minimal effect. This is likely to be due to the fact that the particles have very low charge/mass ratios. The fact that the neutral wind was the most influencial ambient force implied that the gas jets would be the most effective control method.

The problem of particulates scattering sunlight into electromagnetic sensors was examined in the third chapter. The result showed the gas jets to be the most effective of the methods. In the two dimensional case, the gas jets were far more effective than either of the other methods, primarily because of the fact that in this scenario the particles were forced to travel through the centerline of the thruster, where the resultant force is a maximum. In three dimensions, the gas jets were still the most effective. The improvement was less dramatic in this case, however, because the particles were not forced to travel through the jet centerlines. In this case, six gas jets were used and spaced symmetrically about the sensor. It was found that reducing the area ratio of the thrusters increased the angle over which they would be effective, and by reducing the area ratio to the point where the exit Mach number was two (down from six), the effectiveness of the jets was significantly increased. However, it was not as effective as in the two dimensional case.

The electric field and charge modification methods did not show significant effects. The acceleration due to electromagnetic forces follows the formula : $a = qE/m$, where q is the particle charge, E is the electric field and m is the mass of the particle. These two methods involve increasing either the electric field or the charge. The charge on the particle, however, was limited to a function of its dielectric strength (Section 2.5.3) This charge limit was not significantly higher than the initial charge of the particle, and thus, charge modification had little or no effect. The increase in electric field near the high voltage wires was not large enough to result in a large acceleration. This is primarily due to the fact that the q/m ratio was too large. An electron would have a ratio of $q/m = 1.8 \times 10^{11}$ C/kg, and a water ion with unit charge would have a ratio of q/m =

5.4×10^6. The one micron particle at maximum charge had a q/m ratio of .358. This shows that the electric field would be much more effective in moving smaller particles around, but not ones on a size of this scale.

This analysis of these active control methods also included considerations of system cost. The cost of the gas jets was measured in additional mass due to fuel, and the cost of the other two methods was measured in power. As noted in Section 3.3.3, the fuel required by the gas jets would be close to one and a half kilograms per year for the scenario described.

For this case, optimum control method examined was that of the cold gas jets, being the most effective and having an affordable mass penalty. They were the most effective in the two dimensional scenario. This implies that the optimum time to use them would be when the direction of approach of the particles is known, thus forcing the particles to approach closer to the centerline of the gas jet before they reach the sensitive areas of the spacecraft, and allowing the jet to have its maximum effect.

In Chapter 4, this knowledge was used to assess the value of using gas jets to prevent particles from accumulating on the surface of a solar array. Because of knowledge gained in the previous two chapters, only the gasdynamic control method was used in these simulations.

The case presented in Chapter 4 was a more difficult control problem, as the force due to the neutral wind was directly toward the surface to which the contamination needed to be reduced. The gas jets were seen to be far more effective at higher altitudes where the neutral wind is negligible. Additionally, the gas jet was seen to have detrimental effects on contaminants reaching the surface at the lowest altitude examined, causing some particles to impact the surface that would not have impacted the surface in the absense of a control method.

These methods were general, and not optimized. Further optimization may yield improved results in controlling the particles. A different fuel or a higher I_{sp} might result

in improved control of contamination. In addition, regarding cases with smaller particles, posessing higher q/m ratios, the electric field modulation may be much more effective. These should be examined in future research. In addition, control methods unlike the ones examined here may be examined and found to be more effective.

Bibliography

[1] Tribble, A. C. "The Space Environment and its Impact on Spacecraft Design", AIAA 93-0491, 31st Aerospace Sciences Meeting, 1993.

[2] Stewart, T. B., Arnold, G. S., Hall, D. F., Marvin, D. C., Hwang, W. C., Chandler, R. D., and Martin, H. D., "Photochemical Spacecraft Self Contamination - Laboratory Results and Systems Impaces, " *Journal of Spacecraft and Rockets*, Vol. 26, No. 5, Sept.-Oct. 1989, p. 358.

[3] Newkirk, G. "The Optical Environment of Manned Spacecraft", *Planet Space Sci,* 15, 1267, 1967.

[4] Clifton, K. S. and Owens, J. K., "Optical Contamination measurements on early Shuttle missions", *Applied Optics,* 27, 603, 1988.

[5] Robinson, P., Leung, P., Feynman, J., Gabriel, S., Wuerker, R., Wong, A. , Short, E., and Seale, O. "Observations and Impact of Dust Particles on the Magellan Mission to Venus", Internal JPL report, 1991.

[6] Smith, Bruce A. "JPL Monitoring Satellite Systems", *AW & ST*, Oct. 5, 1992, p. 24.

[7] Rawlins, W. T. and Green, B. D., "Spectral signatures of micron sized particles in the Shuttle optical environment", *Applied Optics*, 26,3052, 1987.

[8] Consolmagno, G. J. "Lorentz Forces on the Dust in Jupiter's Ring", *Journal of Geophysical Research,* 88:5607-5612, 1983.

[9] Goertz, C. K. and Ip. W. H. "Limitation of Electrostatic Charging of Dust Particles in a Plasma", *Geophysical Research Letters*, 11: 349-352, 1984.

[10] Havnes, O., Morfill, G. E. and Goertz, C. K. "Plasma Potential and Grain Charges in a Dust Cloud Embedded in a Plasma", *Journal of Geophysical Research*, 89: 10999-11003,1984.

[11] Whipple, E. C., Northrop, T. G. and Mendis, D. A. "The Electrostatics of a Dusty Plasma", *Journal of Geophysical Research*, 90: 7405-7413, 1985.

[12] Havnes, O., Goertz, C. K., Morfill, G. E., Grun, E. and Ip, W. "Dust Charges, Cloud Potential and Instabilities in a Dust Cloud Embedded in a Plasma", *Journal of Geophysical Research,* 92: 2281-2287, 1987.

[13] Gatsonis, N. A. and Hastings, D. E. "A Three Dimensional Model and Initial Time Numerical Simulation for an Artificial Plasma Cloud in the Ionosphere", *Journal of Geophysical Research*, 96, 7623-7639, 1991.

[14] Tribble, A. C. and Haffner, J. W. "Estimates of Photochemically Deposited Contamination on the GPS Satellites", *Journal of Spacecraft and Rockets*, Vol. 28, No. 2, pp. 222-228, 1991.

[15] Wang, J. Electrodynamic Interactions Between Charged Space Systems and the Ionospheric Environment, MIT Ph.D.. Thesis, 1991.

[16] Alpert, Ya. L., Gurevich A. V., and Pitaevskii, L. P. Space Physics with Artificial Satellites. 1965, pp. 20-24.

[17] Dettleff, G. "Plume Flow and Plume Impingement in Space Technology", *Prog. Aerospace Sci,* Vol 28, 1991, p. 14.

[18] van de Hulst, H. C. Light Scattering by Small Particles, 1981, pp. 200-206.